# LORELEI LOCALIZATION AND OVULE ULTRASTRUCTURE IN *ARABIDOPSIS THALIANA*

by

Juleen Dickson

A Dissertation Submitted in

Partial Fulfillment of the

Requirements for the Degree of

Doctor of Philosophy

in Biological Sciences

at

The University of Wisconsin-Milwaukee

August 2019

# ABSTRACT

LORELEI LOCALIZATION AND OVULE ULTRASTRUCTURE IN *ARABIDOPSIS THALIANA*

by

Juleen Dickson

The University of Wisconsin-Milwaukee, 2019

Under the Supervision of Professor Heather Owen

Communication between the male and female gametophyte is vital to successful fertilization during sexual reproduction in plants. One of the proteins known to be important for communication between the male and female gametophyte is LORELEI (LRE). Several studies have shown that there are defects in pollen tube guidance and synergid degeneration, however this is the first study that shows that cell wall thickness in the female gametophyte may also be affected. Previous confocal studies have documented that LRE is present both in the filiform apparatus and found in puncta throughout the cytoplasm. This study confirmed this, but our studies suggest that the proportions maybe different; in the TEM sections we examined a majority of the LRE seems to be localizing to the filiform apparatus. This study also reported that three *Arabidopsis* WT accessions had very similar embryo sac ultrastructure, thus for electron microscopy studies data from all these accessions can be used to add robustness to a study with a low WT sample size.

To:

Grandma Jane and Papa Otto for raising me in a greenhouse and instilling in me a life-long love of books and learning. I would also like to dedicate this to my childhood hero, Mr. Rodgers, for taking me to make believe land and reminding me to feed the fish. Finally, I would like to dedicate this dissertation to the dreams of the future; may my niece Elisabeth follow her dreams down all the rabbit holes of adventure that they bring.

# TABLE OF CONTENTS

LIST OF FIGURES

LIST OF TABLES

# LIST OF ABBREVIATIONS

ANJ: Anjea

*amc*: *abstinence by mutual consent*

CaM: calmodulin

CBLs: calcineurin B-like proteins

Col Wt: Colombia Wild Type

CDPKs: calcium-dependent protein kinases

CI: Confidence Interval

CMLs: calmodulin-like proteins

FA: filiform apparatus

*fer: feronia*

GABA: gamma-Aminobutyric acid

GDNF: glial cell line-derived neurotrophic factor (GDNF)

GEF: guanine nucleotide exchange factors

GPI: Glycophosphatidylinositol

HERL1: Hercules Receptor Kinase 1

Ler: Landsberg erecta

*lre: lorelei* allele usually the null mutant

LRE/LRE: wild type form of lorelei allele

LLG: LORELEI-like-GPI-anchored proteins

NADPH: nicotinamide adenine dinucleotide phosphate

*nta: nortia*

RET: receptor tyrosine kinase

ROP: Rho of Plant

ROS: Reactive Oxygen Species

SD: Standard deviation

SE: Standard error

*syl: scylla*

*ser: sirene*

T-DNA: Transfer DNA

WS: Wassilewskija

WT: wild type line

# ACKNOWLEDGEMENTS

This work would not have been possible without the LRE lines provided to us by our generous collaborators in the Palanivelu laboratory at the University of Arizona. Funding for this project was provided by a UW-Milwaukee Research and Creative Activities Support Grant to H.A.O. I would also like the thank Addie Skillman for running the PCR to confirm the wild type lines.

# Chapter 1: Introduction

## SEXUAL REPRODUCTION IN PLANTS

Although plants are able to reproduce asexually by various means, sexual reproduction is important for maintaining variability within a population. In order for sexual reproduction to occur, the combination of genetic material from two different individuals into one cell must take place during fertilization. Although some of the basal terrestrial plant taxa such as bryophytes and pteridophytes have flagellated sperm, the more derived spermatophytes such as angiosperms have one or two non-flagellated sperm (Wodniok et al., 2011; Dresselhaus and Franklin-Tong, 2013) that are contained within a pollen grain. Although this protects the sperm from drying out and facilitates terrestrial dispersal via wind or animal pollinators, it means that the sperm cannot just 'swim' to the female gametophyte the way they can in more basal land plants. To compensate for this loss of sperm motility, the vegetative cell that is contained in the pollen grain will elongate, forming a pollen tube that will deliver the two sperm cells to the female gametophyte that is contained within the pistil of the flower.

Once a pollen grain lands on the stigma, either through self-pollination or with the aid of wind or insect pollinators, the vegetative cell begins to form a pollen tube which will grow towards the female gametophyte (Heydlauff and Groß-Hardt, 2014). Throughout the process of pollen tube growth there are a number of cell signaling interactions that must take place between the pollen tube and the female gametophyte in order for the pollen tube to successfully deliver the two sperm cells to the egg cell and central cell (Figure 1.1) in a process called double fertilization (Dresselhaus and Franklin-Tong, 2013). The fertilized egg cell will

undergo many cell divisions to form the plant embryo and the fertilized central cell will divide to form the nutrient rich endosperm (Heydlauff and Groß-Hardt, 2014).

## SIGNALING INVOLVED IN POLLEN TUBE GROWTH

### *General signaling in cells*

There are many aspects of cell signaling that must occur throughout pollen tube growth in order for the sperm contained within the pollen grain to reach and fertilize the embryo sac (Table 1.1). Cells can communicate through both long-distance signaling, and also through short range guidance cues. One of the long-range signaling cues that is commonly used in eukaryotic cells is calcium signaling. Another signaling pathway that is used in eukaryotes is the RAC/Rho signaling pathway.

This pathway acts as a molecular switch that can have many downstream effects and is used for a wide variety of cellular functions including cell migration, cell cycle progression and cytokinesis, and microbial killing (involving phagocytosis and NADPH oxidase activity)(Caron, 2003). As with other Rho GTPases present in animals and fungi, Rho of plant (ROP) regulates a number of processes involved in cell polarization and cell shape (Uhrig and Hülskamp, 2001). Although portions of this pathway are conserved, the upstream regulators and downstream effectors in this pathway can be altered depending on the context. These GTPases are active in the guanosine triphosphate-bound state, but inactive in the guanosine diphosphate-bound state so they can act as molecular switches (Uhrig and Hülskamp, 2001). Downstream targets of RAC/ROP signaling include the rearrangement of actin filaments, calcium regulation, and NADPH generated reactive oxygen species (Duan et al., 2014).

*Long range signaling in plants*

If compatible, when the pollen from the anther reaches the stigma, it will stick to the papilla cells at the end of the stigma, and begin to hydrate. The pollen tube will then grow along the transmitting tract, which is made of small cylindrical cells that are situated within an extracellular matrix composed of glycoproteins, glycolipids, and polysaccharides. Pollen tube guidance towards the female ovule is established by gradients of molecules such as GABA, $Ca^{2+}$, and D-serine (Bleckmann et al., 2014). Pollen tubes can detect changes in calcium through the use of calmodulin (CaM), calmodulin-like proteins (CMLs), calcium-dependent protein kinases (CDPKs), and calcineurin B-like proteins (CBLs) (Bleckmann et al., 2014). This calcium detection is also augmented with glutamate-like receptors and other receptors that can detect GABA (Palanivelu et al., 2003; Yu et al., 2014). In addition to these long-distance signaling cues, there are also more localized signaling cues once the pollen tube approaches the female gametophyte.

After the pollen tube has reached the end of the transmittance tract it can interact with ovular pollen guidance cues. High concentrations of GABA have been reported in front of the ovule (Palanivelu et al., 2003; Yu et al., 2014), which are known to influence pollen tube growth (Yu et al., 2014). In normal wild type (WT) only one pollen tube will reach each ovule through a mixture of guidance and repulsion cues that are present before and after fertilization. Guidance cues can come from several different sources such as the synergid cells or the central cell (Liu et al., 2010; Kessler and Grossniklaus, 2011). Once the pollen tube has reached the end of the transmitting tract, the pollen tube extends towards the micropyle, which is the entrance to the embryo sac. The mature embryo sac has seven cells that originated from a single megaspore

mother cell (also called a megasporocyte). Five of these cells are support cells, three antipodal cells and two synergid cells. The other two cells are the egg cell, which will become the embryo after fertilization, and the 2N central cell that results from the fusion of two haploid nuclei which will be the source of the 3N endosperm after fertilization.

*Short range signaling and the Role of synergid cells*

Two of the support cells, called synergid cells, are found in the micropylar region at the entrance to the female gametophyte and are important for pollen tube attraction, repulsion of additional pollen tubes, arresting the growth of the pollen tube once it has reached a synergid cell, and pollen tube rupture (Song et al., 2014). The synergid cells have two different major roles in fertilization, 1) they secrete attractive proteins involved in pollen tube guidance and 2) they induce pollen tube discharge (Leydon et al., 2015).

During the early stages when the pollen tube is entering the micropyle, the synergid cells are important for pollen tube attraction and at least one viable synergid cell is necessary for successful pollen tube attraction (Ferluga et al., 1971). At the micropylar region of these cells there is a specialized structure called the filiform apparatus which contains specialized secretory regions that release small peptides that are involved in pollen tube attraction (Kessler and Grossniklaus, 2011). This structure has many folds which increase the surface area at the point where the pollen tube contacts the synergid cell (Leydon et al., 2015). Leshem et al. (2013) proposes that there may be two sets of attractive signals associated with the synergid cells. The chemical signals secreted at the micropylar end where the filiform apparatus is located could prime the pollen tube for gamete release through the RAC/ROP signaling pathway involving FERONIA (FER), LORELEI (LRE), and most likely NORTIA (NTA), because they

all have similar pollen tube reception defects. Before pollen tube reception NTA is localized to the synergid cytoplasm and then relocates to the filiform apparatus region after pollen tube reception(Kessler and Grossniklaus, 2011). NTA is known to have a calmodulin binding domain and its localization from the cytoplasm to the synergid cells dependent on FER but not LRE (Kessler and Grossniklaus, 2011), thus it is down stream of FER and could be involved in the calcium regulation. If the entry site of the pollen tube is not the filiform apparatus, which was previously suspected, but an alternative site, there may be a second set of chemoattractants for the pollen tube. Although it was difficult to observe under epifluorescence microscopy due to background noise, Leshem et al. (2013) noted that most of the pollen tubes extended along the side of the synergid cells to areas referred to as 'synergid hooks' pockets, which are a narrowing of the synergid cells in the region that is engulfed by cytoplasmic protrusions of the central cell.

The synergid cells are not only important for pollen tube attraction, they also interact with the pollen tube (Higashiyama, 2002; Kumar and Wagner, 2018). After the pollen tube has entered the micropyle, the pollen tube growth must be arrested, and the pollen tube must then burst, releasing the two sperm cells. Synergid cell degeneration may play a key role in both of these events. During normal fertilization events one of the synergid cells, called the 'receptive' synergid cell, will degenerate (Leydon et al., 2015). This synergid can undergo degeneration via two different pathways. It is thought that pollen tube-synergid contact or signaling via secreted molecules initiates synergid degeneration (Leydon et al., 2015). They also found that when the pollen tube bursts, it always does so in a degenerated synergid (Leydon et al., 2015). The persistent synergid will later degenerate after the central cell has been fertilized (Leydon et al.,

2015). Degeneration via the other pathway is initiated after the egg cell and the central cell are fertilized. This activates an ethylene response pathway, which leads to nuclear disorganization and the degeneration of the synergid cell (Volz et al., 2013). The importance of synergid degeneration during fertilization events has also been confirmed in *gfa2* mutants, which have defective synergid cell death and ovules that remain unfertilized (Christensen et al., 2002).

Programmed cell death is not only important in the synergid cells, it is also important for pollen tube rupture that releases the sperm cells. Both reactive oxygen species (ROS) generation and calcium influx seem to be important for pollen tube burst (Kessler and Grossniklaus, 2011). Although treatment with ROS is enough to trigger pollen tube rupture on its own *in vitro*, ROS generation most likely acts along with calcium signaling to bring about pollen tube rupture *in vivo.* ROS production may act to weaken the cell wall of the pollen tube similar to the way it weakens the cell wall to allow for root growth (Duan et al., 2014).

Calcium influx is important during pollen tube reception and also during pollen tube burst. During Phase I, the pollen tube enters the micropyle. This phase is fairly prolonged lasting 40 $\pm$ 15 min in *Arabidopsis*, during which the pollen tube extends and there is an increase in calcium in both the pollen tube and the synergid cells (Leydon et al., 2015). In Phase II, the pollen tube rapid growth phase, the pollen tube burst most likely occurs during a final spike in calcium in the pollen tube which is accompanied by a decrease in the calcium in the receptive synergid cell (Leydon et al., 2015). During the final stage there is another calcium spike in the pollen tube around the time of pollen tube discharge, which will release the two sperm cells. Mutants for the calcium pump ACA9 are able to attract the pollen tube but they fail to burst inside the synergid cells (Schiott et al., 2004). Although $Ca^{2+}$ ion concentration seems to be important in

both the synergid cell and the pollen tube there are a number of other ion channels on the pollen tube that are involved in pollen tube rupture.

The influx of other ions via channels on the pollen tube may also play a role in pollen tube burst, and changes in potassium influx may be important. In *Maize*, ZmES4 is released from the secretory system of the synergid cell and then it binds to KZM1 on the pollen tube, which results in a potassium ion influx and the burst of the pollen tube (Amien et al., 2010). There are also receptors on the pollen tube that could be important for maintaining the integrity of the pollen tube until it has made contact with the synergid cells. ANXUR1 (ANX1) and ANXUR2 (ANX2) are the pollen expressed FER-like receptor-like kinases that have mutants that display premature pollen tube rupture (Boisson-Dernier et al., 2009; Miyazaki et al., 2009). These proteins may receive signals from the synergid cell that initiates pollen tube rupture, and thus there are multiple signaling events between the synergid cell and pollen tube that are important for the successful attraction, growth arrest, and pollen tube rupture needed for fertilization to occur.

## FERTILITY DEFECTS

There are a number of mutants that have fertility defects in the female gametophyte. A few examples of these mutants are *scylla* (*syl*), *lorelei* (*lre*), *feronia* (*fer*)*/sirene* (*ser*)*, nortia* (*nta*), *evan,* and *turan* (Rotman et al., 2008; Tsukamoto et al., 2010; Kessler and Grossniklaus, 2011; Lindner et al., 2015). There can also be male defects that can disrupt pollen tube attraction and fertilization, such as *myb98* (Leydon et al., 2015). In some cases, a mutant genotype must be present on both the male and the female gametophyte in order for fertility defects to occur,

such as in the *abstinence by mutual consent* (*amc*) mutant (Tsukamoto et al., 2010). The *AMC* gene is a peroxin gene that could be important in cell death, and mutants display pollen tube reception defects and defects in synergid cell death when both the male and female gametophytes are positive for the mutant allele (Kessler and Grossniklaus, 2011). This may indicate that peroxin is important for cell death in both the pollen tube and the synergid cells.

Of these mutants there are three, *lre, fer,* and *nta,* that are present in the same RAC/ROP signaling pathway and have been studied in detail in the context of fertility defects. All three of these genes have very similar fertility defects when mutant alleles are present and exhibit defects in pollen tube rupture, the over growth of pollen tubes, and defects in synergid cell death (Kessler et al., 2010; Tsukamoto et al., 2010; Ngo et al., 2014; Li et al., 2015). There are a number of studies that have used these mutant lines as well as complemented lines to begin to understand the function of these proteins and their role in *Arabidopsis* fertility.

## LORELEI FERTILITY DEFECTS

LORELEI (LRE) was first identified due to its fertility defects in mutant lines (Tsukamoto et al., 2010). There are a number of different *lre* alleles that have been identified that are the result of random T-DNA insertions. When the WT version, LRE/LRE, female is pollinated with pollen from the LRE/LRE male 95-98% of the seeds are normal, whereas in the null mutant lines *lre-4, lre-5, lre-6,* and *lre-7,* females that are self-pollinated produce a reduced proportion of normal seeds (22-28%), with an increase in the proportion of aborted seeds (27-43%), and undeveloped ovules (40-75%) (Tsukamoto et al., 2010). These reported defects in seed development could be the result of multiple defects in fertilization.

When examined in more detail, it was found that the *lre/lre* lines had a number of fertilization defects, a number of which involved pollen tube reception. One example of these defects was the presence of supernumerary pollen tubes after fertilization events, which could be the result of either a lack of short-range repulsive cues or the continued presence of attractive cues (Tsukamoto et al., 2010). In female gametophytes in all null mutant lines (*lre4, lre5, lre6,* and *lre7)* 15-20% of the ovules had entry by multiple pollen tubes, and in female gametophytes from heterozygous plants from each line, 7-15% of ovules still had entry by multiple pollen tubes (Tsukamoto et al., 2010). Another one of the pollen tube defects that was reported was the failure of the pollen tube to arrest its growth, resulting in pollen tubes that extended past the synergid cells (Tsukamoto et al., 2010). The pollen tubes that extended beyond the synergid cells also fail to burst, thus sperm cells were not released.

Not only were there defects in pollen tube reception, but there were also defects in the female gametophyte, specifically in the synergid cells. Although a majority of the ovules examined had one synergid cell that was degenerated after pollen tube reception, there were a number of ovules that contained two intact synergid cells with pollen tubes visible (Tsukamoto et al., 2010). There have also been defects in development that occur even after successful fertilization is observed. Some of the aborted seeds (~10%) lacked an embryo but still had proliferating endosperm (Tsukamoto et al., 2010). There are numerous phenotypes associated with *lre* including defects in pollen tube reception, a failure to induce synergid degeneration, a delay in seed development, and aborted seed with endosperm development, thus LRE seems to be important in many aspects of the events leading up to and following fertilization (Tsukamoto et al., 2010).

Some preliminary localization information on LRE was gathered with fluorescent imaging techniques. Complementation studies with a LRE-YFP fusion protein in the null *lre-7* background showed that LRE localizes to the plasma membrane in the filiform apparatus as well as being located intracellularly as puncta in the cytoplasm (Liu et al., 2016). Given this localization pattern and the large range of defects present in the *lre* null mutants, LRE may be involved in several processes during pollen tube reception ranging from pollen tube attraction to proper programmed cell death. Although the LRE that is membrane bound is likely to be acting in the RAC/ROP signaling pathway along with FER, there are many questions remaining as to exactly where the puncta in the cytoplasm are actually localizing at the ultrastructural level and how they may be functioning in pollen tube reception. We know that the truncated version of *lre* that has a deleted transmembrane domain and localized intracellularly is still able to complement the fertility defects (Liu et al., 2016). We also know that both soluble and membrane bound versions of other GPI anchored proteins can function in signaling pathways (Worley et al., 2000). At this point it is still unknown what is the native function of the intracellular LRE proteins.

## MEMBRANE ASSOCIATED LRE

The membrane bound LRE most likely acts in concert with other proteins such as FER and NTA in the RAC/ROP signaling pathway as a GPI-anchored protein (Figure 1.2). It is not surprising then that LRE null mutants have some of the same pollen tube defects as observed in FERONIA (FER) null mutants (Li et al., 2015). Fluorescent imaging has shown that LRE is associated with FER and localizes to the synergid filiform apparatus (Liu et al., 2016). It is known from yeast pull-down studies that LRE interacts with the extracellular domain of FER and that

FER localization is altered in LRE mutants. Although LRE is localized to the female gametophyte, seedlings have a different isoform called LRE-like GPI-AP1 (LL1), which is a paralog of LRE that is present in vegetative tissues. LRE and LLG1 bind to the extracellular juxtamembrane region of FER (Li et al., 2015). It is possible that these different isoforms of the LRE protein may result in different functions of the LRE/FER signaling pathway (Tsukamoto et al., 2010).

LRE and other related LORELEI-like-GPI-anchor proteins (LLG), are thought to be co-receptors with FER for plant hormones and are a necessary extramembrane component for the Rho signaling pathway needed for the polarization of cells (Li et al., 2015). Although this same pathway is present in the female gametophyte, it has been studied the most in the context of cell polarization in roots/leaves and in plant immunity (Duan et al., 2010; Kessler et al., 2010; Li et al., 2015). For the former function, the RAC/ROP signaling pathway (Fig 1.1) is used to modulate calcium levels which will alter the formation of actin filaments and microtubules (Uhrig and Hülskamp, 2001). In the latter function, the ROC/ROP pathway induces NADPH production of reactive oxygen species (ROS) needed for plants to defend themselves against foreign invaders. Both ROS production and regulation of calcium influx are important for pollen tube rupture (Duan et al., 2014) and synergid cell degeneration (Ngo et al., 2014).

FER interacts with guanine nucleotide exchange factors (ROPGEFs) to activate the RAC/ROP GTPase (Duan et al., 2014). This activation can cause nicotinamide adenine dinucleotide phosphate (NADPH) to release ROS, which affects polarization in root hair growth (Duan et al., 2010; Duan et al., 2014). The presence of different GPI co-receptors in this pathway may be important for receptor binding to a diverse array of ligands, and may confer some degree of temporal and spatial specificity to the activation of this pathway in different

contexts. In addition to LRE, which is only expressed in the female gametophyte during very specific stages of ovule development, there are several different LORELEI-like-GPI-anchor proteins GPI-APS 1,2,3 (LLG1,2,3). LRE expression was reported at floral stages 12c and 14 in unfertilized ovules, while LLG proteins are expressed in a broad range of tissues such as pollen, pollen tubes, sporophytic pistil tissues, and in the early stages of the development of the female gametophyte (Tsukamoto et al., 2010). LRE and the LLG proteins have GPI anchor domains and are thought to act as co-receptors with FER in the RAC/ROP pathway (Li et al., 2015).

In other systems the upstream ligand regulators and downstream effectors of signaling pathways can be altered simply by changing the GPI protein which functions as the co-receptor with the primary receptor in the pathway. A classic example of this is in the enteric nervous system (Worley et al., 2000) in which ligands in the glial cell line-derived neurotrophic factor (GDNF) family preferentially bind to receptor tyrosine kinase (RET) receptors that have different GFRα co-receptors (which are GPI anchored proteins). This determines which GDNF ligands will have the highest affinity for binding to the receptors and thus alters the downstream targets of the signaling pathway based on which ligand is bound to the receptor. For example, GFRα-1 preferentially binds to GDNF, while GFRα-2 preferentially binds to neurturin (Worley et al., 2000). In plants, FER can also interact with a number of different ligands. In root and leaf development FER functions in several plant hormone signaling pathways including auxin, abscisic acid (aba), brassinosteroid, and ethylene (Li et al., 2015). In addition to these hormone pathways, FER can also interact with a peptide called rapid alkalinization factor 1 (RALF1) (Li et al., 2015). Although a specific ligand for LRE/FER in the female gametophyte has yet to be

identified (Kessler and Grossniklaus, 2011), the downstream effectors of this pathway seem to be ROS generation and $Ca^{2+}$ regulation needed for the final stages of pollen tube reception and the events leading up to fertilization.

ROS signaling and FER are also needed for regulating calcium levels and for programmed cell death of both the pollen tube and the synergid cells (Ngo et al., 2014). In the female gametophyte there is a high ROS concentration at the entrance to the micropyle (Duan et al., 2014). The *fer-4* mutants not only have reduced ROS production, 80% of the time the pollen tubes failed to rupture (Duan et al., 2014). Although both pollen tube rupture defects and multiple pollen tubes have been observed in *fer-4,* only the pollen tube rupture seems to be affected by ROS (Duan et al., 2014). Inhibiting ROS production leads to pollen tube overgrowth similar to what is seen in *fer,* however it did not affect pollen tube repulsion (Duan et al., 2014). Interestingly, ROS production is not the whole story in pollen tube rupture.

ROS production in pollen tube rupture is calcium dependent. Decreasing the $Ca^{2+}$ concentration in the medium or blocking calcium channels decreased ROS-dependent pollen tube rupture (Duan et al., 2014). ROS signaling is needed for polarized growth in pollen tubes because there is a balance between cell wall rigidity and flexibility to allow for growth, and still provide structure (Duan et al., 2014). The ROS accumulation at the entrance to the micropyle could weaken the cell wall of the pollen tube before it enters the synergid cells (Duan et al., 2014). Then, once the pollen tube enters the synergid cell, ROS-dependent calcium channels are opened and the pollen tube ruptures due to changes in turgor pressure (Duan et al., 2014). LRE is not only important for generating ROS, it also indirectly affects the calcium oscillations in the plasma membrane of the synergid cells (Ngo et al., 2014).

Another protein that is in this same signaling pathway is NTA (Li et al., 2015). *Nta* is a member of the mildew resistance locus family of proteins that is involved not only in pollen tube reception, but also in the invasion of powdery mildew into plant tissues (Kessler et al., 2010). In *nta,* a female gametophyte mutant, there is reduced fertility and pollen tube over growth in the synergid cells, and pollen tubes fail to burst similar to what is observed in *fer* (Kessler and Grossniklaus, 2011). Although NTA has no effect on FER localization, FER is necessary for the relocalization of NTA (Kessler et al., 2010). NTA is first localized to puncta in the cytoplasm, then relocates to the basal portion of the synergid cytoplasm upon pollen tube reception (Kessler et al., 2010)(Figure 1.3). NTA functions to modulate the calcium levels within the synergid cells, and it has a calmodulin-binding domain (Kessler et al., 2010).

## INTRACELLULAR LRE

Although the mature versions of LRE and FER are localized to the plasma membrane, they were originally translated and processed within the cytoplasm of the cell before they are packaged and transported to the plasma membrane. Thus, any upstream events that affect the localization of these two proteins could potentially alter the functioning of this pathway. LRE can also function as an intracellular chaperone of FER to aid in transporting FER from the ER to the filiform apparatus (Liu et al., 2016).

The basic structure of LRE is known. In the unprocessed protein a signal peptide (SP) is located on the N-terminal end of unprocessed pre-pro-protein that is needed for translocation in the endoplasmic reticulum (Liu et al., 2016). Once the SP region has been removed it is now the pro-protein form that is subsequently cleaved by a transamidase to remove the

hydrophobic tail and the GPI anchor (which is made in the endoplasmic reticulum) is added. After the GPI anchor has been added the mature protein travels through the endomembrane system to the cell surface.

The proteins in this signaling pathway not only interact during signal transduction events, they also interact intracellularly and can affect the localization of other proteins in this pathway. One possible function of the intracellular LRE/LLG1 (LLG1) is that it interacts with FER in the endoplasmic reticulum lumen and acts as a chaperone to bring FER to the filiform apparatus (Li et al., 2015). Not only do FER and LRE interact intracellularly, NTA localization is affected by FER. During pollen tube reception, FER is important for the relocalization of NTA from points within the synergid cells to the filiform apparatus when the pollen tube arrives (Kessler et al., 2010).

## FUNCTION OF LORELEI PROTEIN:

The exact role and functions of LRE in arresting pollen tube growth, pollen tube rupture, and synergid cell death is still not completely understood. LRE may have different functions, both as a co-receptor with FER in the ROS/ROP signaling pathway on the surface of the cell membrane and as a chaperone for FER from the endoplasmic reticulum to the plasma membrane. Thus, understanding exactly where LRE localizes is the first step in understanding how it functions during the final stages of pollen tube reception.

One of the most likely roles for LRE is that it is acting as a co-receptor in the RAC/ROP signaling pathway. As was mentioned earlier, previous studies have shown both ROS generation and $Ca^{2+}$ regulation. Both of these are downstream targets of this signaling pathway and are

important for pollen tube growth arrest, pollen tube burst, and programmed synergid cell death, which is consistent with the phenotypes that have been reported in null mutants for different *lre* alleles (Tsukamoto et al., 2010). If this is the primary role for LRE during the final stages of pollen tube reception it would seem likely that LRE attachment to the cell membrane at the filiform apparatus would be necessary.

Preliminary results with confocal imaging have revealed that LRE localizes to both the plasma membrane and in the cytoplasm (Liu et al., 2016). Production of fully functional LRE-YFP fusion proteins in a *lre-7* null mutant background showed that 56% of the YFP signal is localized to the filiform apparatus in the synergid plasma membrane, but there were also puncta of LRE-YPF in the cytoplasm. To further understand how LRE functions, several truncated versions of YFP-tagged LRE protein that have deletions of different protein domains have been used to complement *lre-7* null mutants.

Liu et al. (2016) used one of these truncated YFP-LRE fusion proteins to determine if the GPI anchor domain was important for pollen tube reception. Since the GPI anchor domain is important for LRE to attach to the plasma membrane, removal of this domain should affect its ability to localize to the plasma membrane, which may disrupt its function as a co-receptor in the RAC/ROP signaling pathway. This GPI anchor is also needed for transportation of LRE from the endoplasmic reticulum to the plasma membrane. Although disrupting the GPI anchor altered the localization of LRE it did not alter its function. In all three of the *lre* lines that had truncated proteins, either missing portions needed for the attachment of the GPI anchor or in the LRE-cYFP-TM line, a transmembrane domain replaced the GPI anchor, the LRE protein was still functional and still fully complemented LRE in the *lre-7* null mutant background. It was also

found that LRE-cYFP and LRE-cYFP-TM from the pollen tube could fully restore the *lre* defects in the female gametophyte. This means that external LRE expressed in other cells can potentially complement the non-functioning LRE in the synergid cells.

The function of LRE does not seem to be dependent on localization, but rather the M8CM domain is the most important for LRE function. The *lre-7/lre-7* lines can be complemented with a truncated LRE without the GPI anchor domain and still restore the fertility defects even though the localization of LRE is altered without the GPI domain. Thus, localization does not seem to be important for LRE function during development. LRE function during fertilization is only impaired when the eight-cysteine motif (M8CM) is missing. Liu et al. (2016) showed this experimentally when a *lre-7/lre-7* null mutant was complemented with a truncated LRE protein with a missing eight-cysteine motif (M8CM) that was not able to restore the fertility defects. Perhaps the reason for the importance of the M8CM is because this motif is important for maintaining the proper folding structure of the protein. The M8CM region forms disulfide bridges that maintain the tertiary structure of the scaffold, which is important for the functioning of the protein (Liu et al. 2016).

Additional confocal work was done to see if there was co-localization with organelle markers for Golgi, ER, and peroxisomes, however, there was no indication that LRE localized to any of these organelles. Thus, the purpose of this study was to 1) characterize the ultrastructure of the wild type background for the *lre-7/lre-7* null mutant and compare that with other wild type accessions, 2) compare and contrast the *lre-7/lre-7* null mutant with wild type ultrastructure, 3) used immunogold localization techniques to get a higher resolution of

LRE localization at the ultrastructural level. It is also unknown if the absence of LRE affects the ultrastructure of the ovule, so we also wanted to examine the ultrastructure in more detail.

# CHAPTER 1 TABLE

Table 1. 1 Pollen tube growth and the signaling that occurs during different phases of pollen tube reception. Modified from Dresselhaus and Franklin-Tong (2013).

| Pollen tube growth | Structure | Signaling molecules |
|---|---|---|
| Phase I | Pollen coat components | CRPs: PCPs, SCR/SP11; lipids) |
| | Pollen components | PrpS, $Ca^2$+ |
| | Stigma components | SRK;MLPK;PrsS; ARC1;Exo 70A1; S-azadecalins;Ca2+ |
| Phase II | Stigma components | Exo70A1; $Ca^2$+ |
| Phase III | Pollen tube components | LePRK1&2; POP2;ROS;$Ca^2$+;PI4P;*F-box protein;* SLF,SFB;HT-B |
| | Transmitting tract components | AGPs: TTS;*CRPs:*SCA, LTPs;chemocyanin, plantacyanin; GABA; STIL; RHD4-1;PI4-k β1/β2;S-Rnases |
| Phase IV | Pollen tube components | CNGC18;CHX23 |
| | vule/micropyle ɔmponents | GABA; D-serine;SR1;NO;PDIL2-1;POD1;MAA3;CCG;MYB98 |
| Phase V | Pollen tube components | *CrLK1Ls;* ANX1&2;KZM1;ACA;Ca2+ |
| | Synergid components | *CRP; LUREs, ES1-4*; EA1;CrRLK1L:FER;NTA;*GAPs:*LRE;AMC;VDD;NO, ROS;$Ca^2$+ |

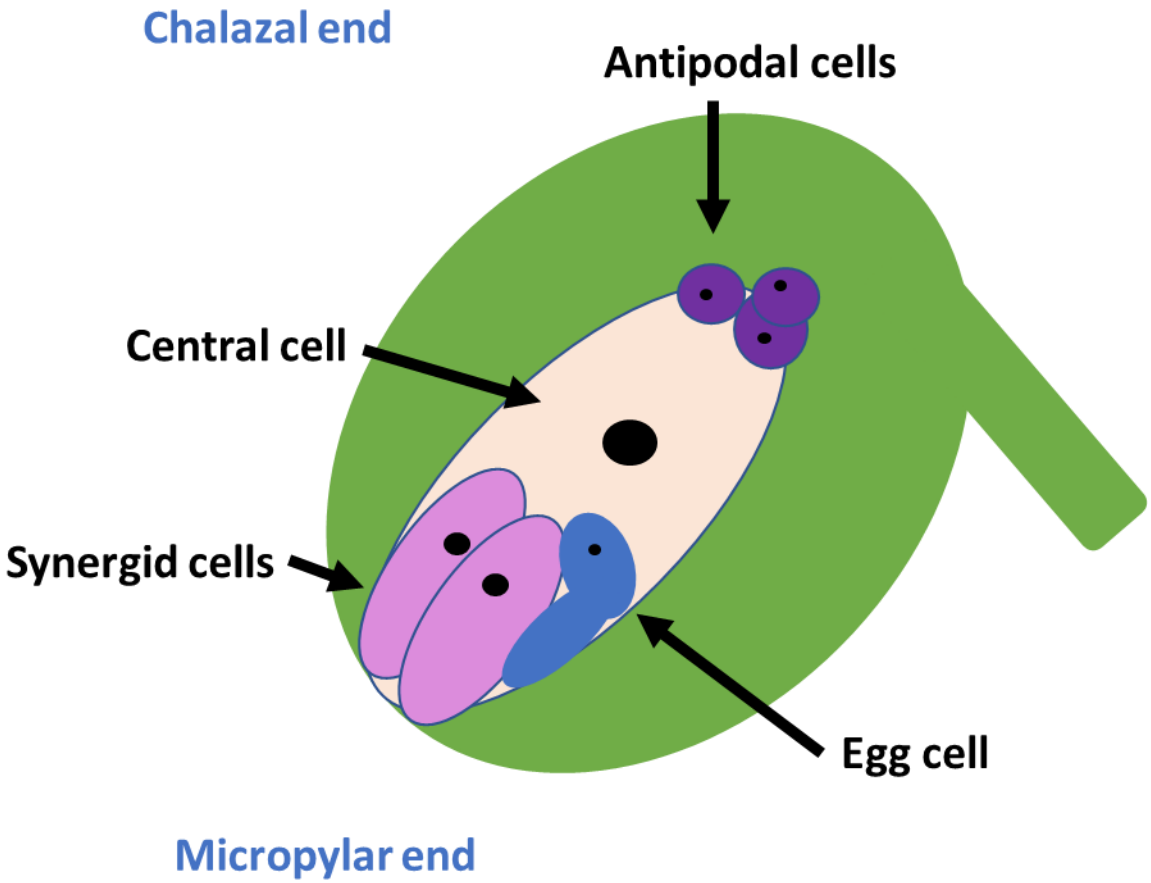


Figure 1. 1 Diagram of the *Arabidopsis* ovule showing the five major cell types within the embryo sac, the synergid cells, egg cell, central cell, and the three antipodal cells. The synergid cells (pink) are located at the entrance to the micropyle. The central cell (light orange) is in the middle. There are three antipodal cells at the chalazal end of the embryo sac. During double fertilization both the central cell and the egg cell will be fertilized. Synergid cells (pink), Egg cell (blue), maternal tissue (green), central cell (light orange), antipodal cells (purple).

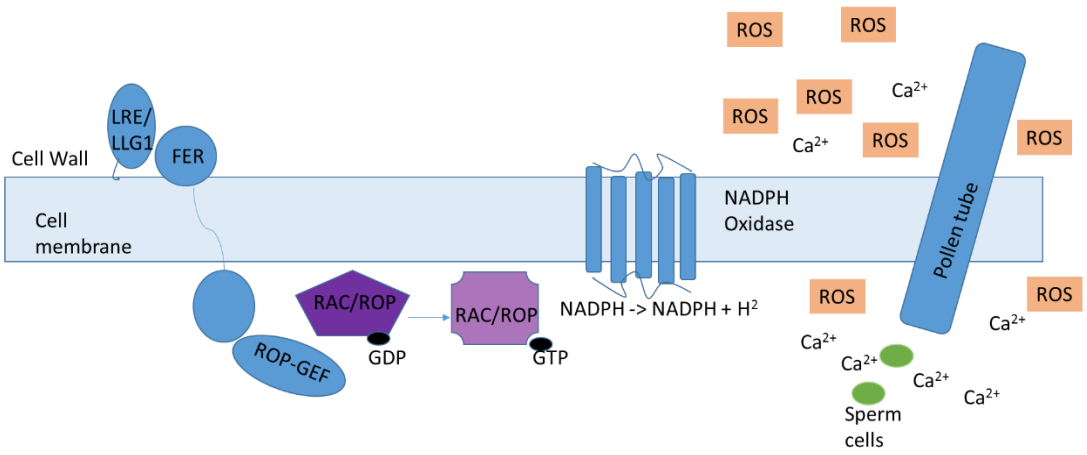


Figure 1. 2 Diagram of FER mediated activation of ROS generation and Ca2+ in the pollen tube prior to pollen tube rupture. FER can form a co-receptor with either the LRE in the embryo sac or the LORELEI-like-GPI-anchored proteins (LLG) in other tissues such as the roots and leaves (modified from Duan et al. (2014). NTA is downstream of the FER, however its exact function in the FER pathway is unknown so it is not included in this diagram. It does have a calmodulin binding domain, thus it could be important for calcium regulation.

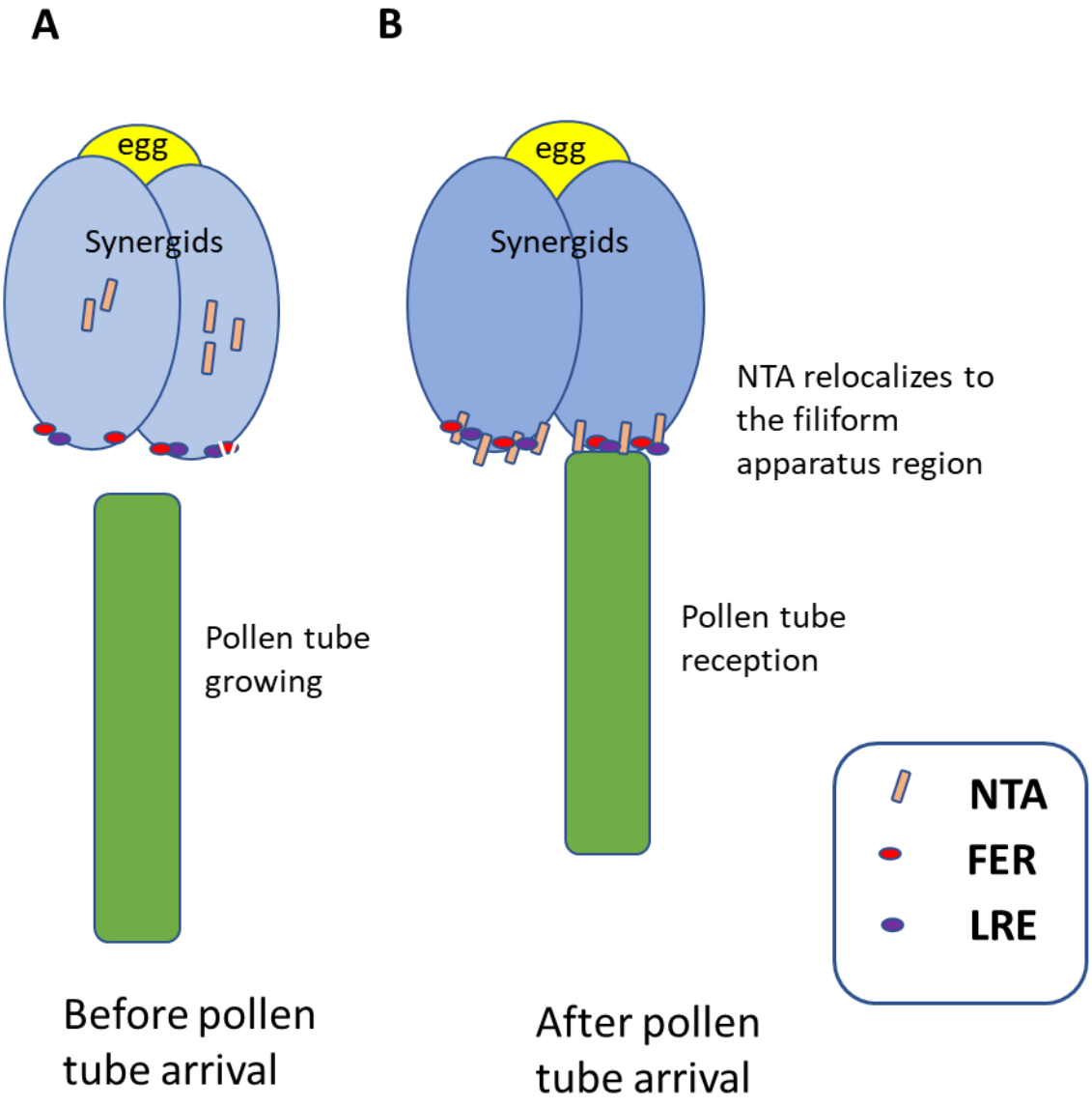


Figure 1. 3 Diagram of the signaling involved in pollen tube reception. A) Signaling before pollen tube arrival showing two intact synergid cells that have FER and LRE localized to the filiform apparatus and NTA and ZmES4 located intracellularly. The male signaling components are ANX1/ANX2 receptors and KSM1 and ACA9, which are ion channels. B) Signaling events after pollen tube arrival in which one of the synergid cells is degenerating. NTA and ZmES4 have now localized to the filiform apparatus in the ion channels in the pollen tube are not open. Taken from Kessler and Grossniklaus (2011).

# Chapter 2: Wild type ovule ultrastructure


## ABSTRACT

This study found that the descriptions of wild type accessions of the mature ultrastructure were similar to the ultrastructural descriptions of the published literature on the Landsberg erecta. While antipodal cell degeneration is common in other species, this study confirmed that antipodal cells are present in the mature embryo sac. This study also noted that while polar nuclei are not fused during the early stages of embryo sac development, they are fused in the mature embryo sac. In addition to the mature ultrastructure, this study also includes descriptions of the ultrastructure during early development and degeneration. The ultrastructure during degeneration was broken up into three different stages: early, mid, and advanced stage degeneration.


## INTRODUCTION

*Arabidopsis thaliana* is the model organism of the plant world for a number of reasons. It grows well in the lab and it has a small genome, 2.5 MB, which has been completely sequenced making it relatively easy to use for molecular biology studies (Bevan, 2011). Arabidopsis from many different regions have similar variations, which is to be expected from a plant that has spread rapidly (Bevan, 2011). The most frequent types of variations are SNPs, copy number variants (changes in the duplication of some regions), and changes in the methylation of cytosines (Bevan, 2011). Many genes can also possess premature stop codons

(Bevan, 2011). Most of the variation was found in genes associated with defense and environmental responses (Bevan, 2011).

In addition to being a general model for genetic studies, it has also been used as a model for reproductive studies. It has been used to identify genes involved in cell to cell communication between the male and female gametophyte. A few examples of these female gametophyte mutants are *scylla* (*syl*), *lorelei* (*lre*), *feronia* (*fer*)/*sirene* (*ser*), *nortia* (*nta*), *evan*, and *turan* (Rotman et al., 2008; Tsukamoto et al., 2010; Kessler and Grossniklaus, 2011; Lindner et al., 2015). There can also be male defects that can disrupt pollen tube attraction and fertilization, such as myb98 (Leydon et al., 2015). In some cases, a mutant genotype must be present on both the male and the female gametophyte in order for fertility defects to occur, such as in the abstinence by mutual consent (amc) mutant (Tsukamoto et al., 2010). The AMC gene is a peroxin gene that could be important in cell death, and mutants display pollen tube reception defects and defects in synergid cell death when both the male and female gametophytes are positive for the mutant allele (Kessler and Grossniklaus, 2011). This may indicate that peroxin is important in cell death of both the pollen tube and the synergid cells.

In order to better understand and use *Arabidopsis* as a model for plant reproduction, we have done and ultrastructural comparison on three different *Arabidopsis* wild type accessions. Currently in the literature the only Arabidopsis line that has been characterized in detail is the Landsberg erecta. It is unknown how similar these lines are and no one has ever characterized any of the developmental differences that occur as the embryo sac matures.

Since *Arabidopsis* is an important model organism and EM studies take a considerable amount of resources such as time, money, and labor, it is important to understand the amount

of variability that exists not only between different *Arabidopsis* WT accessions, but also within a single accession at different stages as the embryo sac develops. For this reason, we determined the ultrastructure of two different *Arabidopsis* accessions, Colombia WT (Col WT) and WT that is likely Wassilewskija WT (WS WT: Fig. 2.1). Then we compared them to what has been reported in the literature for WT Landsberg erecta (Ler). We were also able to document the immature embryo sac ultrastructure as well as the ultrastructure of degenerating WT embryo sacs.

# METHODS

Plant care: Wild-type (Columbia and WS accessions) *Arabidopsis* were sown either directly on soil (Sun Gro Metro-Mix 360) or on agar plates (MS salts 4.3g/L, Su1crose 20g/L, MES. 0.5g/L, pH 5.7, Agar 9g/L). In some cases, the seeds were stratified for 2 days at 4˚C to synchronize their germination, before being transferred to the growth chamber. These plants were germinated and grown in an environmental chamber that was maintained in a 16:8 light:dark cycle at 20˚C with PAR light levels that are 100-125 µmol/$m^2$/s. Seedlings geminated on agar were transplanted to soil. The identity of both WT lines were checked with PCR using the NGA 76 marker from TAIR (https://www.arabidopsis.org/; Figure 2.1).

TEM sample preparation: Fixation of plant tissue for transmission electron microscopy was modified from Holdorf et al. (2012). Flowers were emasculated at the floral stage 12 before the anthers contain mature pollen grains. Unpollinated ovules were removed from the carpels with a fine needle, 12-20 hours after emasculation. For the fixation, washes, and post-fixation steps the ovules were placed in cell strainer baskets (Falcon 352350) with the tabs cut off to fit inside six-well plates (Falcon 353046). Ovules were immersed in fixative (2.5% EM grade glutaraldehyde v/v, 0.02% Triton X-100 v/v, 0.1 M HEPES, pH7.2) overnight at room temperature. The ovules were washed several times (3-5 times for 15 min each) in 0.1M HEPES buffer, pH 7.2, before they were placed into 1% $OsO_4$ w/v in distilled water overnight at room temperature. They were then rinsed five times with distilled water for 15 min each before being placed into 1% uranyl acetate w/v in distilled water for three days. Samples were then washed several times with distilled water.

To embed the ovules in agar, the ovules were arranged on a pad of solidified 4% agar, encased with a top layer of molten 4% agar, and allowed to cool to room temperature. Cubes of agar containing an individual ovule were cut out of the agar. Samples embedded in agar cubes were moved through an acetone dehydration series (10%, 20%, 30%, 40%, 50%, 60%, 70%, 80%, 90%, 100%, 100%, 100%). The ovules were allowed to equilibrate for at least 1 hour at each step in the series, with the exception of the 100% acetone. At this point three changes of 100% acetone were done over a two-hour interval. Infiltration and embedding were done with Modified Spurr's resin (Electron Microscopy Supplies, Hatfield, PA), according to Holdorf, et al. (2012). The samples were infiltrated with increasing concentrations of Modified Spurr's resin in acetone (20%, 40%, 60%, 80%, 100%). Samples were allowed to remain at each step for a minimum of 3 hours, and samples were left in 100% resin for at least two days for complete infiltration. Ovules were oriented in flat embedding molds so that longitudinal sections through ovules could be obtained and polymerized at 60˚C for 48 hours.

Semi-thin sections (0.5 microns thick) were cut and stained with Azure B, and examined by light microscopy to determine where the embryo sac began. Ultrathin sections (60-90 nm thick) were then placed on Pelco 200 mesh or Hex Cu TEM grids that were coated for adhesion using a Coat-Quick "G" grid coating pen (Ted Pella 1556). Sections were stained with 1% uranyl acetate followed by Reynold's lead citrate before they were imaged with a Hitachi H-600 transmission electron microscope (TEM) operating at 75kV. Micrographs were captured on Kodak 4489 film and, following development, digital images were acquired from the negatives using an Epson Perfection V750 Pro scanner. Plates were assembled in Photoshop (version 5.5).

Image analysis was carried out in ImageJ and statistical analyses were done in either JMP 14 or R statistical software.

## RESULTS

Our initial findings on WT ovules suggests that mature Col and WS WT embryo sac ultrastructure is similar to that of Landsberg erecta (LER) WT described in Mansfield et al. (1991). We also documented some developmental changes, such as the immature embryo sac and also the degenerating embryos sac. These descriptions should be used to compile a reference library for female gametophyte ultrastructure.

### Mature Embryo Sac is Similar to LER

The *Arabidopsis* ovule contains two different types of tissue, the 2N maternal tissue and the 1N embryo sac, which is the female gametophyte. There are two distinct poles, a chalazal end, where the ovule attaches to the transmitting tract via the funiculus, and the micropyle end, which is the small opening in the integuments through which the pollen tube enters. The maternal tissue that surrounds the embryo sac includes the layers of the inner and outer integuments which surround the embryo sac and the nucellus, which is present at the chalazal end above the embryo sac (Figure 2.2). The *Arabidopsis* embryo sac contains seven different cell types; three antipodal cells, the central cell, the egg cell, and two synergid cells (Figure 2.2). The two synergid cells, which receive the pollen tube, are positioned at the opening to the micropyle. Located closer to the chalazal end above the synergid cells is the egg cell, which when fertilized will form the zygote that develops into the embryo. The elongated cell in the middle of the embryo sac is the central cell, which after it is fertilized will become the nutritive

tissue known as the endosperm. Next to the central cell and closest to the chalazal end of the embryo sac are the antipodal cells.

The embryo sac is surrounded by an electron dense cuticle-like wall that separates the embryo sac from the inner integument (Figure 2.2). There are typically two layers of outer integument cells and two layers of inner integument cells. When the embryo sac was mature, the cells of the outer integument are characterized by the presence of a large vacuole that took up the majority of the cell. The inner integuments may also have a large vacuole, but there is more cytoplasm visible in them. There are no plasmodesmatal connections between the cells of the inner integument and the embryo sac. There are plasmodesmatal connections between the inner integument cells, and between the outer integument cells, but there are no plasmodesmatal connections between the two integuments. The cuticle that surrounds the embryo sac extends up into the chalazal region before it terminates (Figure 2.2). Therefore, it is possible to distinguish between the nucellus cells and the integument cells well into the chalazal region. Near the antipodal cells and down the sides of the central cell there may be cells undergoing cell death (Figure 2.2). It is presumed that these are nucellus cells that are degenerating.

In general, nucellar cells are irregular near the antipodal cells and more regular in shape closer to the chalazal end. Some of the nucellus cells adjacent to the antipodal cells may have a dark cytoplasm similar in appearance to the antipodal cells. Thus, it can be hard to distinguish some of the nucellus cells from the antipodal cells in some sections, so several sections need to be examined. The cytoplasm of the nucellus cells is dense and contains many mitochondria. Other features of the nucellar cytoplasm are that there are very few vacuoles and plastids and a

high ribosome density. This can be very different than some of the other cells in the embryo sac.

*Antipodal cells are present at the chalazal end of the embryo sac*

The antipodal cells are located closest to the chalazal end of the embryo sac. They are situated between the central cell and the nucellus (Figure 2.3). They are easily identifiable by their dark (electron dense) cytoplasm, and their shape, which ranges from triangular to cuboidal. There is a thick cell wall that surrounds them, and it is easy to distinguish plasmodesmatal connections between both other antipodal cells and the central cell.

There were antipodal cells present in all the ovules examined, with no visible signs of degeneration, which can occur in antipodal cells in other species. In some of the sections it appears that there may be more than the three antipodal cells (Figure 2.3). The literature has always reported them as three, so this is most likely an artifact due to sectioning resulting in two-dimensional views, perhaps one cell has been sectioned through more than once due to its three-dimensional orientation. It is also possible that some of these cells are electron-dense nucellus cells, since nucellus cells can have a wide variety of morphologies. In the future serial sections with a three-dimensional reconstruction need to be done to determine if this is in fact correct since developmentally there should only be three antipodal cells, and we have seen no evidence of the antipodal cells dividing.

The cytoplasm of the antipodal cells appears to be very electron dense, perhaps due to the extremely high density of ribosomes in the cytoplasm. Mansfield et al. (1991) reported that there were no vacuoles or dictyosomes in the antipodal cell cytoplasm of Landsberg erecta (LER) accession, however there appears to be at least one Golgi body present in the antipodal

cell (Figure 2.3). There are numerous mitochondria present, however there are no large vacuoles that are typical of plant cells. In sections where the nucleus is visible it takes up almost 1/3 of the cell.

*Central cell is the largest cell in the embryo sac*

The largest cell in the embryo sac is the central cell (Figure 2.4). It is in contact with the antipodal cells at the chalazal end and the egg and synergid cells at the micropyle end. This cell is specialized for storage with numerous vacuoles, including a large central vacuole. The central cell has a large vacuole that is situated towards the chalazal end of the cell (Figure 2.1). Throughout the central cell there is a thin layer of cytoplasm that is adjacent to the cell membrane, with most of the cytoplasm concentrated at the micropylar end surrounding the nucleus. The cell wall is continuous except at the micropylar end where it articulates with the egg and synergid cells. At the intersection of the egg cell and the synergid cells, the plasmalemma is very thin and it is unknown if there are any cell wall components. In the micropyle region thin portions of the central cell extend down the sides of the synergid cells, which has been previously described as 'synergid hooks' (Figure 2.5).

A majority of the central cell cytoplasm and the nucleus was situated at the micropylar end of the central cell. The cytoplasm was specialized for storage so there were a lot of starch grains and lipids. There were numerous plastids present with and without starch grains present. The plastids with starch granules that were concentrated near the large diploid nucleus, and there were also electron dense lipid accumulations near the nucleus. This cell was metabolically active, there were a lot of mitochondria present within the cytoplasm.

*Egg Cells have thin plasmalemmas which would facilitate communication between cells*

The general shape of the egg cell is a broad oval cell body at the chalazal end with a tapered triangular projection that extends towards the micropyle end along the lateral edge of one of the synergid cells (white arrow: Figure 2.5). The nucleus is contained within the oval shaped portion of the cell body at the chalazal region of the egg, and there is a large vacuole that is present in the triangular projection and can extend into the main cell body of the egg as well, this is especially apparent in sections before or after the nucleus. The cell membranes between the egg cell, the central cell, and the synergid cell are quite thin and sometimes appear to be discontinuous (black arrow: Figure 2.5). The egg cell does not appear to have thick cell walls, but it does have a plasmalemma that is in contact with the plasmalemmas of the central and synergid cells. There can be thicker regions along this plasmalemma, and it is unknown if there are any cell wall components that are associated with this thicker region. In addition to this there are often times electron dense circular structures associated with the egg plasmalemma (white arrowheads; Figure 2.5).

A majority of the cytoplasm is contained in the main body of the egg cell at the chalazal end of the egg cell along with the nucleus. The cytoplasm of the egg cell has a few Golgi bodies and a moderate density of mitochondria, most of the mitochondria and Golgi bodies are found in the main cell body but there are also a few in the portion of the cell that is located next to the synergids. There are fewer plastids in the egg cell than are usually observed in the central cell (Figure 2.5). These plastids are typically found near the nucleus and may contain some starch granules.

*Synergid cells are positioned at the micropyle to receive the pollen tube*

The synergid cells are located at the micropyle end of the embryo sac (Figure 2.6). There is a pair of these cells that are ultrastructurally similar, with no noticeable differences. These cells are typically elongated cells, with a vacuole at the chalazal end and a specialized cell wall structure known as a filiform apparatus at the micropyle end. The filiform apparatus is a convoluted structure that increases the surface area at the cell wall interface. The nucleus is in the middle of the cell between the vacuole and the filiform apparatus (Figure 2.7). There is a nuclear envelope and the condensed chromatin that comprise the nucleolus is clearly visible in the mature embryo sac.

In the cytoplasm, the synergid cells have a large concentration of endoplasmic reticulum. Although there are abundant mitochondria in the synergid cells, there does not appear to be a higher concentration of them near the filiform apparatus as was noted by Mansfield et al. (1991) in the sections that I have examined. There are numerous Golgi bodies with active vesicle formation present indicating that these are very metabolically active cells. The synergid cell cytoplasm contains many mitochondria, Golgi bodies, and a few plastids. Mitochondria profiles tend to be oval or circular in appearance and have well developed cristae. There is also abundant rough endoplasmic reticulum.

## Developmental Differences Between Immature and Mature Embryo Sac Ultrastructure

*Central cell has polar nuclei fusion before embryo sac maturity:*

Developmentally the nucleus of the central cell becomes 2N after the fusion of the two polar nuclei. Before this occurs two polar nuclei were clearly seen in the central cell. One of the most obvious indication of an immature embryo sac was if either two separate or two polar

nuclei were in the process of fusing (Figure 2.8). The two polar nuclei were smaller in appearance than the final 2N in a mature central cell.

*Young Synergid cell ultrastructure differs from mature synergid ultrastructure:*

Another indication that the embryo sac was young was the appearance of the synergid cells. Although in the mature embryo sacs synergid cells typically did not have starch grains in their plastids, in young synergids a few large starch granules were present (Figure 2.8). Another important characteristic was the aspect ratios (width: length) of the synergid cells, which were considerably lower for the mature synergid cells (Figure 2.8). This gave the immature synergid cells a boxy appearance instead of the elongated shape that was typical for mature synergids.

## Developmental Differences: Degenerating embryo sac

After the embryo sac had matured the next stage in the life cycle was to undergo fertilization which was associated with degeneration of some of the cells. One of the most notable characteristics of the degeneration process was the formation of elongated channels with circular electron dense structures that continued to expand. The progression of this process as well as the appearance of the nucleus were the major features in determining the three major stages of the embryo sac degeneration: Early, Mid-stage, and Advanced degeneration (Figure 2.9-2.10). It was unknown whether the degeneration was natural or due to poor fixation, however all the degenerating ovules had the same characteristics and early degeneration of the synergid cells was one of the phenotypes noted in other studies on *lre/lre,* thus a detailed description of the degeneration of synergid cells in the WT ultrastructure was needed in synergid cells and other cell types within the embryo sac.

*Early stage degeneration involved ultrastructural changes in the cytoplasm*

During the early stages of degeneration there were a number of changes to the ultrastructure of the cells within the embryo sac. In the early stages of degeneration there was the early formation of extensive elongated channels with electron dense structures. At this stage the vacuoles were visible, but they were not elongated and were not a significant feature in the cytoplasm. They were also not elongated but irregular in shape. They usually had at least one larger circular structure in them with numerous smaller structures. At this point the edges of the nuclear envelope were becoming jagged and showed irregularities, however the overall shape of the nucleus was still fairly normal looking. At this point there were also a lot of extra mitochondria present. This was true for the egg cell, the central cell and the synergid cells.

*Mid-stage degeneration had clear changes in the nuclear morphology*

In the mid-stage degeneration there were more changes but the cell walls separating the egg, central cell, and synergid cells were still present. There were elongated vacuoles with electron dense circular structures that were organized linearly within the elongated vacuoles. There were mitochondria present, but they were not at the densities observed in the early stages of degeneration, nor were they as pronounced (Figure 2.9). The nuclear envelope was starting to become irregular in shape, but had not yet broken down. The nucleolus was still circular or oval in shape (white arrowheads; Figure 2.9).

*Advanced stage degeneration had the breakdown of plasmalemmas*

In the advanced stages of degeneration there were huge changes in the ultrastructure. At this point there was no distinct separation between the synergid cells, the egg cell, and the central cell. No plasma membrane was visible at the intersection of these four cells. It was

possible to see the remnants of the cell wall collapsed in the synergid cell (black arrow heads; Figure 2.10). The filiform apparatus was still intact, however, the cell walls that make up the sides of the synergid cells where the synergid hooks of the egg cell would be, had become free and unattached (black arrowheads; Figure 2.10). They were usually visible as coiled or zig-zagged structures along the sides of the synergids. The cytoplasm of the synergids was very different at this stage. The circular electron dense structures found throughout the cytoplasm in the mid stage of degeneration had expanded, and were more variable in size and were no longer organized in appearance (white arrowheads; Figure 2.10). These structures had a vacuole-like appearance with the numerous circular electron dense structures. At this stage the circular electron dense structures were not uniform in size and some of them were more elongated and oval in shape.

## SUMMARY

In this study we found that the ultrastructure appeared to be similar among different wild type accessions. The ultrastructural descriptions of the antipodal cells, central cell, egg cell, and synergid cells in this study were similar to what had been reported in Landsberg erecta. In addition to the mature ovule ultrastructural descriptions, both the early embryo sac development and the degeneration of the embryo sac were also described for the first time during this study. This study also confirmed some of the major findings, most notably the antipodal cells were present in the mature embryo sac and did not appear to proliferate. Also, polar nuclei fusion happened before the embryo sac is mature. Therefore, a digital library or repository of general wild type ultrastructure should be created to be used by the scientific community.

# CHAPTER 2 FIGURES

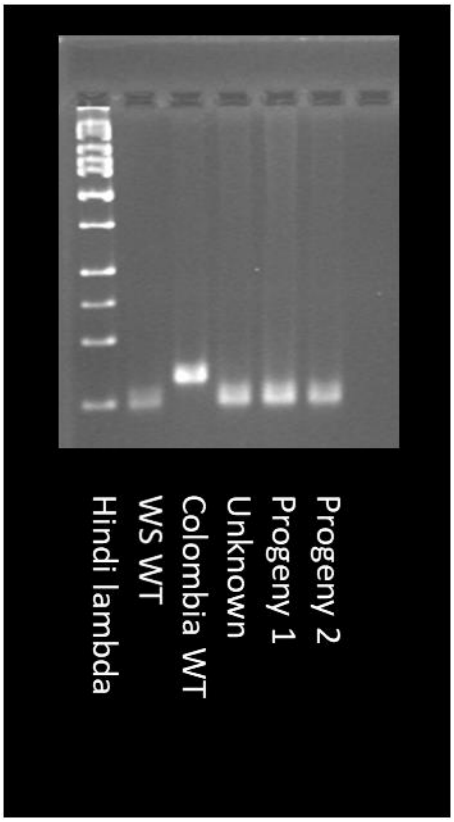


Figure 2. 1 PCR results with the NGR76 marker confirming there are two different wild type accessions, Colombia and another wild type accession that is about the same size as Wassilewskija (WS). There is both the original parental generation (unknown), and the F1 (progeny 1) and the F2 (progeny 2) generation in the second wild type accession. This means that the pooled wild type descriptions from this data set have more genetic variability than with a single wild type accession. The Colombia product length is 220-231 bp and the WS product is between 199-200 bp. The product from the unknown wild type is of similar size to the WS wild type product.

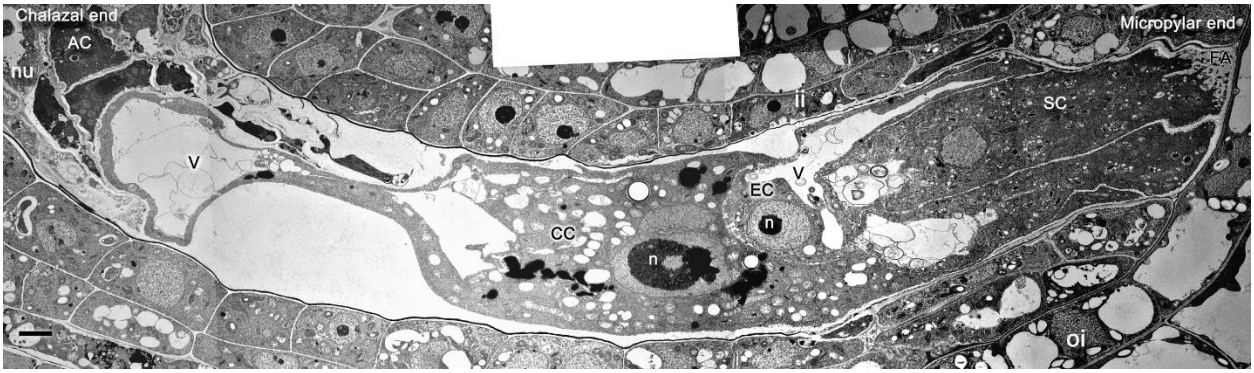


Figure 2. 2 Montage of electron micrographs reconstructed to show the entire embryo sac. The chalazal end is on the left and the micropylar end is on the right. There are three antipodal cells present at the chalazal end of the embryo sac. In the middle of the embryo sac there is a large central cell. This central cell has a large chalazally located vacuole. At the micropylar end of the central cell there is a nucleus and a majority of the cytoplasm. At the micropylar end of the embryo sac is the egg and the two synergid cells. The nucleus for both the egg and the central cell are located near each other. The filiform apparatus is a specialized structure at the micropylar end of the synergid cells. The embryo sac is then surrounded by maternal tissue including the inner and outer integument cells located laterally along the side of the embryo sac and the nucellus cells at the chalazal end of the embryo sac. Antipodal Cells (AC), Central Cell (CC), Egg Cell (EC), Filiform Apparatus (FA), Inner Integument (ii), Outer integument, Nucellus (nu), Nucleus (n), Synergid Cell (SC), and Vacuole (V). The scale bar is 10 microns.

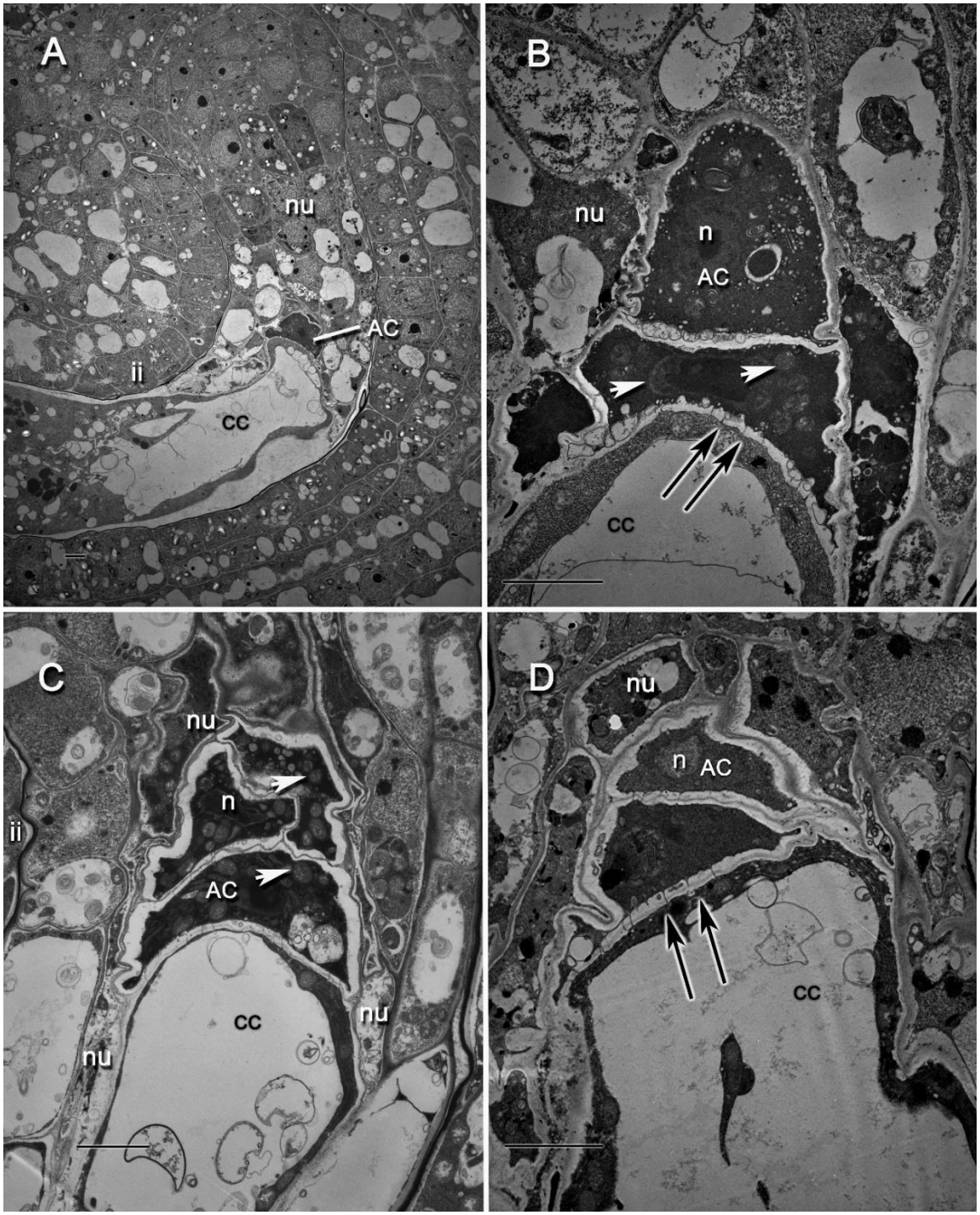


Figure 2. 2 Electron micrograph of antipodal cells. Antipodal cells can be identified by their electron dense cytoplasm, triangular shape, and their position at the chalazal end of the embryo sac, adjacent to the large central cell vacuole. A) A low magnification image of antipodal cells with surrounding tissue in the wild type. B) Antipodal cells in wild type. Although there appears to be more than three antipodal cells in this section, it is likely a sectioning artifact. C) Antipodal cells in Colombia wild type. There are degenerating nucellus cells on the lateral edges surrounding the central cell. D) Antipodal cells in the Colombia wild type. Antipodal Cell (AC), Mitochondria (white heads), Nucleus (n), Nucellus (nu), Plasmodesmata (black arrows), inner integument cells (ii), central cell (CC). The scale bar is 10 microns.

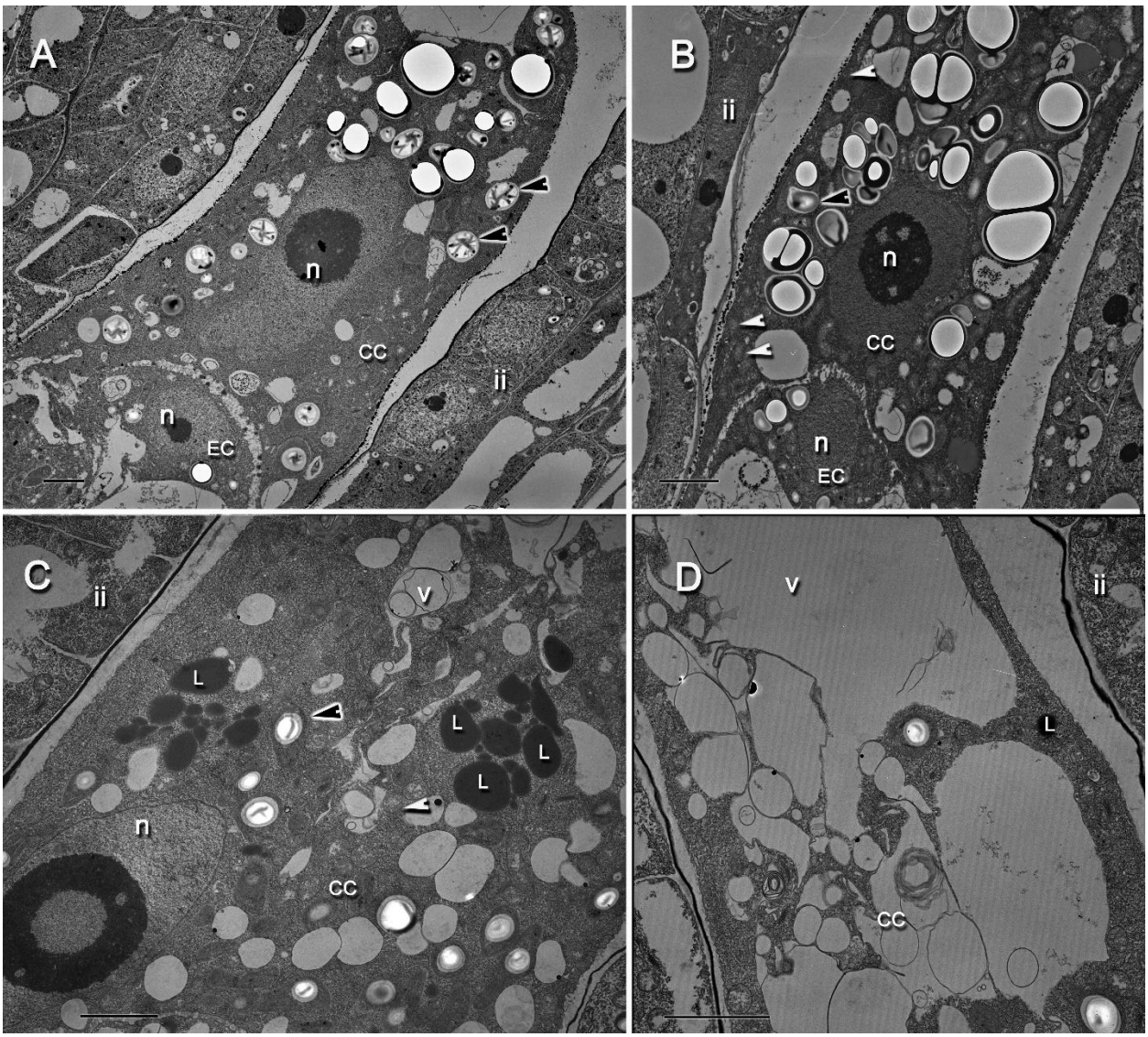


Figure 2. 3 Electron micrographs of the central cell. The central cell is the largest cell in the embryo sac and it appears to be specialized for storage. A) and B) are micrographs from Colombia WT that show that the large 2N nucleus is situated close to the egg cell nucleus. C) Shows a high magnification micrograph of the cytoplasm above the nucleus and D) shows the large vacuole at the chalazal end of the embryo sac. Both C) and D) are from the other wild type accession. C) A high magnification image of the cytoplasm surrounding the nucleus, which contains large amounts of electron dense lipids and also numerous starch granules. D) Is a high magnification view of the large central vacuole that is present that the chalazal end of the central cell. Inner Integument Cells (ii), Mitochondria (white arrowheads), Nucleus (N), Lipid (L), Vacuole (V), Egg Cell (EC), Starch grains (black arrowheads). The scale bar is 10 microns.

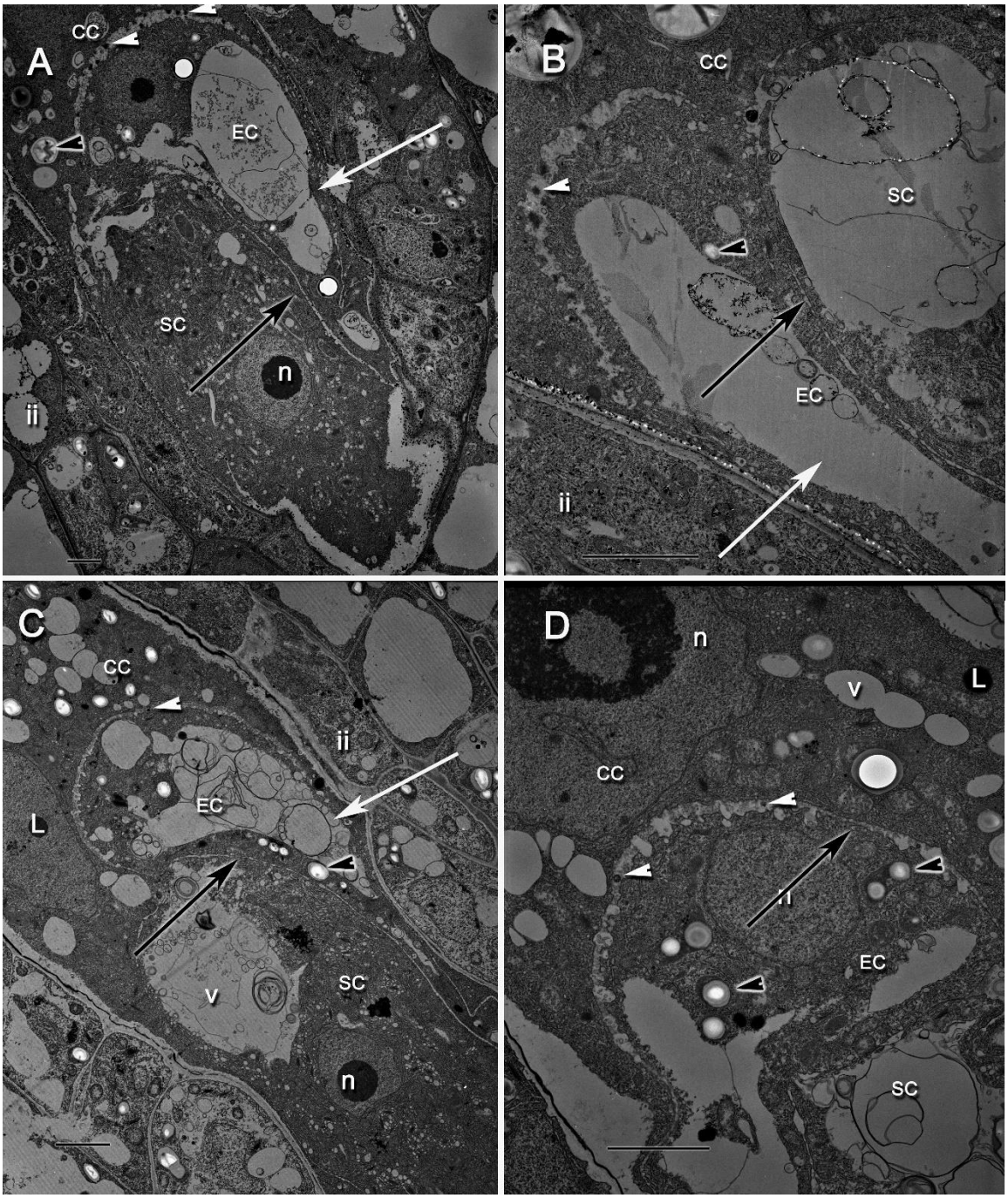


Figure 2. 4 Electron micrograph of an egg cell situated at the micropyle end of a central cell. A) and B) show Colombia WT. A) The main body of the egg is situated chalazally relative to the synergid cells with an extension known as the 'synergid hook' extending along the side of the synergid cells. A higher magnification image of B) showing that the vacuole can extend into the body of the egg cell in sections that do not contain the nucleus. C) The 'synergid hook' of the egg cell extends down the side of the synergid cells in the WT. D) A High magnification WT showing the very thin plasmalemma separating the egg cell, the central cell, and the synergid cell, making communication possible between the cytoplasm of these three cells. Egg Cell (EC), Vacuole (V), Nucleus (n), Central Cell (CC), Synergid Cell (SC), starch (black arrowheads), electron dense circular structures in the plasmalemma of the egg cell (white arrowheads), plasmalemma (black arrow), synergid hooks (white arrow). The scale bar is 10 microns.

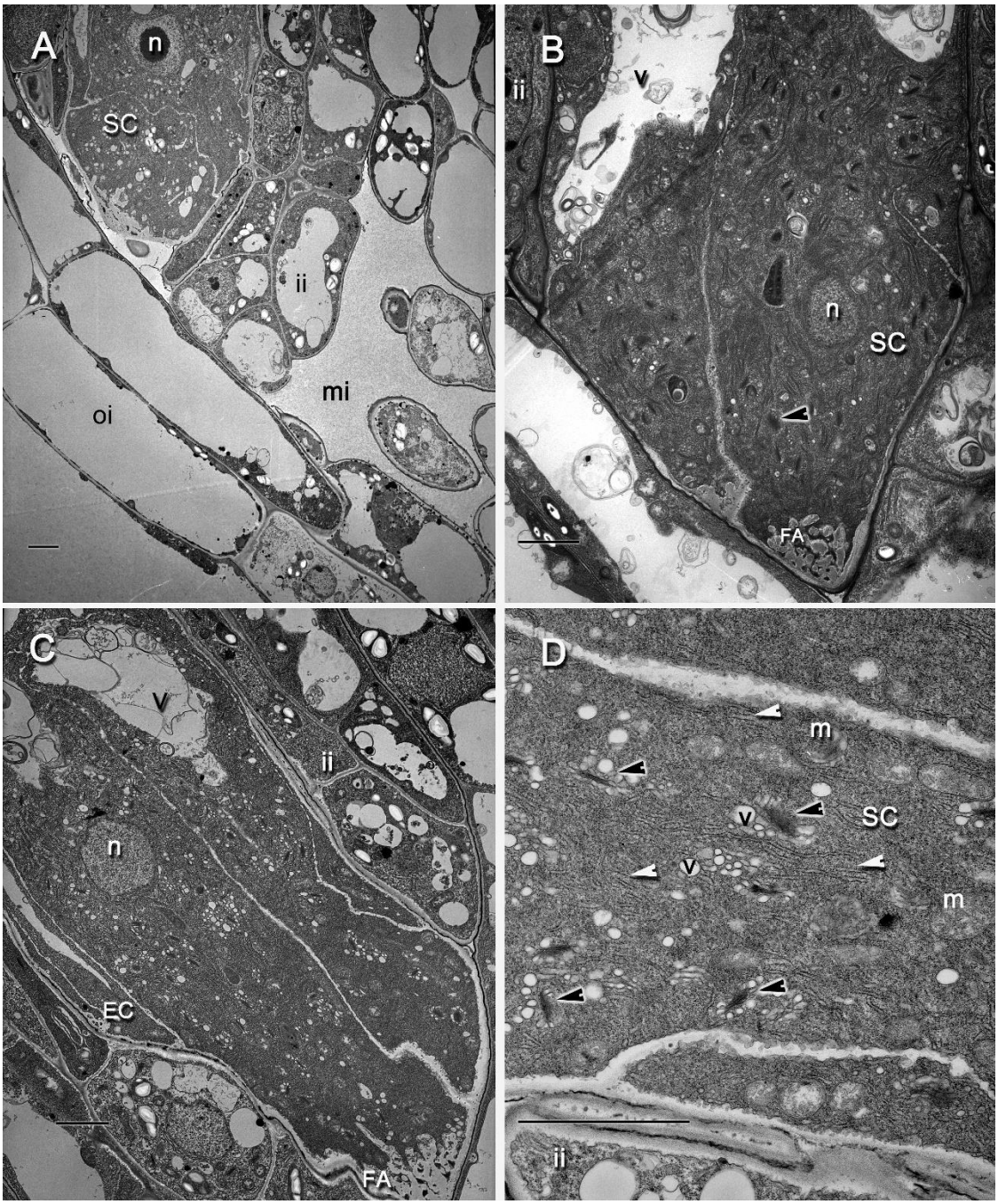


Figure 2. 5 Electron micrographs of the synergid cells. A) The synergid cells are at the entrance to the micropyle in WT. A higher magnification view of synergid cells in B) Col Wt and C) WT showing the filiform apparatus is at the micropylar end of the synergid cells. The nucleus is in the middle of the synergid cell, and there are large vacuoles at the nucellar end of the synergid cell. A high magnification view of the D) synergid cytoplasm. The cytoplasm is very metabolically active with many Gogi bodies producing vesicles. There is also a lot of endoplasmic reticulum and many mitochondria. Central cell (CC), Egg Cell (EC), Endoplasmic Reticulum (white arrowheads), Filiform Apparatus (FA), Golgi Bodies (black arrowheads), Inner Integument (ii), Micropyle (mi), Mitochondria (m), Nucleus (n), Outer Integument (oi), Synergid Cell (SC), Vacuole (V). The scale bar is 10 microns.

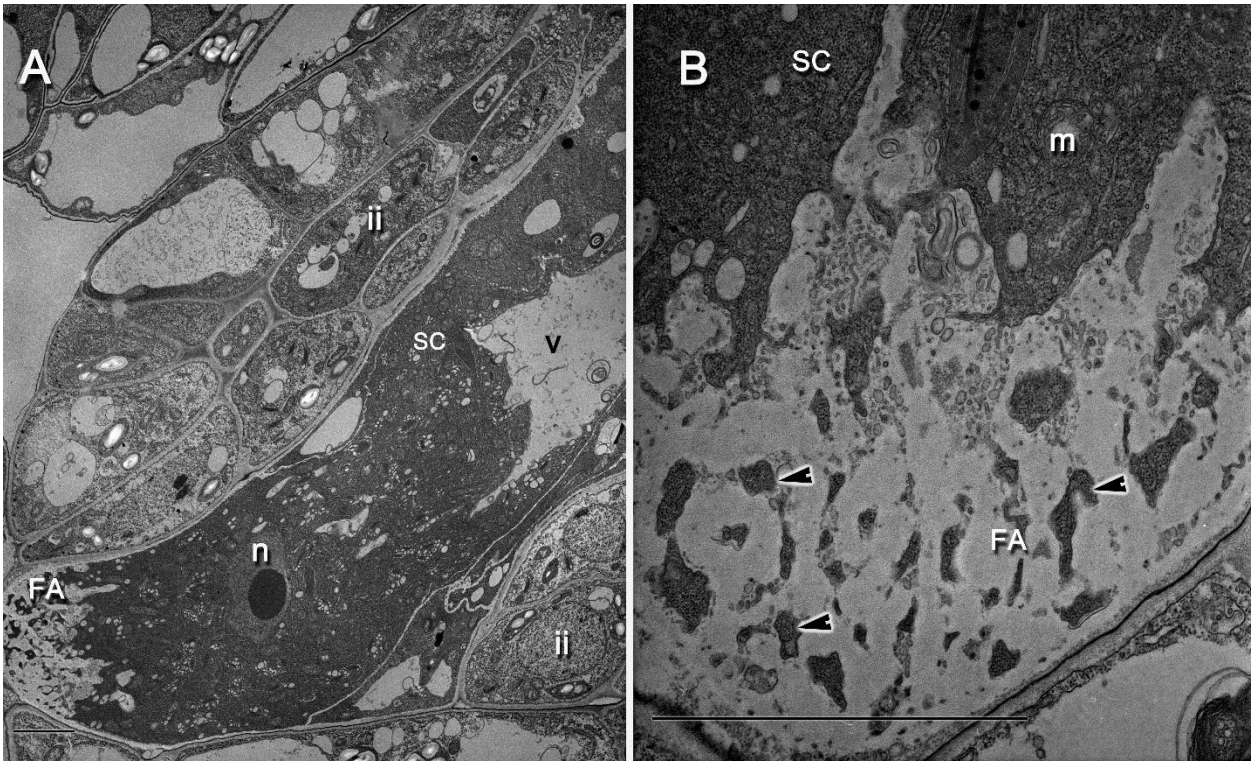


Figure 2. 6 Electron micrographs of the synergid cell showing the filiform apparatus. A) A low magnification view of the WT showing the vacuole, the nucleus, and the location of the filiform apparatus at the micropylar end of the synergid cell. B) A high magnification micrograph of the filiform apparatus in the WT showing the convolutions in the cell wall of the filiform apparatus that increases the surface area. Filiform Apparatus (FA), Inner Integument (ii), Nucleus (n), Mitochondria (m), Convolutions in the filiform apparatus (black arrowheads). The scale bar is 10 microns.

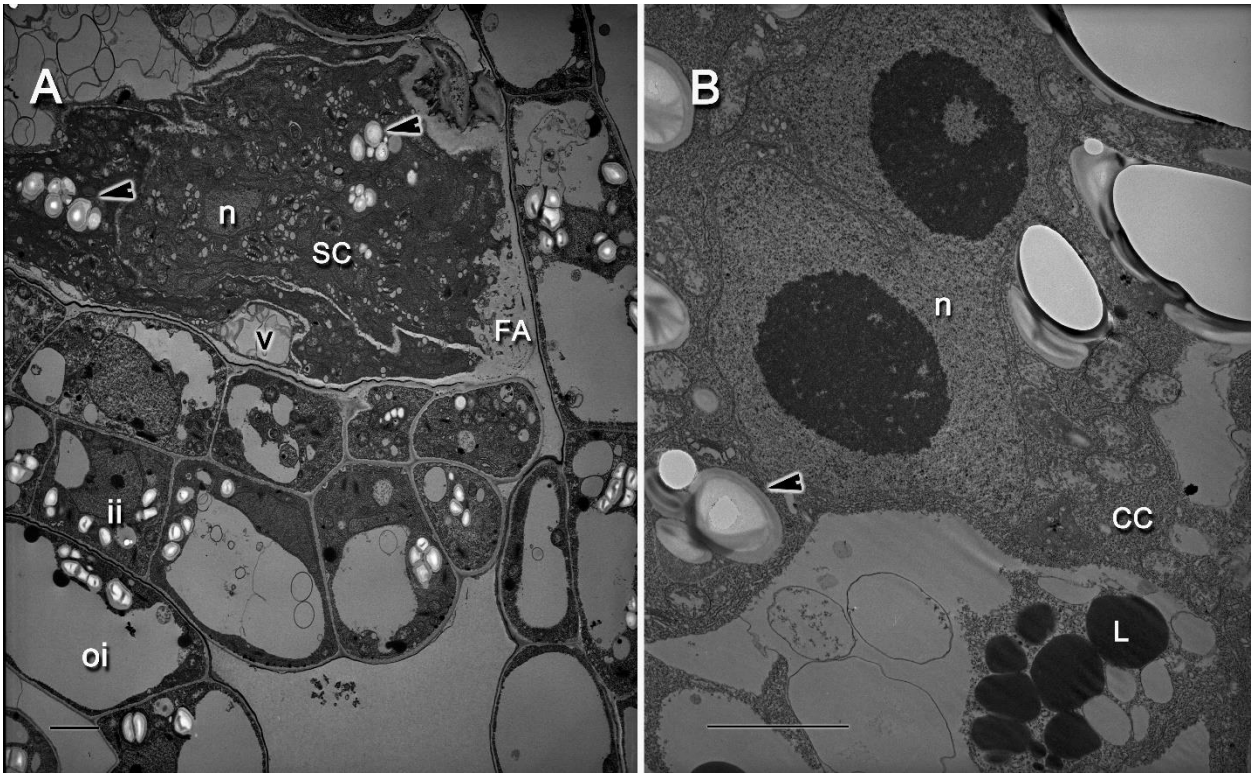


Figure 2. 7 Electron micrographs of developmental differences in the immature embryo sac in WT. A) Starch granules present in immature synergid cells. The synergid cells are not as elongated, resulting in a length and width that are closer in size than in the mature embryo sac. B) Polar nuclei fusing in the central cell Central Cell (cc), Filiform Apparatus (FA), Nucleus (n), Lipid (L), Synergid Cell (SC), Inner Integument (ii), Outer Integument (OI), Starch Granules (black arrowheads). The scale bar is 10 microns.

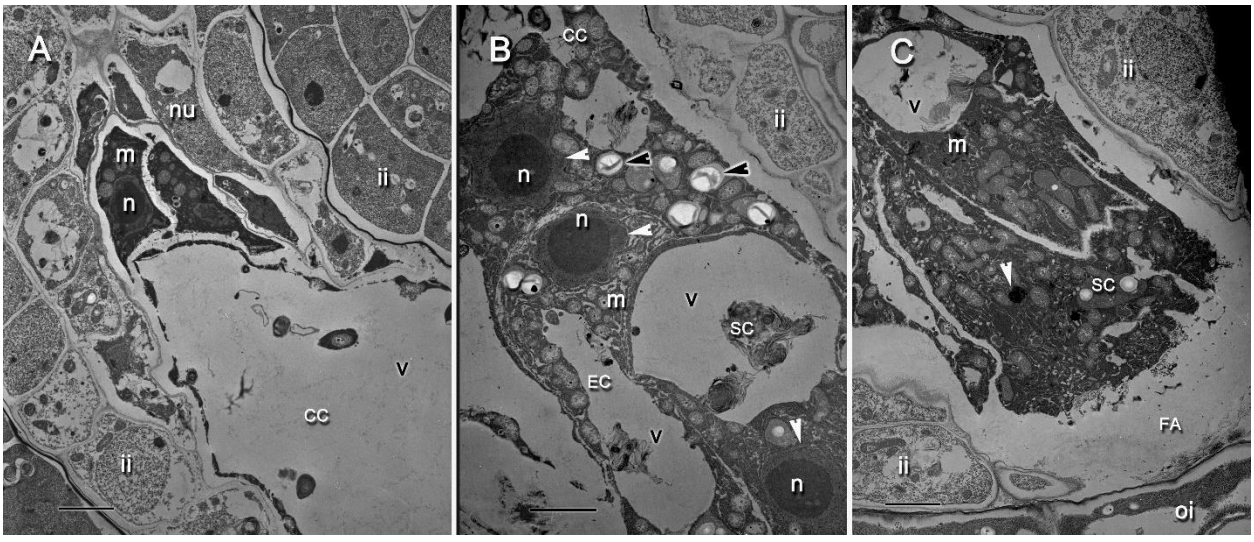


Figure 2. 8 Electron micrographs of the mid-stage degeneration showing the A) antipodal cells, B) central cell, and C) synergid cells. The nuclear envelope is in the early stages of breaking down as noted by the irregular shape of the nuclear envelope (white arrowheads) and there are many mitochondria present in the cytoplasm of all three cell types. Central cell (cc), Filiform Apparatus (FA), Mitochondria (m), Nucleus (n), Nucellus (nu), Synergid Cell (SC), Inner Integument (ii), Outer Integument (IO), Starch Granules (black arrowheads). The scale bar is 10 microns.

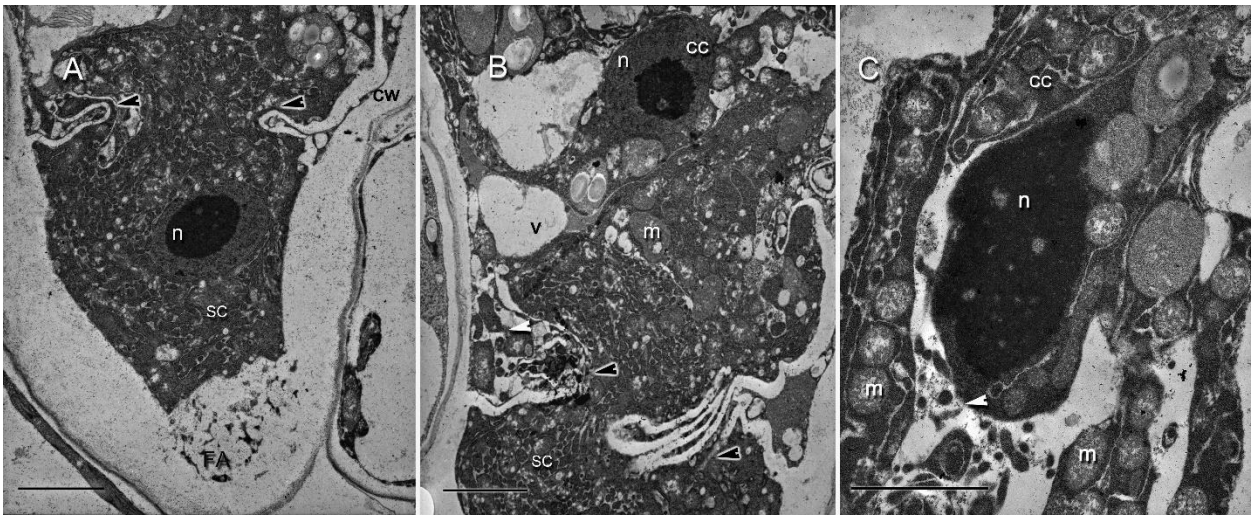


Figure 2. 9 Electron micrographs of the advanced stage degeneration showing the A) synergid cell, B) egg cell and synergid cell degenerating, and C) Central cell nucleus. In A) and B) the cell walls of the synergid cell are breaking down and there is no longer a separation between the cytoplasm of the synergid cell, egg cell, and the central cell (black arrowheads). In C) the nuclear envelope has broken down in the central cell and the shape of the nucleolus is irregular. In the degenerating cytoplasm there are large vacuole-like structures with circular electron dense structures (white arrowheads). Central Cell (cc), Cell Wall (cw) Filiform Apparatus (FA), Mitochondria (m), Nucleus (n), Synergid Cell (SC). The scale bar is 10 microns.

# Chapter 3: lre-7/lre-7 Ultrastructure

## ABSTRACT

The ultrastructure of the wild type (WT) and *lre-7/lre-7* had several notable differences. There were several changes to the filiform apparatus, which would reduce the surface area. The filiform apparatus area of the *lre-7/lre-7* was at the lower end of the range for the filiform apparatus area that were present in the WT. There was a higher percentage of *lre-7/lre-7* that had reduced convolutions. In the synergid cells, there were no differences in the endomembrane system, including the Golgi body counts, and the number of vesicles associated with those Golgi bodies. In this sample data the aspect ratios of the synergid cells, in general, appeared to be more square and boxy, than some of the more elongated WT synergid cells. In the other cell types such as the antipodal and the egg cell there was an increased variability in the cell wall thickness. Overall, *lre-7/lre-7* ovules had several ultrastructural changes in the ovules with high penetrance of the *lre-7/lre-7* phenotype.

## INTRODUCTION

This chapter had a detailed analysis and ultrastructural comparison between the WT and *lre-7/lre-7* embryo sac. Since this was the first study to look at the *lre-7/lre-7* mutant ovules an exploratory inductive reasoning approach was taken. Previous confocal studies had shown that LRE localizes only to the synergid cells and a large percentage of LRE was concentrated at the filiform apparatus. For this reason, the original focus of this study was to 1) compare the ultrastructure of the synergid cells and more specifically the filiform apparatus, however, in the interest of not biasing our observation we also did 2) a comparison of other cell types within

the embryo sac to determine if any ultrastructural differences between synergid cells in WT and *lre-7/lre-7* embryo sacs were observed.

## METHODS

The experimental procedures were similar to those previously described for Chapter 2 with the following modifications: Homozygous *lre-7/lre-7* seeds were germinated on antibiotic selection plates (MS salts 4.3g/L, Sucrose 20g/L, MES. 0.5g/L, pH 5.7, Agar 9g/L, Basta 10 µg/mL) before being transplanted to soil to confirm that the *lre-7* T-DNA insertions were maintained. To supplement the visual observations, measurements (Cell wall thickness: measurements were at easily identifiable landmarks; endomembrane system: the number of Golgi Bodies and their associated vesicles were counted in the synergid cytoplasm in the area between the filiform apparatus and the nucleus) were taken in ImageJ on several structures that were suspected to be phenotypes to determine if any patterns in the data such as changes in the central tendency (sample means, and population mean estimates), spread of the data (standard deviation), or any outliers using JMP14 statistical software even with the low sample sizes typical in an electron microscopy data set were detectable. Note that these statistical analyses were meant to detect and summarize patterns in this sample data to identify promising areas for future studies and are not intended to be representative of actual population estimates like they would in ecological or biomedical studies with a large sample size.

# RESULTS

Transmission electron microscopy was used to investigate the ultrastructure of *lre-7/lre-7* ovules and compare them with the ultrastructure of WT ovules. Initially all the observations were visual. During these initial observations several structures were noted to be abnormal. After our initial observations were made, it was clear that there was a great deal of overlap between both the WT and the *lre-7/lre-7* ovules but that there were a few *lre-7/lre-7* ovules with abnormally severe phenotypes. Although visual observations were adequate in cases where there was a low variability in the range of morphological structures and the mutant and WT samples did not overlap, a wide range of variability was observed in the morphology and there appeared to be a lot of overlap between the morphology of the mutant and the WT samples. The visual observations were supplemented with some measurements to account for any base rate bias which is the tenancy to emphasize specific information instead of general information. By summarizing the morphological data with measurements and displaying them in a graph it was possible to see if the range of variability in the measurements for the structures fell within the range of the morphological variability for the WT, or if there were a number of outliers in the *lre-7/lre-7* that were well outside that of the normal range of variability of the WT. Therefore, the data was displayed three different ways: 1) a plate with a representative WT and a *lre-7/lre-7* example with high penetrance 2) a plate with several *lre-7/lre-7* micrographs showing the range of variability, and 3) a graph of the measurements of a structure at a specific landmark that puts the amount of variability of the *lre-7/lre-7* samples into context with the range of variability found in the WT samples. Please note that it was expected that the actual raw numbers from the measurements could have changed depending

on the position of the landmark that was chosen, but the overall patterns in the data seemed to be very consistent regardless of the landmark position and cell types that were chosen. Therefore, it was demonstrated that there was strong evidence of an increase in the variability of morphological structures (usually cell wall thickness) in *lre-7/lre-7* and it was likely that this pattern is present in the *lre-7/lre-7* population. The limitations of electron microscopy data from populations with high variability indicate that the sample mean (average) and the frequency that a specific phenotype was observed in the sample set were not accurate representations of the population means and frequencies, however a pattern emerges that provides an estimate about the magnitude of the variability between the WT and mutant structures.

An unexpected phenotype that was noted in the *lre-7/lre-7* ovules was an abnormal thickening of the cell walls of several cells within the embryo sac including the antipodal cells and the egg cell, which have not been reported to have LRE expression. A more detailed analysis on the synergid cells was done, which included looking at the endomembrane structures and metrics associated with the filiform apparatus, including the area and typing the convolutions present within the filiform apparatus.

### Antipodal cells have structural variability in cell wall thickness

Another likely *lre-7/lre-7* phenotype was a thickening of the antipodal cell walls. In the WT ovules, for the raw cell wall thickness the sample mean was 217 nm, and the standard error (SE) was 117 (n=6). For *lre-7/lre-7,* the sample mean was much higher, 639 nm with a SE of 128 (n=7)(Figures 3.1-3.3). There was no significant difference between the sample means, however

the standard errors (range where the population mean would be expected to fall) for the two groups did not overlap. There was also an increase in variability in the *lre-7/lre-7* lines as compared to the WT lines as indicated by the standard deviation, 199 and 47 nm, respectively.

These patterns were confirmed by using another approach that would account for some of the developmental variation in cell wall thickness due to growth. The inner integument cell wall thickness (which is visible in almost every micrograph that has antipodal cells) was used as a baseline when calculating the relative thickness (ratio of the antipodal cell wall thickness: inner integument cell wall thickness). The same patterns that were found in the raw cell wall thickness were also present in the relative cell wall thickness. The WT sample mean relative thickness was 2.95, with a standard error of 1.66 (n=6) and the *lre-7/lre-7* relative thickness mean was 8.5 with an SE of 2.15 (n=6). Both sample means were far apart and the standard error (estimate of where the population mean would fall) do not overlap, which suggested that the population means could be different. The lack of significance may have been an artifact of a low sample size and high variability in the data. The standard deviation (which was an estimate of variability), increased in the *lre-7/lre-7* as compared to the WT, 7.19 and 1.2 respectively. This means that in both the raw and relative measurement the *lre-7/ lre-7* had a higher average thickness, and there was also an increase in the amount of variation or spread of the data as evident by the standard deviations in the *lre-7/lre-7.* In both cases, the raw and relative thickness, there were a number of *lre-7/lre-7* ovules that were well outside the upper 95% CI of WT and there was a dramatic increase in the variation (as estimated by the standard error) in antipodal cell wall thickness in *lre-7/lre-7* ovules sampled.

For both of these approaches, raw vs relative cell wall thickness, the same patterns in the data were observed. The sample mean of *lre-7/lre-7* was much higher than the WT and the standard errors did not overlap, suggesting that there could be a difference between the population means. There was an increase in the amount of variation in the *lre-7/lre-7* as indicated by the standard deviations. Although there were technically no significant differences between these two lines, this was not surprising because there was a lot of noise (variability, equal variances are ideal) in the data and the low sample size that could be obtained with electron microscopy samples.

### Egg cells with cell wall thickenings at the cell wall apex

At the chalazal apex of the egg cell there were several *lre-7*/*lre-7* ovules that had a thickening of the cell wall. For *lre-7/lre-7* the sample mean raw thickness was 681.00 nm and SE was 329.28 (n=7), while the WT mean was 911.75 nm with a SE of 355.66 (n=6). The relative thickness (raw thickness of egg: integument raw thickness) for *lre-7/lre-7* had a sample mean of 14.26 and SE of 6.95 (n=7). The WT had a relative sample mean of 7.98 and a SE of 7.50 (n=6). For both approaches, the raw and the relative thickness, the standard errors overlap for both the *lre-7/ lre-7* and the WT (Figure 3.4-3.6). This indicated that the range of values were both the WT and the *lre-7/lre-7* would be found overlap, so there was probably no difference in the population means, however there were clear outliers in the *lre-7/lre-7* sample. The variation as estimated by the standard deviation increased in the *lre-7/lre-7* ovules as compared to the WT ovules, 20.69 and 3.91 respectively. In summary, the sample means had not provided a lot of

information, but there was a huge increase in variability in the *lre-7/lre-7* ovules and there were clear outliers that were well above the 95% CI in the *lre-7/lre-7* data set.

### Synergid cells have boxy shapes

The aspect ratio (width:length) of synergid cells were compared in both the *lre-7/lre-7* and the WT ovules. The sample mean for *lre-7/lre-7* was 0.40 and the standard error was 0.04 (n=6). The sample mean for WT was 0.37 and the standard error was 0.05 (n=3). This means that there were some WT synergid cells that were longer than the *lre-7/lre-7* synergid cells, however this sample data suggested that it was unlikely that there was a difference in the population means due to the overlap of the SE. The variability was greater in the WT. For *lre-7/lre-7* the standard deviation was 0.09 and the WT is 0.12 (Figure 3.7). This noise in the data may have been due to developmental differences and low sample size, due to the fact that these were very large cells, so it was difficult to obtain images with the entire cell intact. This metric should be re-examined using a technique where it was easier to collect more data.

### Synergid endomembrane system

The Golgi counts in the cytoplasm region between the nucleus and the filiform apparatus for *lre-7/lre-7* were within the range of the WT counts. The WT sample mean was 16.00 Golgi bodies with a SE of 2.26 (n=13) as compared to *lre-7/lre-7* which was 12.8 Golgi bodies with a standard error of 3.09. Both the WT and the *lre-7/lre-7* had outliers that were beyond both of their 95% CI. The amount of variation as measure by the standard deviation for both *lre-7/lre-7* and WT were similar, 7.08 and 8.39 respectively (Figure 3.8). In addition to the number of Golgi bodies, the number of vesicles that were near the Golgi apparatus was

measured for *lre-7/lre-7* sample mean was 12.4 vesicles/Golgi body with a standard error of 0.75, while the WT sample mean was 9.77 vesicles/Golgi body with a standard error of 0.48 (Figure 3.8). The variation which was indicated by the standard deviation was 5.80 for the *lre-7/lre-7* and it was 3.22 for the WT. There was a significant difference between the two when compared with a student's t-test (p=0.0041).

### Filiform apparatus has reduced surface area

Since the filiform apparatus was the place where LRE has been reported to localize, this was one of the major structures that was focused on. It was thought that the function of the filiform apparatus was to increase the surface area where signaling molecules that were important for communication between the male and female gametophyte were located. There were two different metrics used to analyze the filiform apparatus information; 1) an analytical/descriptive statistics approach to measure filiform apparatus area in imageJ and 2) a representativeness heuristic approach to categorize the types of the convolutions. The sample mean for the area of the WT filiform apparatus average was 23.71nm$^2$ with a standard error of 6.06 and the sample mean of the area of the *lre-7/lre-7* filiform apparatus was 18.77 nm$^2$ with a standard error of 9.34. This data suggests that there was no difference between sample or population means of WT and *lre-7/lre-7*. This would suggest that additional sampling would likely shift the sample mean and thus the WT to a larger value.

It was thought that the purpose of the filiform apparatus was to increase the surface area of the cell membrane. Since it was not possible to quantitatively measure the convolutions in the filiform apparatus, this data was categorized using a representativeness heuristics

approach. To estimate whether the surface area of the filiform apparatus was altered they were grouped into types (Figure 3.9-3.10), where Type 1= very reduced, there were no visible convolutions, Type 2= convolutions that were present but not fully formed, Type 3= filiform apparatus appears normal with fully formed convolutions present. In the WT, 71% of samples had normal Type 3 convolutions, 14% had Type 2 reduced convolutions, and 14% had the Type 1 reduced type of filiform apparatus with no convolutions (n=14). This contrasts with the *lre-7/lre-7* distributions of the Types, 43% Type 3, 28.5% for Type 2, and 28.5 % Type 1 (n=7). The data from this sampling suggests that the WT has a higher proportion of synergids with a Type 3 fully formed filiform apparatus (Figure 3.11). The strengths of using a representativeness heuristics approach, was that it involved a simplification that can be used to quickly estimate the probability of something happening. This data was classified into categories called 'types' based on the types of convolutions they have. It should be noted that with a representativeness heuristics approach, the major limitations associated with this approach are the base rate fallacy and other cognitive biases. This approach also imposed discreet categories on a continuous data set for morphological structures, therefore some of the resolution in the data set was lost.

# CHAPTER 3 FIGURES

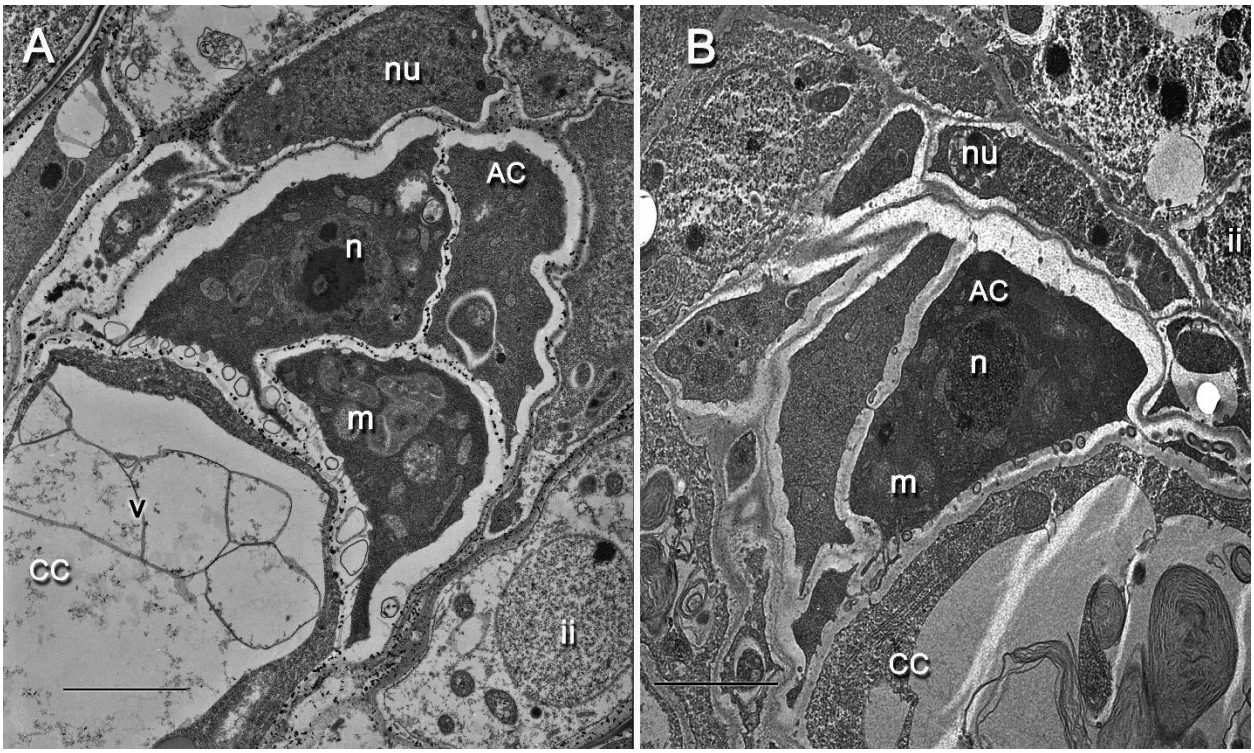


Figure 3. 1 Electron micrographs of antipodal cells from A) Col Wt and B) *lre-7/lre-7.* The antipodal cells from both have electron dense cytoplasm and a general triangular shape. Both are positioned adjacent to the central cell and the nucellus. In the section in B) it appears that the *lre-7/lre-7* cell wall may be thicker than the A) wild type section. Antipodal cell (AC), Central Cell (CC), Inner Integuments (ii), Mitochondria (m), Nucellus (nu), Nucleus (n), Vacuole (V). The scale bar is 10 microns.

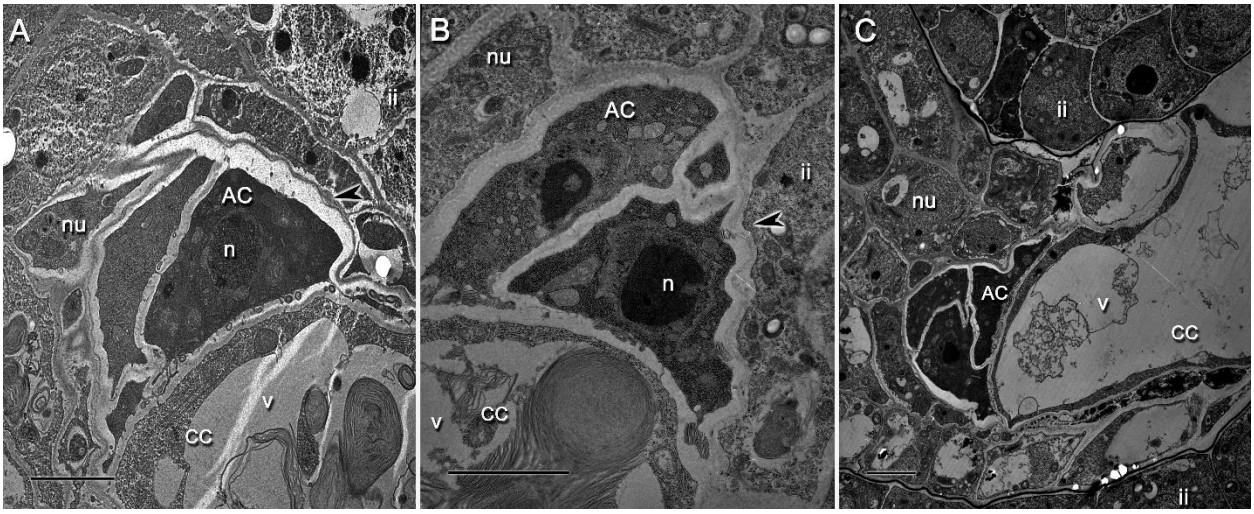


Figure 3. 2 Electron micrographs with the range of *lre-7/lre-7* antipodal cell wall thickness. In A) and B) it appears the cell walls of the antipodal cells are thicker (black arrowheads). In C) the cell walls appear to have thickness similar to that observed in the wild type. Antipodal cell (AC), Central Cell (CC), Mitochondria (m), Nucleus (n), Nucellus (nu), Vacuole (V). The scale bar is 10 microns.

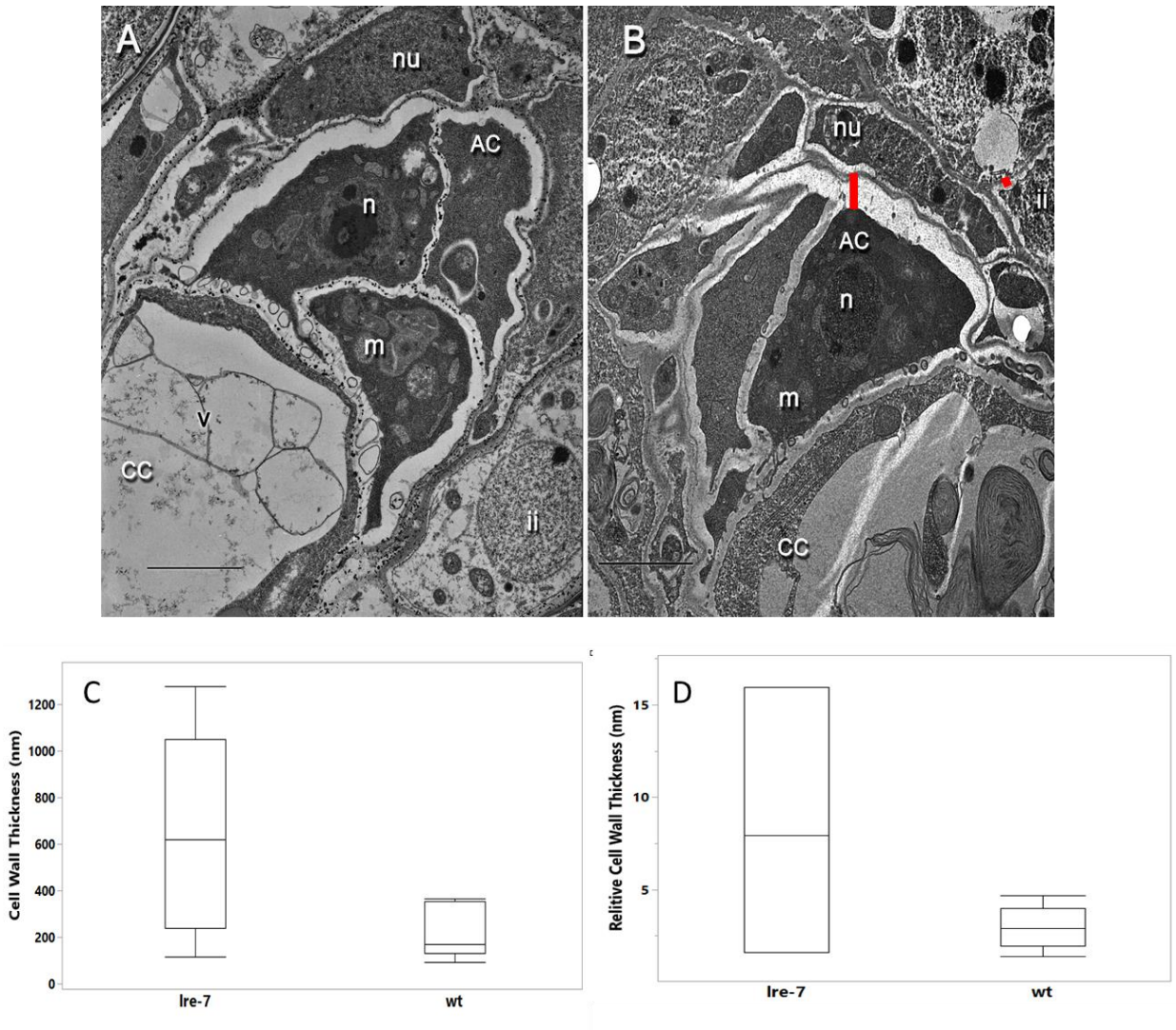


Figure 3. 3 The raw and relative cell wall thickness of the antipodal cells showing *lre-7/lre-7* has a wider range of variability in cell wall thickness than the wild type. Transmission electron micrographs showing A) wild type antipodal cells and B) *lre-7/lre-7* antipodal cell with a high penetrance of the cell wall thickness phenotype and the landmark, the top right corner of the bottom cell touching the central cell, that was used to sample the cell wall thickness. The boxplots show the C) raw cell wall thickness and D) relative cell wall thickness, which is a ratio that has the relative cell wall thickness divided by the cell wall thickness of the integument cell, which was used as an internal control to account for the within ovule cell wall thickness. In both cases the same pattern is present, the *lre-7/lre-7* ovules have more variation in cell wall thickness than present in the wild type. The transverse lines in the middle of the boxplot, indicate the sample median, the upper and lower edges of the boxplot are the 25$^{th}$ and 75$^{th}$ quartile. Antipodal cell (AC), Central Cell (CC), Egg Cells (EC), Mitochondria (m), Nucleus (n), Vacuole (V). Raw thickness: WT: (Maximum excluding outliers = 1779 nm, minimum excluding outliers= 181 nm, median = 730 nm, n= 6). *lre-7/lre-7*: (Maximum excluding outliers= 2089 nm, minimum excluding outliers= 38 nm, median = 279 nm, n=17). Relative thickness: WT: (Maximum excluding outliers= 5, minimum excluding outliers= 1, median = 3, n= 6). *lre-7/lre-7*: (Maximum excluding outliers= 16, minimum excluding outliers= 2, median= 8, n= 6). Long red line indicates thickness of antipodal cell wall measured and short red line indicates integument cell wall thickness measured. The scale bar is 10 microns.

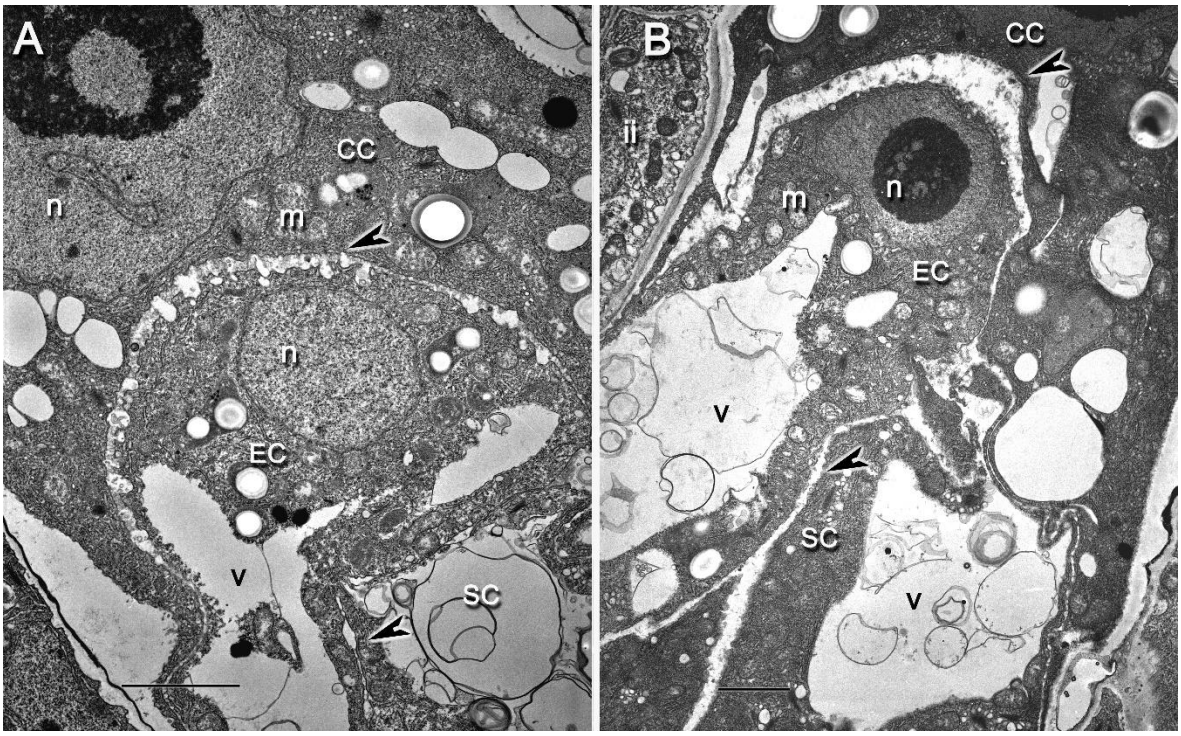


Figure 3. 4 Transmission electron micrographs showing the A) WT and B) *lre-7/lre-7* egg cell wall. In the wild type cell wall, it is quite thin in places, while the *lre-7/lre-7* egg cell example has a high penetrance of the cell wall thickening defect (black arrowhead). This thickening of the cell wall in the *lre-7/lre-7* egg cell is especially pronounced near the nucleus. Central Cell (CC), Cell Wall (arrow heads), Egg Cells (EC), Mitochondria (m), Nucleus (n), Synergid Cell (SC), Vacuole (V). The scale bar is 10 microns.

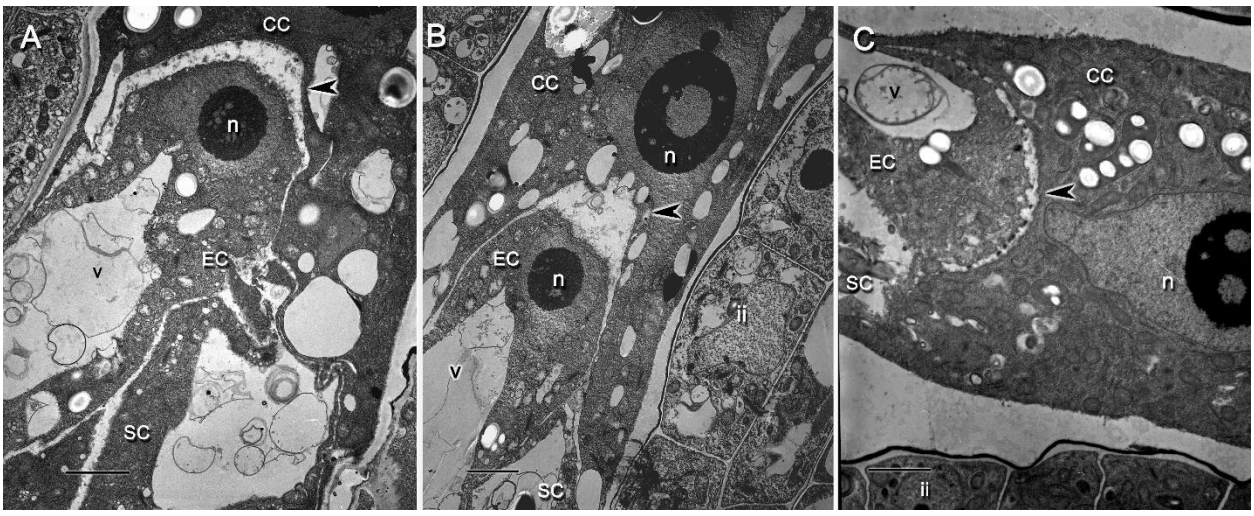


Figure 3. 5 Transmission electron micrographs showing the range of *lre-7/lre-7* egg cell wall thickness with the two ovules A) and B) that had the severest of the cell wall thickening (black arrowhead). There were also C) relatively normal *lre-7/lre-7* egg cell walls. Central Cell (CC), Egg Cells (EC), Mitochondria (m), Nucleus (n), Synergid Cell (SC), Vacuole (V). The scale bar is 10 microns.

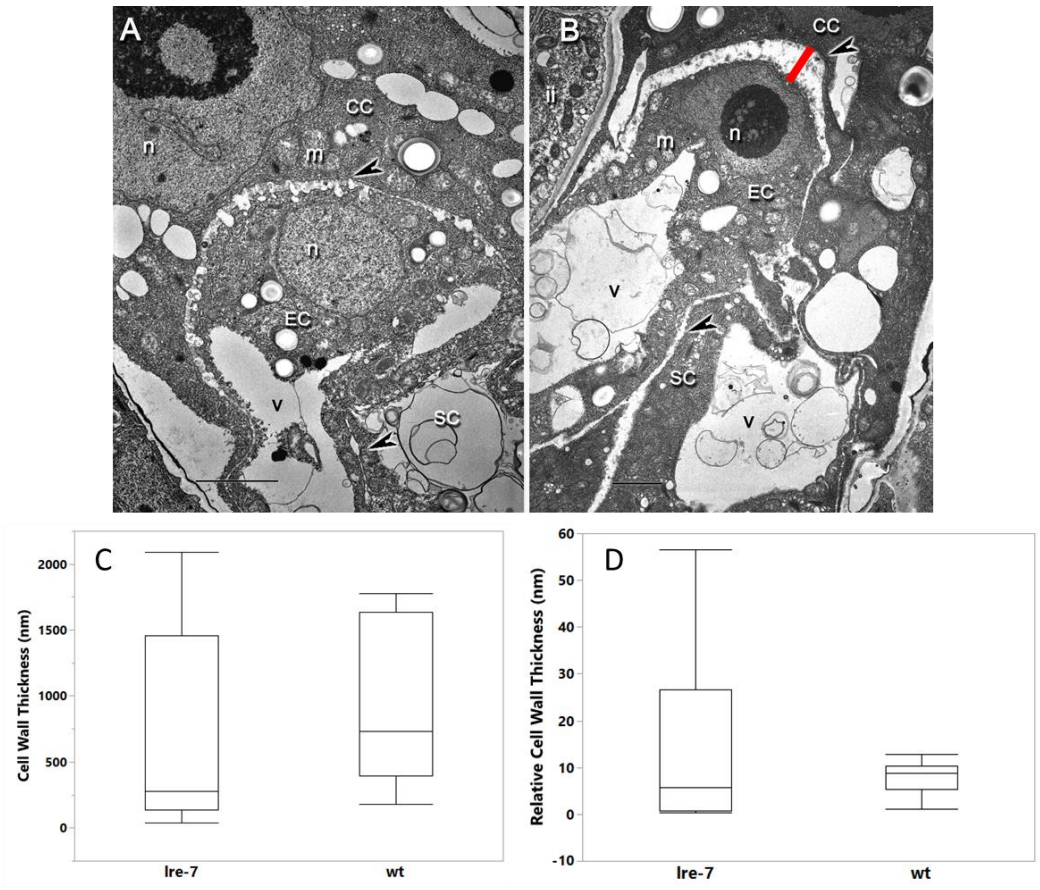


Figure 3. 6 The raw and relative cell wall thickness of the egg cell. Transmission electron micrographs of A) the wild type egg cell and B) the *lre-7/lre-7* egg cell with high penetrance of the cell wall phenotype. The boxplots show the C) raw cell wall thickness and D) relative cell wall thickness, which is a ratio that has the relative cell wall thickness divided by the cell wall thickness of the integument cell, which was used as an internal control to account for the within ovule cell wall thickness. In both cases the same pattern is present, the *lre-7/lre-7* ovules have more variation in cell wall thickness than present in the wild type. The relative thickness accounts for some of the within ovule variation in cell wall thickness, thus the pattern in the data is clearer in the relative cell wall thickness. The transverse lines in the middle of the boxplot, indicate the sample median, the upper and lower edges of the boxplot are the 25$^{th}$ and 75$^{th}$ quartile. Central Cell (CC), Egg Cells (EC), Mitochondria (m), Nucleus (n), Synergid Cell (SC), Vacuole (V). Raw thickness: WT: (Maximum excluding outliers= 360 nm, minimum excluding outliers= 94 nm, median= 171 nm, n= 6). *lre-7/lre-7*: (Maximum excluding outliers= 1276 nm, minimum excluding outliers= 118 nm, median= 619 nm, n= 7). Relative thickness: WT: (Maximum excluding outliers= 13, minimum excluding outliers= 1, median= 9, n= 6). *lre-7/lre-7*: (Maximum excluding outliers= 56, minimum excluding outliers= 0, median= 6, n= 7). The scale bar is 10 microns.

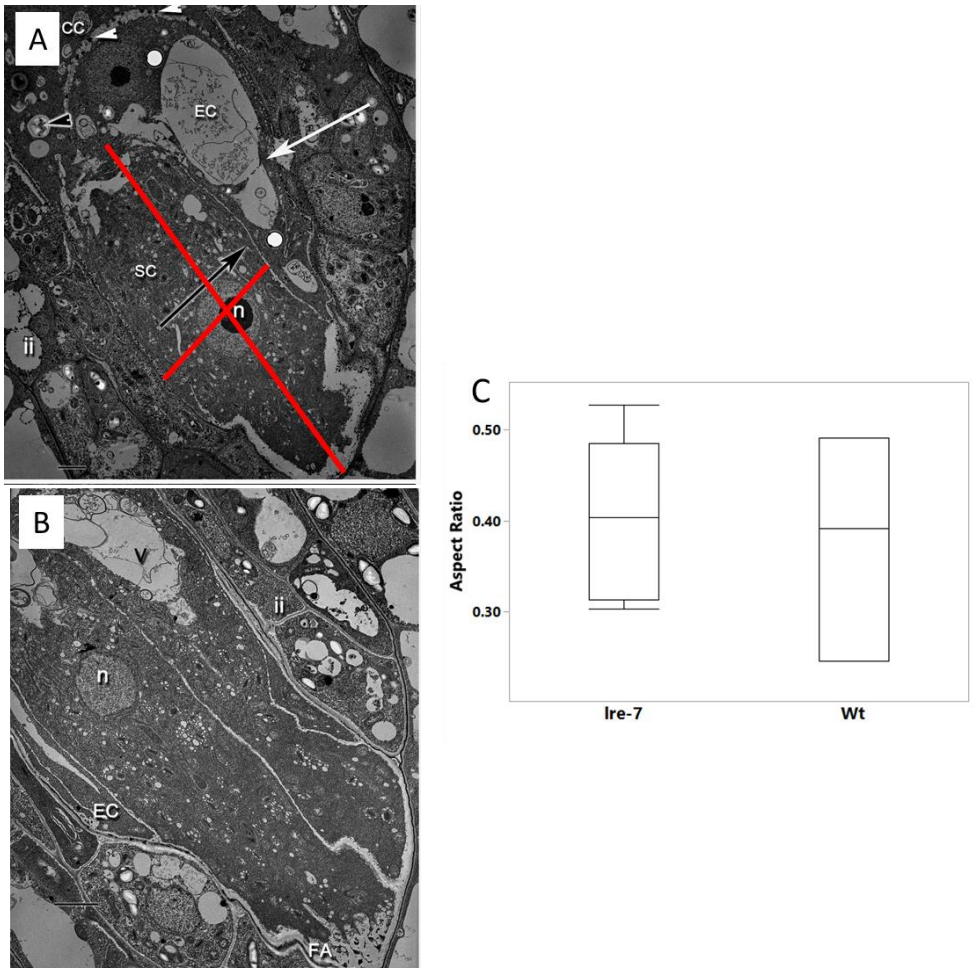


Figure 3. 7 The aspect ratio of the synergid cells. Micrographs of synergid cells with A) higher aspect ratio, which is more boxy in shape, and B) synergid cells that are more elongated. C) Boxplots of synergid cell aspect ratios. In general, the *lre-7/lre-7* sample data seems to be closer to the 1:1 ratio indicating that *lre-7/lre-7* synergid cells have a more boxy appearance. The transverse lines in the middle of the boxplot, indicate the sample median, the upper and lower edges of the boxplot are the 25$^{th}$ and 75$^{th}$ quartile. Central Cell (CC), Egg Cells (EC), Mitochondria (m), Nucleus (n), Synergid Cell (SC), Vacuole (V), Filiform Apparatus (FA), Inner Integument (ii). Starch (black arrowheads), Electron dense circular structures in the plasmalemma of the egg cell (white arrowheads), Plasmalemma (black arrow), Synergid Hooks (white arrow). WT Aspect ratio: WT: (Maximum excluding outliers= 0.49, minimum excluding outliers= 0.25, median= 0.39, n= 3). *lre-7/lre-7*: (Maximum excluding outliers= 0.53, minimum excluding outliers= 0.30, median= 0.40, n= 6). The scale bar is 10 microns.

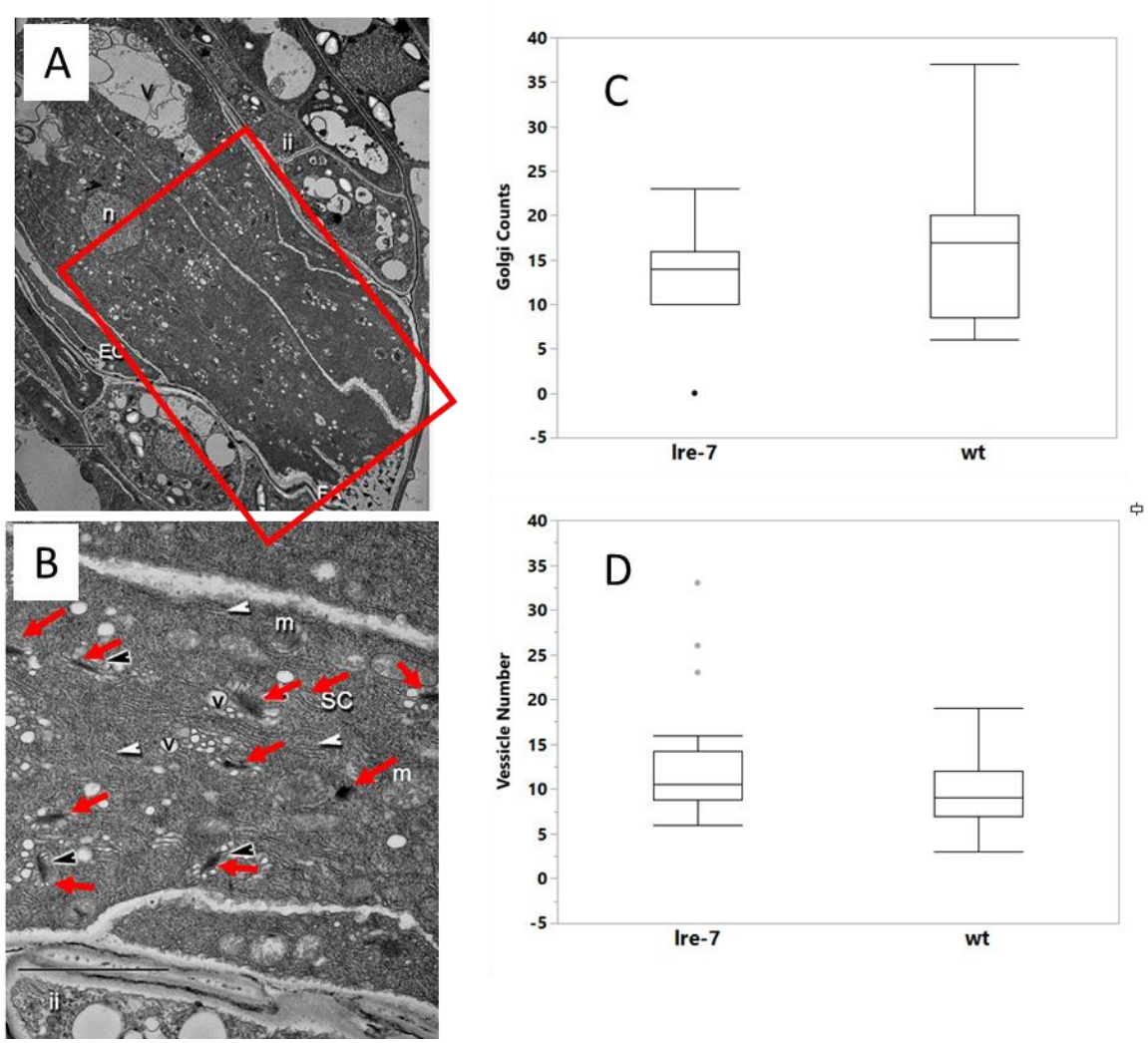


Figure 3. 8 Analyses for the endomembrane system in the synergid cytoplasm. Micrographs of the synergid cytoplasm showing that A) the counts took place in the area between the filiform apparatus and the nucleus and B) the Golgi bodies present in the cytoplasm of the synergid cell. Boxplots showing the C) Golgi body counts and D) vesicle number for vesicles associated with the Golgi bodies. The *lre-7/lre-7* Golgi counts fall within the range observed for the wild type Golgi counts. The *lre-7/lre-7* vesicle numbers for Golgi bodies fall within the range of vesicle numbers, however a portion of the of the *lre-7/lre-7* sample data is above the 75% quartile of the wild type sample data. The transverse lines in the middle of the boxplot, indicate the sample median, the upper and lower edges of the boxplot are the 25$^{th}$ and 75$^{th}$ quartile. There are three outliers that have vesicle numbers that are beyond the 90% confidence intervals. Mitochondria (m), Synergid Cell (SC), Vesicle (v), Endoplasmic Reticulum (white arrowheads). Golgi Body count (red arrows) at the micropylar end of the synergid cell (red box); WT: (Maximum excluding outliers= 37, minimum excluding outliers= 6 nm, median= 17 nm, n= 13). *lre-7/lre-7*: (Maximum excluding outliers= 19 nm, minimum excluding outliers= 3 nm, median= 9 nm, n= 7). Vesicle number around Golgi bodies (Black Arrowheads); WT: (Maximum excluding outliers= 16 vesicles/Golgi body, minimum excluding outliers= 6 vesicles/Golgi body, median= 9 vesicles/Golgi body, n= 73 Golgi bodies). *lre-7/lre-7*: (Maximum excluding outliers= 16 vesicles/Golgi body, minimum excluding outliers=6 vesicles/Golgi body, median= 11 vesicles/Golgi body, n= 73 Golgi bodies). The scale bar is 10 microns.

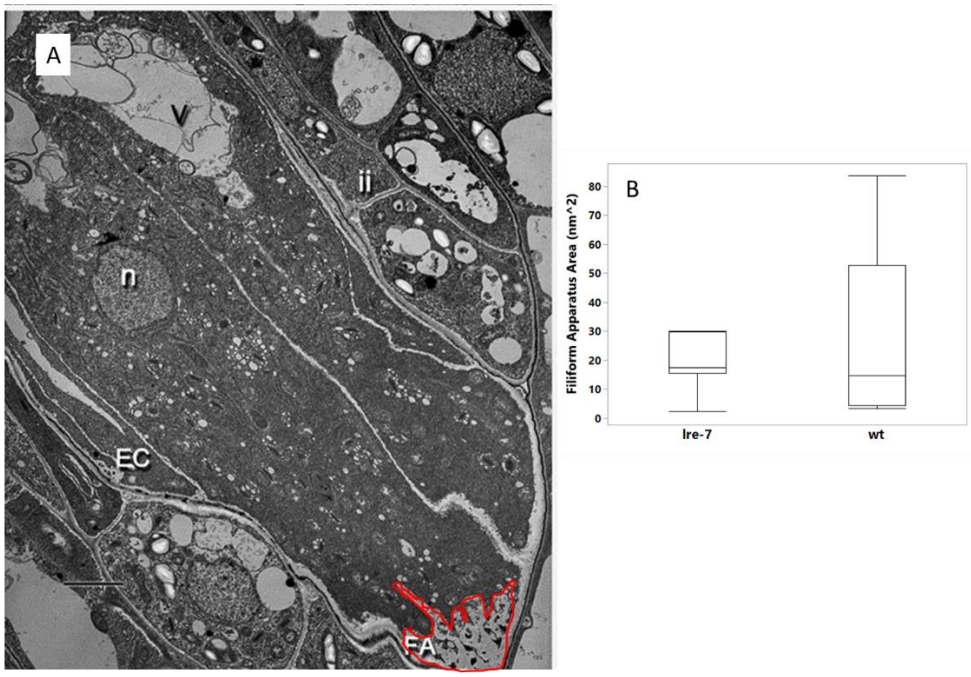


Figure 3. 9 Transmission electron micrographs of the filiform apparatus area that is outlined in red in A) and B) boxplots of the filiform apparatus area in the *lre-7/lre-7* and the wild type. The *lre-7/lre-7* filiform apparatus area is found at the lower end of what is observed in the wild type sample distribution. The transverse lines in the middle of the boxplot, indicate the sample median, the upper and lower edges of the boxplot are the 25$^{th}$ and 75$^{th}$ quartile. Egg cells (EC), Filiform Apparatus (FA), Inner Integument (ii), Nucleus (n), Vacuole (V). WT: (Maximum excluding outliers= 84 nm$^2$, minimum excluding outliers= 4 nm$^2$, median= 15 nm$^2$, n=11). *lre-7/lre-7*: (Maximum excluding outliers= 30 nm$^2$, minimum excluding outliers= 2 nm$^2$, median= 17 nm$^2$, n=17). The scale bar is 10 microns.

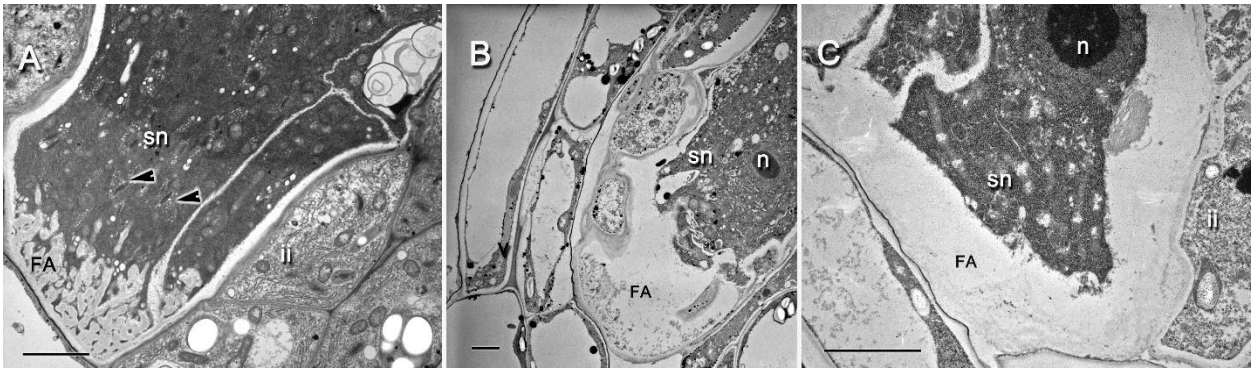


Figure 3. 10 Electron micrographs showing the typing of the convolutions in the filiform apparatus that increase the surface area. A) is a representative example of a type 3 phenotype with normal convolutions, B) is a type 2 phenotype filiform apparatus with reduced convolutions, and C) is a type 1 phenotype filiform apparatus with no convolutions, which is often accompanied by a thickening of the cell wall. There are more of the type 3 phenotypes with a normal filiform apparatus in the wild type, while *lre-7/lre-7* have a higher proportion of the type 1 and type 2 convolutions. Filiform apparatus (FA), Inner Integument (ii), nucleus (n), synergid cell (sn). The scale bar is 10 microns.

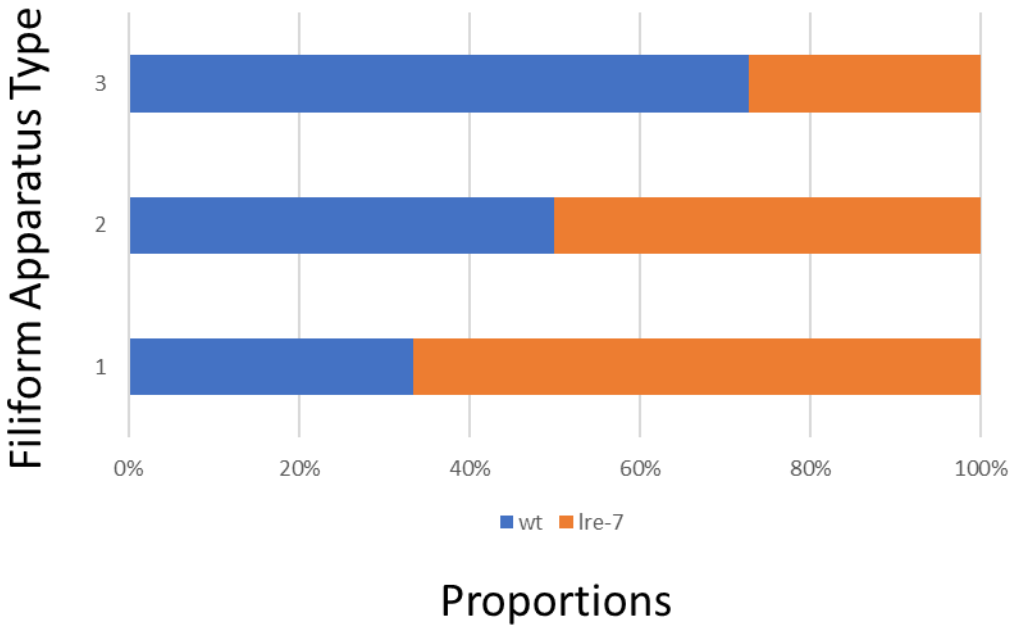


Figure 3. 11 Results from the typing of the filiform apparatus using the types identified in the previous figure 3.10. The wild type (blue) has the highest proportion of normal, type 3, convolutions, while the *lre-7/lre-7* (orange) has the highest proportion of the abnormal type 1, with severely reduced or absent convolutions. WT: (n=12); *lre-7/lre-7*: (n=7).

# CHAPTER 4: Immunogold localization

## ABSTRACT

In order to better understand the function of LRE during development, it was necessary to determine the localization of the LRE protein. Previous studies have used confocal studies to determine that LRE is localized to the synergid cells and was present in both the cytoplasm and the filiform apparatus. Since the filiform apparatus was an important structure that was important for LRE localization, several antibodies for cell wall components were used to understand the composition of the filiform apparatus cell wall. The objective of this study was 1) determine the localization of LRE with greater resolution, and 2) determine some of the components in the cell wall composition of the filiform apparatus. These results indicated that a majority of the LRE protein localizes to the filiform apparatus cell wall. One of the major cell wall components that localized to the filiform apparatus was arabinogalactan, also known as Gum Arabic, which can be involved in intercellular signaling indicating that the filiform apparatus is an important structure for signaling. This was also the first study to show that cell wall components were localizing to the plasmalemma region of the egg cell. This study showed that LRE and other cell wall components that were important for cell signaling were present at the filiform apparatus cell wall.

## INTRODUCTION

In the previous chapter differences in cell wall thickenings were noted between some of the cells in WT and *lre-7/lre-7* embryo sacs. Thus, the goal of this chapter was two-fold. First, to quantify the location of the LRE and distribution of the cell wall components. This was

particularly important for the filiform apparatus and the egg cell. Mansfield et al. (1991) described the filiform apparatus as a thickening of the cell wall based on his observations, however there was no immunogold labeling with antibodies for cell wall components to confirm this. Another phenotype that was noted in the *lre-7/lre-7* mutant was a thickening of the egg cell wall. The cell wall around the egg was previously described in the literature (Mansfield et al., 1991) as a plasmalemma, not as a standard cell wall. Therefore, it was of interest to know if there were, in fact, cell wall components associated with the egg cell plasmalemma.

One goal of this study was to determine what the distribution of LRE was within the embryo sac at a finer resolution than is possible with confocal microscopy. Since cell wall defects were found in cells were no LRE was detected in previous light microscopy studies, it was necessary to look at the distribution of LRE at higher resolution than was possible with light microscopy. It should be noted that if the LRE it weak in some cells, it could have been indistinguishable from background labeling and, therefore, would have been undetectable with our approach. The limitations of immunogold labeling were different than the limitations of other approaches with light microscopy. For example, confocal microscopy indicated that there was a large percentage of the light intensity coming from the synergid cytoplasm which should be confirmed with another approach. Due to the point spread function and the low axial resolution of confocal light microscopy it was possible that in areas with high amounts of fluorescence intensity the amount of LRE is underestimated. In areas of lower density of LRE the light from a single fluorophore could have been overestimated due to the point spread

function. Since a weak signal would theoretically be amplified by fluorescence microscopy, it was necessary to confirm these findings with EM immunogold labeling techniques.

## Hypothesis

We hypothesized that ~50% of the LRE in synergid cells localized to the filiform apparatus and ~50% localized to the cytoplasm. Previous studies have shown that LRE localizes to the filiform apparatus and it was also located intracellularly, where it has a role in chaperoning FER from the ER to the synergids (Li et al., 2016; Liu et al., 2016). The GPI domain has an important role in localizing the LRE to the filiform apparatus, but this domain was not required for LRE function.

## Methods

*Plant care:*

Plant growth conditions were largely the same as reported in Chapter 2, with the following modifications. The LRE lines were obtained from the Palanivelu lab at the School of Plant Sciences, University of Arizona, Tucson, AZ. The seeds were surface sterilized and germinated on agar plates with antibiotic selection (*lre-7*: Basta at a final concentration of 10µg/ml or YFP-LRE: Basta at a final concentration of 10µg/ml together with hygromycin at a final concentration of 20µg/ml) to maintain the YFP fusion protein. Next the seeds were stratified at 4˚C for 2-3 days. The seeds were transferred to the growth chamber at 20˚C with a 16:8 light dark cycle for 7-10 days. After the seeds germinated, resistant seedlings were transplanted into soil (Metro 360 soil mix) and grown under the same conditions as the Colombia WT line. The LRE-YFP line were screened under confocal microscopy to confirm that

YFP was being expressed in the filiform apparatus where LRE expression was reported in this line.

*TEM sample preparation for immunogold localization:*

Fixation of plant tissue for transmission electron microscopy was modified from Holdorf et al. (2012). Flowers were emasculated at the floral stage 12 before the anthers contain mature pollen grains. Unpollinated ovules were removed from the carpels with a fine needle, 12-20 hours after emasculation. For the fixation, washes, and post-fixation steps the ovules were placed in cell strainer baskets (Falcon 352350) from which the tabs were removed so that they fit inside six-well plates (Falcon 353046). Ovules were immersed in fixative [Either Trumps fixative (4% EM grade paraformaldehyde, 0.1M HEPES buffer pH 7.2, .020% Triton X-100, 1% EM grade glutaraldehyde) or 2.5% EM grade glutaraldehyde v/v, 0.02% Triton X-100 v/v, 0.1 M HEPES, pH7.2] overnight at room temperature. Next the ovules were washed several times (3-5 times for 15 min each) with distilled water before being placed in the secondary fixative (1% uranyl acetate w/v in distilled water) for three days at room temperature. For embedding the ovules in agar, the ovules were arranged on a pad of solidified 4% agar, encased with a top layer of molten 4% agar, and allowed to cool to room temperature. Cubes of agar containing individual ovules were cut out of the agar. Samples embedded in agar cubes were dehydrated through a graded acetone or ethanol series (10%, 20%, 30%, 40%, 50%, 60%, 70%, 80%, 90%, 100%, 100%, 100%). These ovules were allowed to equilibrate for at least 1 hour at each step in the series, with the exception of the 100%. At this point three changes of 100% acetone or ethanol were made over a two-hour interval.

Ovules were infiltrated with either the slow or fast infiltration procedure (based on the methods of McDonald (2014). The slow infiltration procedure was as follows: the samples were then infiltrated with increasing concentrations of Hard Grade LR White resin in acetone (20%, 40%, 60%, 80%, 100%). Samples were allowed to remain at each step for a minimum of 3 hours. Samples were left in 100% resin for at least two days for complete infiltration. Ovules were placed in flat embedding between two foil dishes and polymerized at 50˚C for 48 hours.

The fast infiltration procedure has the following modifications based on McDonald (2014). The ovules were not embedded in agar. After the ethanol dehydration, samples were transferred to 1.8 ml microfuge tubes containing the LR white dilutions. For each dilution the microfuge tubes were spun at 6,000 rpm (2,000g) for 30 seconds and was repeated for each step of the infiltration. For polymerization, the ovules were transferred to an Aclar imbedding mold [glass like slide with a piece of Aclar (50 x 30mm) that was taped down with a circular well that was created by a 13 mm Secure Seal (EMS cat. # 70327-13S). Then a second piece of Aclar (40 x 25 mm) was placed on top of the well. Ovules were polymerized at 100˚C oven for two hours. In order to exclude oxygen from the oven, 100 mL of liquid nitrogen in a beaker was placed in the oven at the same time as the samples. After the polymerization was complete, the samples were allowed to cool, and then individual ovules were cut out and glued (Devcon 2 Ton Epoxy 5E157) to blocks. The glue was allowed to cure for at least 24 hours before the block was trimmed.

*Immunogold labeling*

Semi-thin sections (0.5 microns thick) were examined and stained with Azure B to determine the location in the ovule. Once the egg sac was reached, ultrathin sections (60-90

nm thick) were cut and placed on Pelco 200 mesh Ni TEM or SPI 150 mesh Hexagonal grids without support films. Sections were incubated in blocking solution (PBS pH7.4, 0.02% Tween, 0.02% Sodium Azide, 5% Milk) for 45 min. The primary antibody was diluted in blocking solution according to Table 4.1, and the grids with sections were incubated in drops in a hydration chamber overnight at 4˚C. Grids were then washed 5 times for 10 min each in the blocking solution before they were transferred to the appropriate secondary antibody conjugated to gold nanoparticles (Table 4.2) which was diluted in the antibody buffer (20nM Tris pH 8.2, 154 nM NaCl, 1% BSA, 0.02% Sodium Azide). Sections were rinsed in antibody buffer 5 times for 10 min each, then once with once in PBS, before being transferred to 2% aqueous glutaraldehyde for 5 min at room temperature. After this the sections were rinsed with distilled water 5 times for 10 minutes each and then were allowed to dry overnight on filter paper. Many of the sections on grids were also lightly carbon coated in the carbon evaporator to increase the stability of the LR White sections. A few sections were stained with uranyl acetate and/or Reynold's Lead Citrate to increase image contrast, however it was found that automated particle counts using ImageJ did not always work as well on images captured from sections that had been counter stained, therefore the majority of sections were imaged without staining. Sections were imaged with a Hitachi H-600 TEM operating at 75kV. Micrographs were captured on Kodak 4489 film and, following development, digital images were acquired from the negatives using an Epson Perfection V750 Pro scanner. For nanoparticle quantification images were taken at 20,000x and the number of nanoparticles per image were quantified with ImageJ using the particle counter tool (Figure 4.9). Whenever possible three micrographs of each cell

type within an ovule were counted. Statistical analyses were conducted in either R or JMP 14 statistical software. All graphs were constructed in JMP 14 statistical software.

## Results

Results from this part of the study provided insights into the localization of LRE and revealed the composition of some of the walls that surrounded embryo sac cells, such as the egg cell and the filiform apparatus, which was previously unknown. The composition of the filiform apparatus cell wall components differed from that of those in the middle lamellae. The distribution of the LRE in the synergid cells was also different than was previously found in other studies.

### *Cell wall antibody labeling*

Although the literature presumes that the filiform apparatus was a modified cell wall because it appeared very similar to other plant cell walls when viewed by transmission electron microscopy, this had not been confirmed and it was unknown if the composition of the cell wall components in the filiform apparatus was the same as that of other cell walls within the ovule. During this study it was confirmed that there was a high density of JIM 13-positive cell wall components in the filiform apparatus and the synergid cytoplasm (Figures 4.1-4.5). For the filiform apparatus the median counts were 1742 nanoparticles per image area taken at 20x, the synergid cytoplasm was 1877 nanoparticles per image area, antipodal were 55 nanoparticles per image area, and the integument cells were 95 nanoparticles per image area (Figure 4.2). Localization experiments using the homogalacturonan antibody that is specific for partially methyl-esterified pectin, JIM 7, was very clean, with little or no labeling in the filiform apparatus, whereas the inner integument cells were densely labeled (Figure 4.3). It was found

that in the wall surrounding integument cells the area with the highest concentration of homogalacturonan labeling (JIM 7) was in the middle lamella (Figure 4.1).

In the egg cell there was some labeling with JIM 13 (which has a high labeling density in the filiform apparatus) around the edges of the egg cell wall, however there was no JIM 13 labeling in the cell wall thickening at the apex of the egg cell (Figure 4.4). This indicated that there were cell wall components near the plasmalemma of the egg cell, however the composition of those cell wall components appeared to be different than that of the filiform apparatus.

*LRE localization*

The highest concentration of LRE protein was detected in the filiform apparatus region, with a median of 1066 nanoparticles from micrographs taken of the filiform apparatus, whereas the median particle counts from micrographs of the synergid cytoplasm was 20 nanoparticles (Figures 4.6-4.7). The labeling densities in the antipodal and integument cells overlapped with the labeling density of the filiform apparatus secondary antibody controls, so if there was a low amount of LRE signal in the cytoplasm, it should have been indistinguishable from background labeling with our sampling methods. In addition, it was also possible that the puncta visible with confocal microscopy maximum projections were in large aggregations in distinct regions that were simply not present in those specific sections that we examined, thus it was not able to detect these aggregations. So either A) the maximum projections of the confocal data did not yield an accurate estimate of the distribution of the LRE because of the limitations of the sampling methods, or B) the high resolution images in the standard TEM sections only provided information about a section through the three-dimensional object and information not

contained in the plane of the section was lost. In this instance a three-dimensional TEM reconstruction could be used to clarify the discrepancy between the estimates collected by these two different approaches. It was possible that the confocal data could be used as the maximum estimate of the distribution of the LRE that could be present in the cytoplasm and the TEM data could be used as a minimum estimate for the potential LRE distribution in the cytoplasm. In both cases more than a majority of the LRE was accumulating in the filiform apparatus cell wall, thus it is possible that LRE was functioning in the FER pathway.

# CHAPTER 4 TABLES

Table 4. 1 Primary antibody list with dilutions, target, and vendor. All but the last antibody in the table, anti-GFP, are from the Carbosource Services, University of Georgia, for the cell wall carbohydrates, including John Innes Monoclonal (JIM) antibodies, JIM 7 and JIM 13. Since several of the JIM antibodies label the same cell wall components, data analysis was done on labeling with the JIM7, JIM 13, and Torry Pines anti-GFP antibodies.

| 1˚ Antibody | Type | Animal | Dilution | Type | Target | Vendor |
|---|---|---|---|---|---|---|
| CCRC-M38 | IgG1 | Mouse | no dilution | Monoclonal | Homogalacturonan | CarboSource Services |
| JIM 5 | IgG2a | Rat | 1:10 | Monoclonal | Homogalacturonan (partially methyl-esterified) | CarboSource Services |
| JIM 7 | IgA | Rat | 1:10 | Monoclonal | Homogalacturonan (partially methyl-esterified) | CarboSource Services |
| JIM 8 | IgG2a | Rat | 1:10 | Monoclonal | Arabinogalactan | CarboSource Services |
| JIM 13 | IgM | Rat | 1:10 | Monoclonal | Arabinogalactan | CarboSource Services |
| MAC 207 | IgM | Rat | no dilution | Monoclonal | Peribacteroid Membrane | CarboSource Services |
| Anti-GFP | IgG | Rabbit | 1:100 | Polyclonal | GFP | Torry Pines Biolabs-TP401 |

Table 4. 2 Sec Secondary antibody list with gold nanoparticle size, dilutions, target, and vendor. Most of these antibodies are conjugated to a 10nm gold nanoparticle, with the exception of 12nm gold IgM.

| 2˚ Antibody | Dilution | Type | Vendor |
|---|---|---|---|
| 10nm gold IgG | 1:50 | Goat anti-Mouse | BBInternational |
| 10nm gold IgG | 1:50 | Goat anti-Rat | BBInternational |
| 12nm gold IgM | 1:50 | Goat anti-Rat | Jackson ImmunoResearch Laboratories |
| 10nm gold IgG | 1:50 | Goat anti-Rabbit | BBInternational |

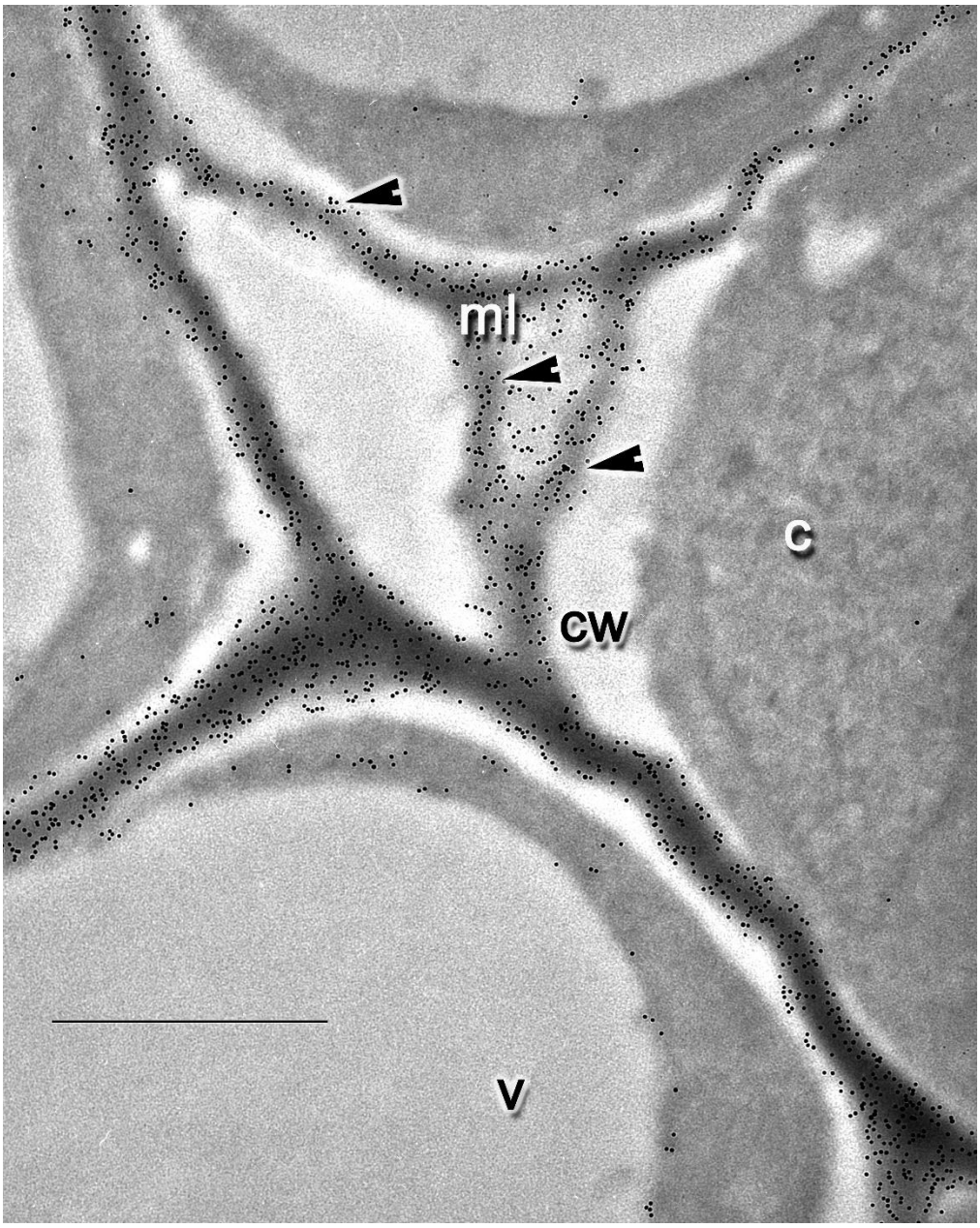


Figure 4. 1 An example of JIM 7 labeling (arrow heads) on leaf cells is concentrated in the middle lamellae. JIM 7 labels partially methyl-esterified homogalacturonan, which is important for the compliancy of the cell wall. Cell Wall (CW), Cell Body (C), Middle Lamellae (ml), Vacuole (V). The scale bar is 5 microns.

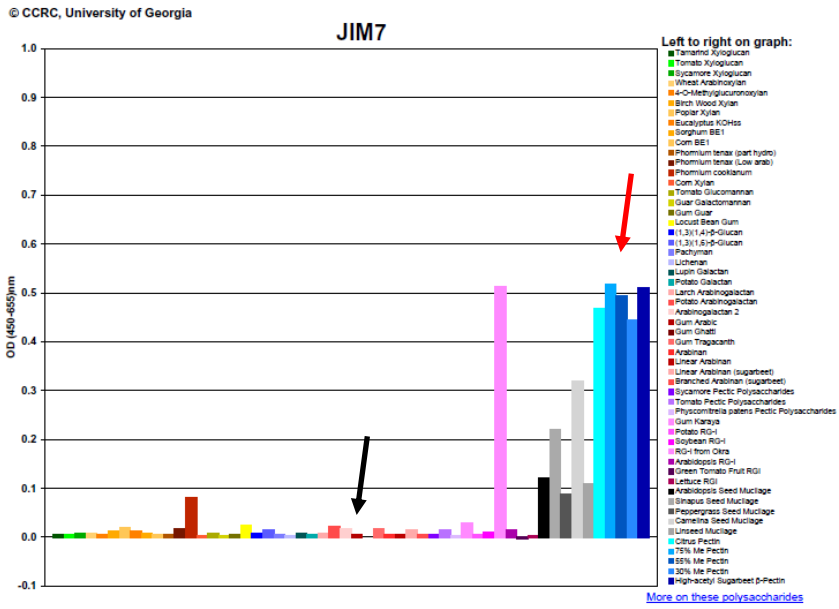


Figure 4. 2 JIM 7 labeling affinities of different cell wall components. The major cell wall component this antibody labels is pectin (Red Arrow), however it does cross react with some other cell wall components in other species. There is low cross reactivity with Gum Arabic (Black Arrow) which is labeled by JIM 13 (see figure 4.6), thus JIM 7 and JIM 13 are labeling different cell wall components. From CCRC website.

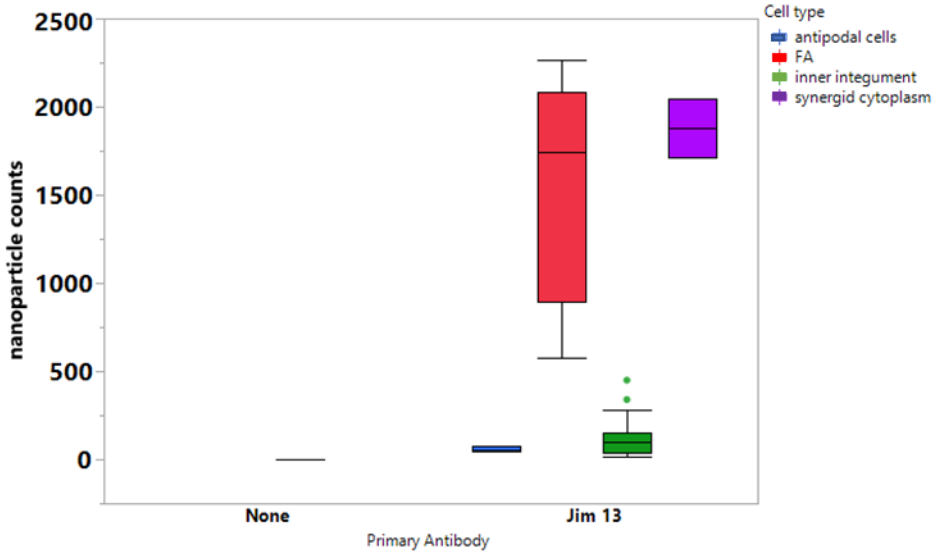


Figure 4. 3 Jim 13 labeling densities on various cell types. The filiform apparatus (red) and the synergid cytoplasm (purple) has the highest labeling densities. The inner integuments have a low labeling density but it is still higher than the Anti-Rat, secondary only control in filiform apparatus tissue. There is some labeling detected in the antipodal cells (blue), however it is extremely low and only slightly higher than the background labeling. Anti-Rat secondary only: (median= 10 nanoparticles/image). Jim 13: (median for antipodal cells= 56 nanoparticles/image, median for inner integument =95 nanoparticles/image, median for synergid cytoplasm= 1877 nanoparticles/image, median for filiform apparatus = 1742 nanoparticles/image, n= 6). The scale bar is 10 microns.

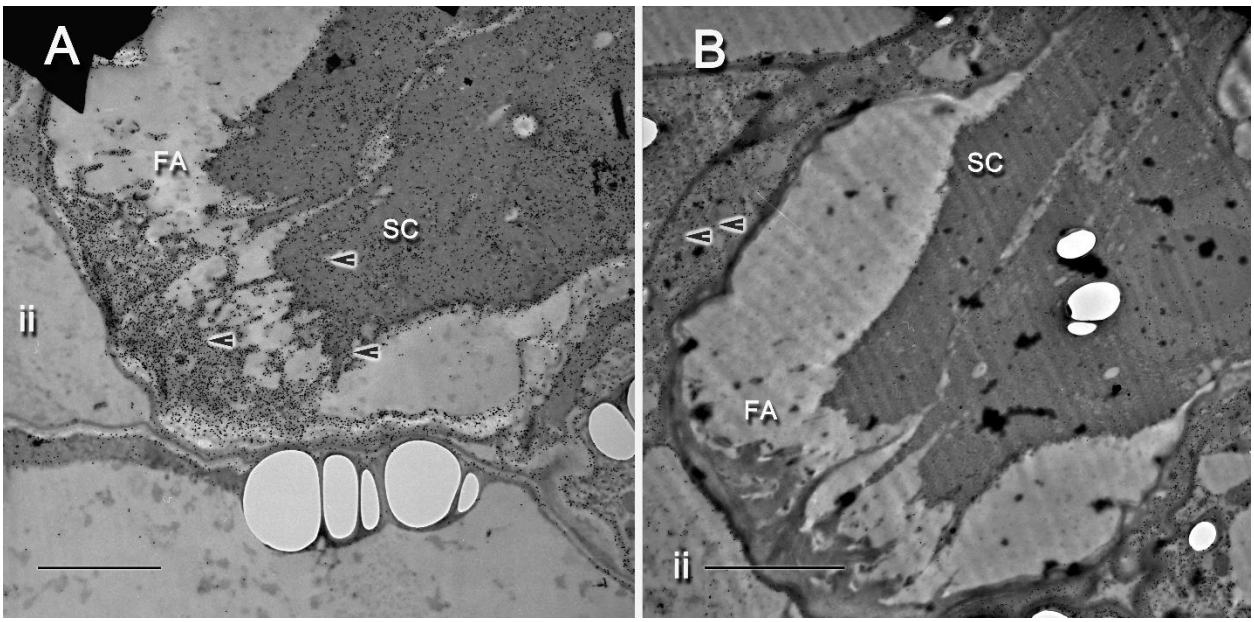


Figure 4. 4 Electron micrograph of A) JIM 13 and B) JIM 7 immunogold labeling (arrow heads) in the filiform apparatus of a WT ovule. The JIM 13 antibody, which labels arabinogalactan, a major component of Gum Arabic, has heavy labeling in the filiform apparatus. Arabinogalactan has two different functions, 1) as an intercellular signaling molecule and 2) as glue to seal plant wounds. Thus, it is not surprising that there is heavy labeling at the filiform apparatus which is thought to be important for intercellular communication. Filiform Apparatus (FA), Inner Integument, Synergid Cell (SC). The scale bar is 10 microns.

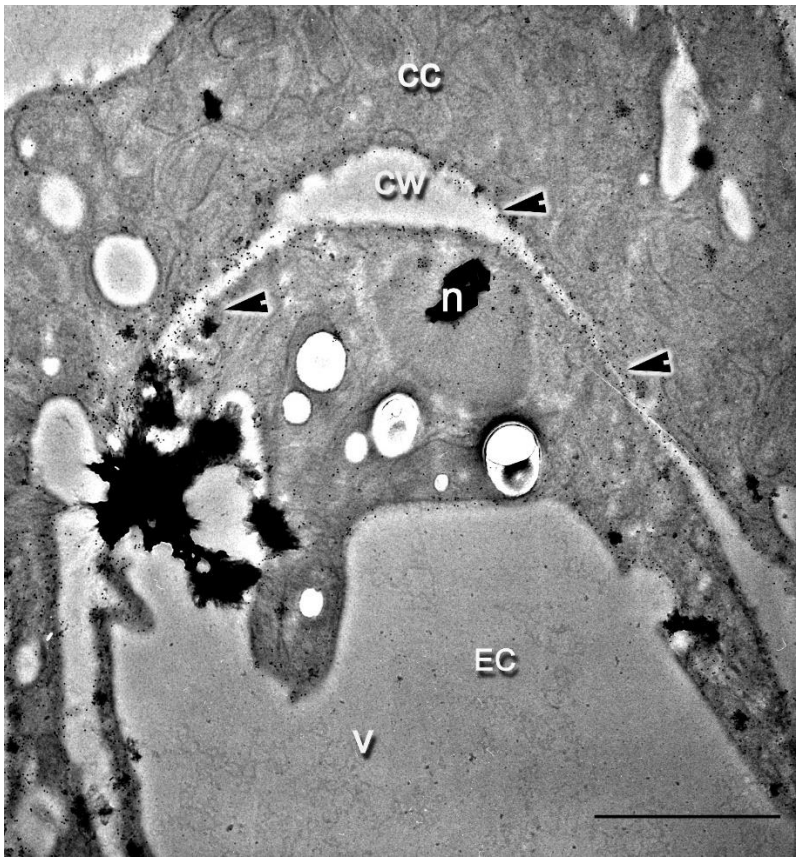


Figure 4. 5 TEM micrograph of JIM 13 labeling (arrow heads) on the egg cell. This confirms that the egg cell has cell wall components in addition to the plasmalemma. The JIM 13 antibody, which labels arabinogalactan, is a major component of gum Arabic. Arabinogalactan has two different functions, 1) as an intercellular signaling molecule and 2) as glue to seal plant wounds. In this context it is likely that the arabinogalactan could be important for intercellular signaling. Central Cell (CC), Cell Wall (cw), Egg Cell (EC), Nucleus (n), Vacuole (V). The scale bar is 10 microns.

starch (black arrowheads), electron dense circular structures in the plasmalemma of the egg cell (white arrowheads), plasmalemma (black arrow), synergid hooks (white arrow

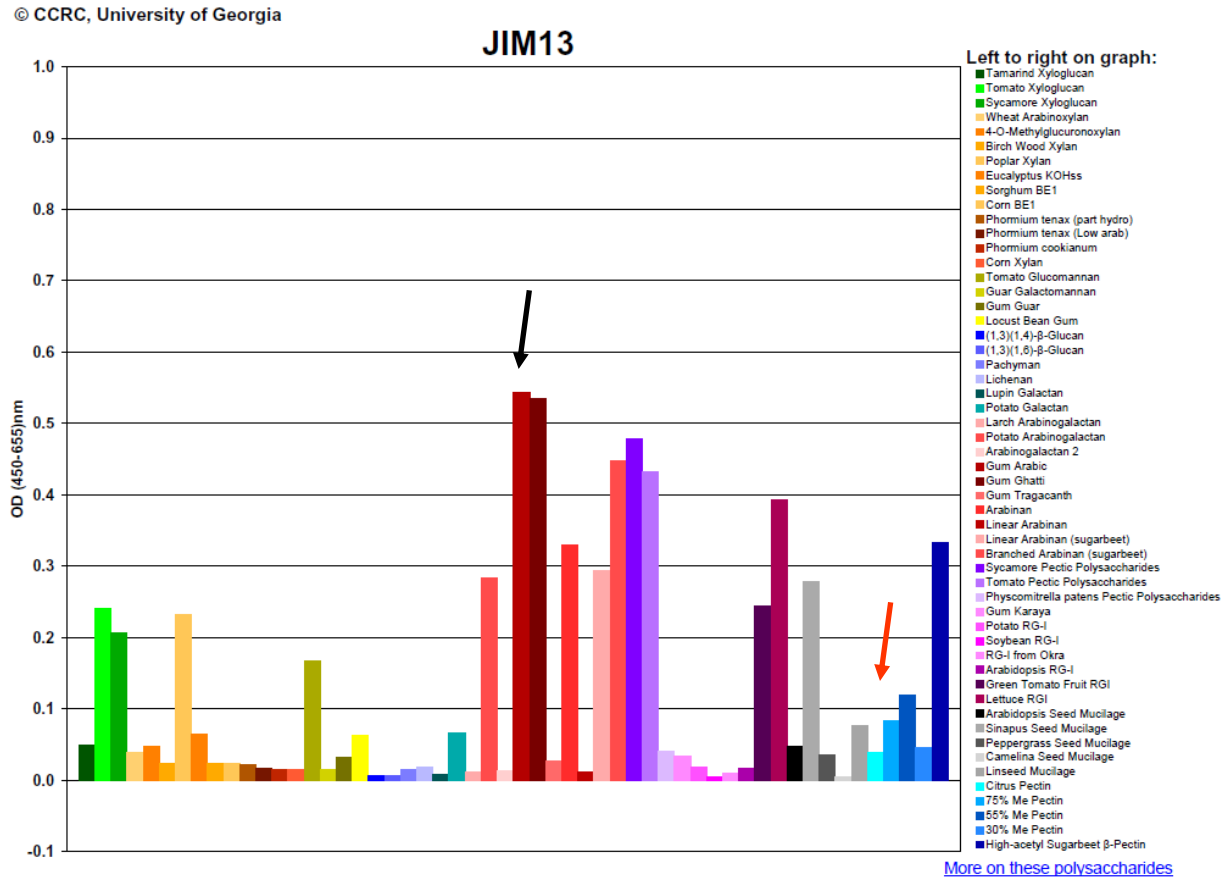


Figure 4. 6 JIM 13 labeling affinities of different cell wall components. The major cell wall component this antibody labels is Gum Arabic (Black Arrow), however it does cross react with some other cell wall components in other species. There is low cross reactivity with pectin (Red Arrow), thus JIM 7 and JIM 13 are labeling different cell wall components. From CCRC website.

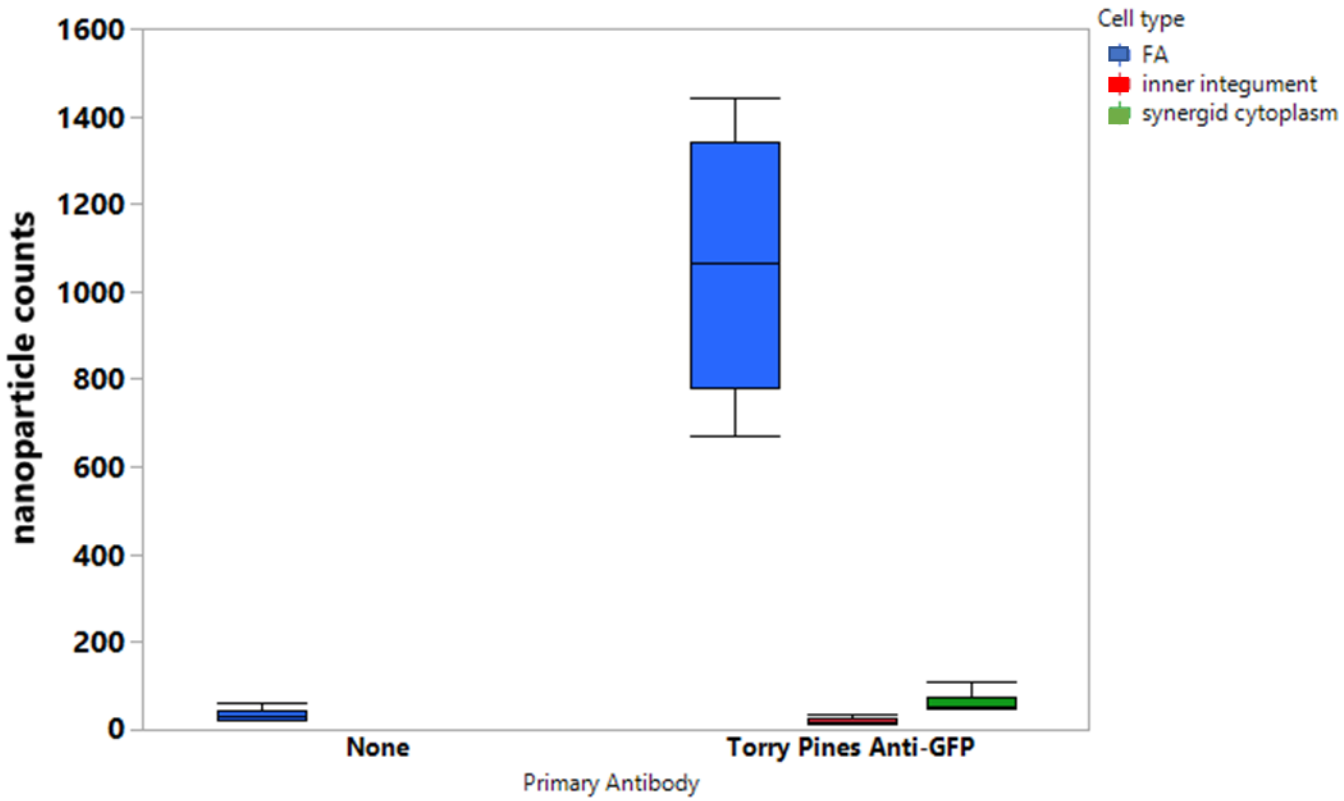


Figure 4. 7 Anti-GFP labeling densities from the GFP reporters in the LRE-YFP/*lre-7* lines. The filiform apparatus (blue) had the highest labeling densities. Both the inner integument, the synergid cytoplasm, and the anti-Rabbit secondary only control had low labeling densities in filiform apparatus tissue. Anti-Rabbit secondary only: (median= 31 nanoparticles/image). Torry Pines anti-GFP: (median for inner integument = 20 nanoparticles/image, median for synergid cytoplasm= 54 nanoparticles/image, median for filiform apparatus = 1066 nanoparticles/image, n= 6).

f

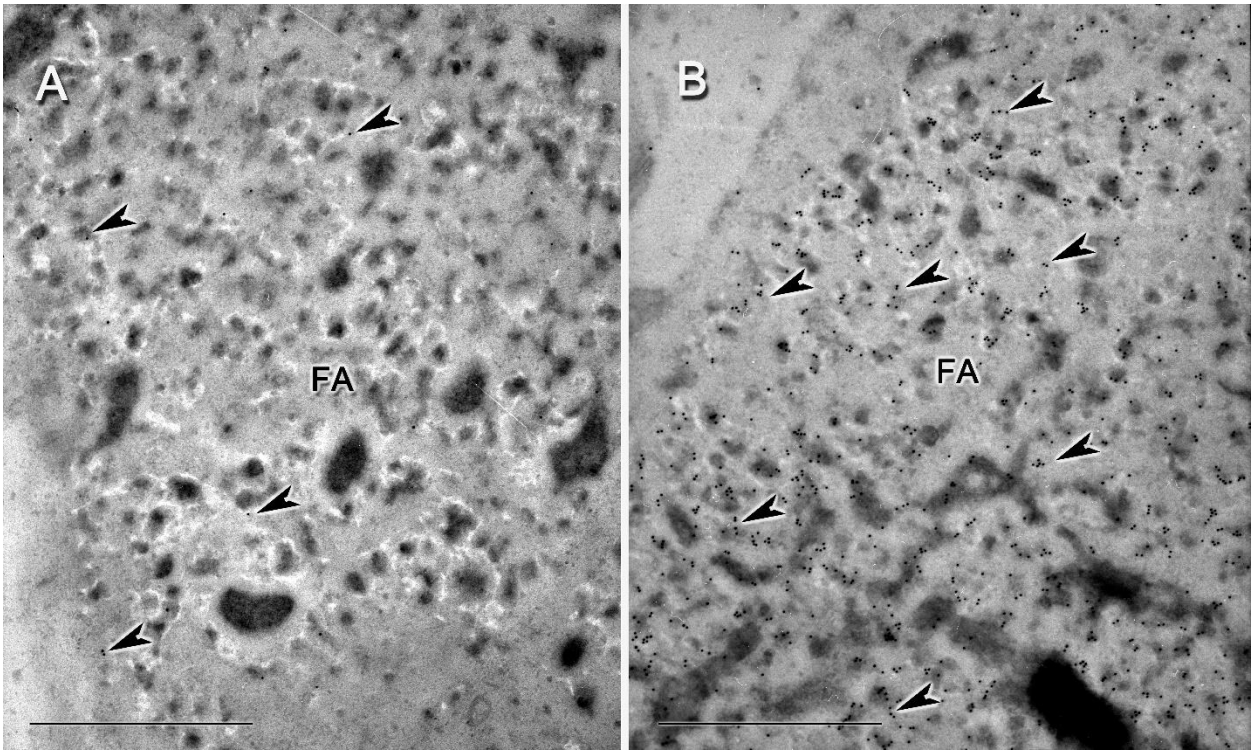


Figure 4. 8 Electron micrographs for the anti-GFP immunogold labeling in the Filiform Apparatus of the Synergid Cells. Background labeling is shown for the A) secondary only negative control and the labeling with the B) primary anti-GFP labeling. The background labeling was very low as compared to the high labeling densities on tissue that had the primary anti-GFP antibody. Immunogold labeling (arrow heads), and filiform apparatus (FA). The scale bar is 5 microns.

# Chapter 5: Conclusions and future directions

This study was a thorough and extensive study of *Arabidopsis* ovule ultrastructure, with the goal of better understanding the role of LRE in plant sexual reproduction. Since other studies had already shown that LRE was important for reproduction, the next step was to understand how LRE functions at the cellular and molecular level to produce the abnormalities in reproduction that were observed in null mutant lines. The next immediate big picture questions that should be understood are whether LRE acts in the FER pathway, does it have a novel function, or is it a combination of the two? The purpose of this study was to determine if there was any ultrastructural evidence that would help determine the direction of future studies. The evidence collected from this study was consistent with LRE acting through the FER pathway. This conclusion was based on 1) ultrastructural defects in the cell wall and 2) the use of higher resolution techniques to understand the localization of LRE, showing that it disproportionally localizes to the filiform apparatus.

This was the first study that was able to detect defects in the cell walls of the embryo sac in *lre-7/lre-7*, as well as resolving some of the unanswered questions that arose during previous studies on LRE. It is known from these studies that other LORELEI-like proteins can form co-receptors with FER and influence cell wall growth in the context of root and leaf development (Li et al., 2016), however this was the first study that has demonstrated that *lre-7/ lre-7* may have either direct or indirect effects on cell walls, and thus the development and growth of the embryo sac. This study suggested that in addition to the immediate impacts that the LRE protein can have on pollen tube reception, there were potentially indirect long term

effects that LRE could have on the cell wall ultrastructure which would impact the pollen tube reception such as 1) a reduction in the surface area of the filiform apparatus and 2) a generalized thickening of other cell wall structures throughout the embryo sac. Both of these ultrastructural cell wall defects could have been the result of a de-localization of ROS signaling that occurs due to a disruption in the FER pathway and will be discussed in more detail below.

This study clarified the localization of LRE with a precision that was unattainable with the resolution of light microscopy. Confocal data indicated that there was a larger portion of the LRE that was localizing to the synergid cytoplasm, however with immunogold labeling we found that the majority was localized to the filiform apparatus. This would make sense if LRE was acting in the FER pathway. It was found that, when in the cytoplasm, LRE appeared to localize to vacuoles, however, there still needs to be better ultrastructural preservation to be used in conjunction with the immunogold labeling technique to get enhanced resolution of LRE localization in the synergid cytoplasm.

*WT study consistent with findings from previous ultrastructure studies on other WT accessions*

This study was able to expand upon the foundation of the WT ultrastructure that has been previously reported. In the literature there was an ultrastructural description of the embryo sac of the Landsberg erecta WT accession, but no description of the Colombia WT or WS WT ultrastructure, both of which are common WT backgrounds for transgenic studies. It was unknown how much variation there was in the embryo sac ultrastructure between the different ecotypes, thus it was important to characterize the Colombia WT ultrastructure, which was the background for the lre-7/lre-7 mutants.

Having a low sample size for the control population in ultrastructural studies was always a concern because it was possible to have missed some of the variability in the controls, and thus ultrastructural variation in the mutants could have been mistaken to have been a phenotype even though it could have been present in the control but just not seen in the samples that were observed. Due to the large amount of resources such as time and money needed for EM, however, it was not possible to get large sample sizes. Based on the findings in this study it appeared that the amount of ultrastructural variability in ovules was very low between ecotypes, thus it would have been appropriate to augment these findings by including data from other studies on WT ovule ultrastructure. These findings were further reinforced in the *lre-7/lre-7* ultrastructural studies where pooled data from the Col WT and WS accessions showed significantly less variation than was present in the homozygous null mutant *lre-7/lre-7* which were all ovules from the Col WT background. In fact, pooling data from different ecotypes should maximize the variability thus any variability found in the mutants should have been due to actual differences from the mutation, not because of not having had a large enough sample size.

This study also raised the need for more electron micrographs to be submitted as a reference library rather than just a few representative images that illustrate a point or a major finding in a study. While collection of all the baseline WT data along with the transgenic or mutant samples was ideal and was possible for a light microscopy study where large amounts of data could have been collected in a short amount of time, it was not always possible in studies where the resources are limited. We determined that the basic descriptions of Landsberg (Ler) wild type accession were consistent with the ultrastructure in Col Wt and

unknown Wt, thus it seemed appropriate to augment EM studies with data from other ecotype lines. This would maximize the variability in the baseline control data set because it would include a larger genetic variability than the *lre-7/lre-7* null mutants, thus one would expect to see more structural variability in the controls. If there were still large differences between the mutant line and the WT data which included this additional variation, one could be confident the differences were not an artifact of low sample size nor from other sources of genetic variability, but variability comes directly from the *lre-7* mutation. The variability in the WT data should have been well beyond the variability encountered in a single ecotype with carefully controlled sample preparation. These WT findings should be published as an on-line book chapter, so these micrographs can serve as a reference library for other studies.

### Developmental differences in the synergid and the egg cell

In this study, it was possible to expand on the developmental descriptions of the *Arabidopsis* embryo sac. These images of immature embryo sacs captured at the time that the polar nuclei were fusing and the stages of degeneration of the embryo sac were also documented. Polar nuclei fusion in *Arabidopsis* happened before fertilization, unlike in some species such as wheat where polar nuclear fusion occurred after the sperm has fertilized the central cell. In other studies, they have found the polar nuclei fusion early was not only a mitochondria-dependent process, it also represses programmed cell death in the antipodal cells (Kawashima and Berger, 2015). The central cell and antipodal cells may also have a link during degeneration. It is known that one protein, SYCO, was necessary for the mitochondria in the central cell to maintain their integrity (Kagi et al., 2010). If this protein was lacking, the mitochondria will loose their cristae. If the mitochondria activity was repressed in the central

cell, then the antipodal cell will undergo programmed cell death. Both of these processes, polar nuclei fusion and the synergid degeneration, were documented during this study in the WT embryo sac and appear to occurred as one would expect.

Since all of these ovules were dissected out from flowers that were roughly the same stages (12-24 hours after flowers were emasculated at the 12c stage), this study documented the amount of developmental variation found within this time frame. For the degenerating embryo sac ultrastructure, it was unknown if this was a natural process. Perhaps older unfertilized embryo sacs would not have naturally degenerated if they were not fertilized by some critical point, although this could also represent fixation artifacts because some of the ovules were not well preserved. Whatever the cause, all of the embryo sacs that were degenerating had similar characteristics in their ultrastructure and thus it was worth reporting as a reference for other studies on embryo sac ultrastructure.

Not much was known about the antipodal cells in *Arabidopsis*. This study confirmed the findings of Song et al. (2014) that antipodal cells were present in a mature embryo sac and even into the early stages of seed development. It was demonstrated that antipodal cells persist in the degenerating embryo sac (Figure 2.9). Antipodal cells in the degenerating embryo sacs had very visible mitochondria, and perhaps this was a sign of programmed cell death. In some species such as maize and rice, the antipodal cells underwent proliferation, which was unlikely to have been occurring in *Arabidopsis*. Song et al. (2014) also reported that there were three antipodal cells when they used a fluorescent reporter for nuclear localization (CDC123::H2B:YFP), however, in some of these micrographs, both in WT and *lre-7/ lre-7* micrographs, it looked like there could have been more than three (Figure 2.1). This could have

been either an artifact of the two-dimensional view produced by sectioning, or it could have been that some of the nucellus cells have an electron dense cytoplasm similar to the antipodal cells. It was previously reported that the antipodal cells in *Arabidopsis* degenerate prior to fertilization (Murgia et al., 1993), but this was reported in a starchless mutant. Our results confirmed that antipodal cells were present in the mature embryo sac in the WTs of *Arabidopsis* studied. It was unknown what role that the antipodal cells have since in most Eudicots the antipodal cells degenerate (Holloway and Friedman, 2008). It has been found that developmentally antipodal cells can adopt either a central cell or an egg cell fate if they were induced by molecular signaling (Gross-Hardt et al., 2007; Moll et al., 2008; Pagnussat et al., 2009).

This was especially important for this study because previous studies have shown that one of the phenotypes that female *lre-7/lre-7* ovules exhibit was that synergid cells may degenerate earlier than in WT (Leydon et al., 2015; Liu et al., 2016), before pollen tube reception, thus it was useful to characterize the ultrastructure of degenerating synergid cells in WT embryos. Tsukamoto et al. (2010) reported that 94.4% of the LRE/LRE pollinated embryo sacs that had a zygote had a degenerated synergid cell. In *lre-5/lre-5* they found that only 26.4% of pollinated embryo sacs had a zygote with a degenerated synergid cell, in 52% both synergids degenerated and that 21.5% had both synergid cells present. In both of these abnormal synergid cell phenotypes there was no zygote present and the egg and central cell nuclei were present, indicating that fertilization had not occurred.

Documenting the process of synergid degeneration in WT ovules was an important frame work for understanding the developmental impacts of LRE in other studies (Leydon et al.,

2015). One question that may be of interest to examine in future studies would be to identify heterochronic differences in development of morphological structures. Heterochrony is changes in the timing during development, such as in onset, offset, or rate of development. This was thought to be an important mechanism that can result in morphological changes and in plants cell walls were important for growth. Thus, if the cell wall thickness was altered, there may have been a difference in the cell growth, and the size of cells like the synergid cell could have been affected. One would suspect there may be some dissociated heterochrony occurring during embryo sac development, i.e. cells such as the central cell still have the polar nuclei fusing and could reach some aspects of a mature embryo sac, however there was a slowing of the maturation of other aspects of cell development. For example, it was suspected that the allometric growth rates of the elongation of the synergid cells was reduced. What impact that has on reproduction, if any, was unknown. This data set was not able to show this with this EM data when the aspect ratios of the *lre-7/lre-7* and WT synergid cells were compared, because of the low sample size (n=3 for the WT), but this should be investigated with light microscopy techniques that are able to collect a relatively large sample size in a reasonably small amount of time.

### Morphological variability in LRE is present in the cell wall thickness and other structures

The LORELEI protein was first discovered and described in terms of fertility defects in mutant lines. Here novel *lre-7/lre-7* phenotypes were described that were only detectable at the ultrastructural level. These phenotypes both deepen the understanding of some of the fertility defects that have been reported previously, and broaden the understanding of the *lre-7/lre-7* mutation beyond just the scope of the fertility defects. As with many mutant

phenotypes, there was not a 100% penetrance of any one characteristic, however there were emergent patterns that arise from the data as *lre-7/lre-7* with a strong phenotype.

Previous studies that have described the null allele *lre-5,* and reported that LORELEI was important in pollen tube reception because most ovules (72.9%) did not allow pollen tube reception, while 27.1% had normal pollen tube reception (Tsukamoto et al., 2010). For those that do have normal pollen tube reception, there was a delayed seed development and there was also a fraction of seeds that were aborted (Tsukamoto et al., 2010). In aborted seeds there was endosperm development but no zygote, so the egg likely did not get fertilized (Tsukamoto et al., 2010).

When examined in more detail, it was found the *lre-5/lre-5* had a number of fertilization defects. There were several pollen tube defects. One such defect was the presence of supernumerary pollen tubes after fertilization events, which could have been the result of either a lack of short-range repulsive cues or the continued presence of attractive cues (Tsukamoto et al., 2010). In the female gametophytes for all null mutants examined (*lre4, lre5, lre6,* and *lre7)* there were 15-20% of the ovules that had multiple pollen tubes, and in heterozygous female gametophytes, 7-15% of ovules still had the entry of multiple pollen tubes (Tsukamoto et al., 2010). This study showed that there was evidence for an increase in the thickness of the cell walls of many of the cells of the embryo sac.

In addition to the previous reported defects, this study has revealed that there can be an abnormal thickening of the cell wall at the ultrastructural level in *lre-7/lre-7*. This thickening of cell wall material can be present in the antipodal cells, the egg cell, and the synergid cells. This

was unexpected since in LRE, Liu et al. (2016) found that LRE-YFP localized to the synergid cells, so this may have been an indirect result of changes in the expression of other genes or interactions with other cell signaling pathways. The thickening of the cell wall that can occur in the egg cell may potentially explain why some of the fertilized seeds are aborted, because they do not form embryos. While there were many normal looking *lre-7* egg sacs, there were several outliers (ovules 12,18) that had cell wall thickening in at least two cell types that were noted as outliers in the graph (Figure 3.3, 3.6). Ovule 18 had outliers in several structures including, Golgi counts, Type 1 filiform apparatus, and antipodal cell wall thickness. Ovules 12 and 15 had outliers in the egg cell thickness. Thus, it was proposed that ovules 18, 12, and 15 have a high penetrance of the *lre-7/lre-7* phenotype.

### Cell wall components in the filiform apparatus

This was the first study which directly showed that some of the cell wall components are localized to the filiform apparatus. There was a strong localization of pectin antibodies to the middle lamellae of cell walls, especially between the integument cells (Figure 4.1). This makes sense since it was the primary cell wall component that makes up the middle lamellae, as well as being present in all primary cell walls. Pectin was deposited in cell walls by exocytosis of vesicles coming from the Golgi.

The filiform apparatus has the highest concentration of arabinogalactan (Figure 4.3) that was observed in the embryo sac. This cell wall component has the potential to have been very important in reproduction because of its role in many aspects of cell interactions such as signaling molecules, cell identity determinants, morphogens, nutrient sources, and support for pollen tube growth (Pereira et al., 2015). They typically had a high sugar content and a GPI

anchor. It should have been noted that the GPI anchor was a glycolipid that can be attached to the c-terminus end of a protein as it undergoes post-translational modification. This means that it was possible that either an enzyme could cleave the sugars and release them into the extracellular fluid where they could have acted as signaling molecules, morphogen, or nutrients (Pereira et al., 2015). The other possibility was that the entire GPI anchor was cleaved and thus the entire protein can act as a signal. Arabinogalactan was likely to play an important part in reproduction since it would have been found in the pollen grain, the transmitting tract (Pereira et al., 2014), and also in the ovule (Pereira et al., 2015).

### Cell wall thickness defects are present in LRE

One of the major findings from this study was the fact that there were cell wall defects in cells throughout the embryo sac, not just in places where LRE was expressed. This study measured the cell wall thickness in the antipodal cells and at the apex of the egg cell. In both of these locations there was a huge increase in the variation observed in cell wall thickness, including several outliers that were above the 95% CI. There were no statistical differences in the sample mean, however this is expected because of the low sample size and because there was a lot of noise (variation) in the *lre-7/lre-7* samples. It was known from other studies on *lre* null mutants that not every single ovule in a *lre* null mutant line will have a phenotype, and this added noise to the data when looking at just sample means. When the LRE female was pollinated with the LRE male 95-98% of the seeds were normal, where as in the *lre-4, lre-5, lre-6,* and *lre-7* females that were self-pollinated there was a reduced proportion of normal seeds (22-28%), and an increase in the proportion of aborted seeds (27-43%), and undeveloped ovules (40-75%) (Tsukamoto et al., 2010). Therefore, it was expected that at least 1/4 of the

ovules would have looked like WT ovules. Since there were multiple other phenotypes, these reported defects in seed development could have been the result of a combination of multiple defects that resulted in reduced fertilization.

This was the first time that LRE had been associated with cell wall defects because it was only expressed in the female gametophyte, and without ultrastructure data it was not known that there were cell wall thickenings until this study. It was not known if LRE can form a co-receptor with FER, and that in other tissues the FER pathway can influence cell wall growth. Previous studies have shown that application of auxin cannot recover root hair growth in FER null mutants (Duan et al., 2010). It was also known that auxin and ethylene were typically upstream of ROS signaling (Andriunas et al., 2012). Therefore, there may have been a connection between ROS, cell walls, cell growth, and the FER pathway that should be investigated further in the future.

### Filiform apparatus has a high density of LRE localization in immunogold studies

The filiform apparatus was the structure that LRE has been reported to localize to in confocal studies. The complementation studies with a LRE-YFP fusion protein in the null *lre-7* background showed that LRE localized to the plasma membrane-rich filiform apparatus as well as being located intracellularly as puncta in the cytoplasm (Liu et al., 2016). Given this localization pattern and the large range of defects present in the *lre* null mutants, LORELEI may have been involved in many processes ranging from pollen tube attraction to proper programed cell death. Although the LRE that was membrane bound was likely to be acting in the RAC/ROP signaling pathway with FER, previous confocal studies left many questions remaining as to exactly where the puncta in the cytoplasm were actually localizing to, and how

they may have been functioning in pollen tube reception. It was known that LRE can act as a chaperone for FER, so it would have been expected to see some amount of LRE in the cytoplasm. Data from previous studies have shown that intracellular versions of the LRE protein (LRE-2ω, LREΔGAS) were able to complement the general fertility defects (Liu et al., 2016), however it was unknown if this occurred normally during pollen tube reception, which would have suggested a second alternative novel function for LRE, or if this was some sort of developmental redundancy that had evolved as a compensatory mechanism if the primary role of LRE fails due to some mutation in the protein. Since pollen tube reception was vital to the passing on of genetic material it would have made sense that there had evolved redundant alternative pathways that could function even if the primary mechanism, such as the LRE-GPI anchor version in the FER pathway, was compromised due to a mutation in one of the proteins within the pathway. In pollen tube reception, the native LRE protein would have most likely have involved the FER pathway in the filiform apparatus to some degree. Thus, an increase in the thickness of the wall and the number of convolutions of the filiform apparatus could have had an impact on fertility in *lre-7/lre-7*. There were a number of different ways fertility could have been affected. If surface area was diminished, this might have reduced the need for pollen tube guidance. This could have explained some of the pollen tube growth defects that have been reported within *lre* mutants (Tsukamoto et al., 2010; Liu et al., 2016). The thickness at the filiform apparatus could also have affected the actual pollen tube reception.

A lot of proteins involved in proper pollen tube reception were likely located at the filiform apparatus region. GPI-anchors were known to have been involved in signaling, and the cell wall material they attach to was the arabinogalactan cell wall component (Schultz et al.,

1998). Using immunogold labeling, it was found that there was a high density of arabinogalactan at the filiform apparatus region. Since LRE proteins had GPI anchors, it would have made sense that previous studies reported their localization at the filiform apparatus region.

It was known that ROS signaling could have initiated the formation of wall ingrowths in other cell types, such as transfer cells (Andriunas et al., 2012). In transfer cells the wall ingrowths increased the rates of nutrient exchange across apo- and symplastic interfaces. In that study they demonstrated that $H_20_2$ functions downstream of ethylene to activate cell wall biosynthesis. Another important finding from this paper was that if there were a de-localization of $H_20_2$, there was de-localized cell wall deposition. Thus, the increase in the surface area in the filiform apparatus may have had a similar function to increase the amount of communication. To examine this, a representativeness heuristics approach was used to establish three categories for the amount of convolutions that were present in the filiform apparatus. The WT had the highest proportion Type 3 (normal convolutions), while that of the *lre-7/lre-7* had a lower proportion of the Type 3 convolutions. This could have been one possible explanation for the increase in the cell wall thickness throughout the embryo sac. Now that it is known that there can be differences in the area of the filiform apparatus, future studies need to determine the range of variation in the area of the filiform apparatus that is normally present in WT. Some fluorescence light microscopy techniques would be needed to collect a large data set for proper statistical analyses and a 3D reconstruction of electron micrographs would also be needed to get an idea of the differences between *lre-7/lre-7* and WT in the three-dimensional area of the filiform apparatus.

## LRE and the FER pathway

These immunogold labeling results supported the hypothesis that LRE was likely acting in the FER pathway. It was known from studies on the FER pathways in other plant structures such as roots and leaves, that the FER pathway could have led to several different responses such as ROS generation, actin/microtubule arrangement, and regulation of hormones. In the ovule, *lre* could have been involved in the generation of ROS in the synergid cytoplasm (Duan et al., 2014; Ngo et al., 2014). The ligand for the receptor-like kinase, FER, was unknown, but other RLK receptors bind to LURE proteins released from the filiform apparatus (Galindo-Trigo *in prep).* In addition to LRE and FER there were other proteins that had been studied that also influence fertility. A recent study found that HERK1 and ANJ acted redundantly in the filiform apparatus, but not during vegetative growth, and can bind both with LRE and/or FER. They found that modified HERK1 and ANJ with no kinase activity could still have complemented the reproductive phenotypes, thus kinase activity was not important for their roles here (Galindo-Trigo *in prep*). FER localization was dependent on LRE, and NTA localization was dependent on FER. There was also reduced ROS production in both the *lre-5* and *fer-4* ovules, with the reduction being greater in the *fer-4* ovules. FER is upstream of ROS signaling while HER1, ANJ, and LRE were not required for this process. They proposed that FER was involved in both ROS generation and in the calcium fluxes needed for pollen tube burst, but HER1, LRE, and ANJ may only have been acting in the pathway that involved calcium flux, because there were only slight changes in the amount of ROS generation if those genes were knocked out (Galindo-Trigo *in prep*). Thus, ROS generation should have been impacted by the loss of LRE and it was known from studies on transfer cell that a de-localization of ROS signaling would have resulted in a de-

localization of cell wall material (Andriunas et al., 2012). It would not have been surprising if there was a loss of cell wall material in the filiform apparatus, but a general cell wall thickening in other cell walls throughout the embryo sac.

These findings confirm that there was a high concentration of LRE in the filiform apparatus, and even though LRE was also present in the synergid cytoplasm it was not nearly as high in this study as was reported with confocal microscopy. This could have been due to an artifact of the data collection methods. With light microscopy there was a low axial resolution and individual fluorophores emit light as a cone according to the point spread function. Thus, as light was collected it radiates from a point so using light intensity as in estimate of LRE concentration may have over-estimated the amount of fluorophores present in a low fluorophore density area. At the same time, it may have underestimated the amount of fluorophores present in high density areas, since their light cones overlap and it was impossible to distinguish the number of individual fluorophores. If the highest concentration of LRE was in the filiform apparatus, and not split between the cytoplasm and the filiform apparatus it was likely LRE was functioning as a co-receptor with FER in the FER pathway. If LRE acted indirectly in the FER pathway it would also have explained some of the results that were noted with the cell wall defects. It was known that FER null mutants had leaf and root growth defects due to its effect on the cell wall in non-reproductive structures. It was known that ROS signaling could have been important for cell wall development and the development of cell wall convolutions similar to those found in the filiform apparatus. Therefore, it would have made sense that a loss of LRE could have produced cell wall phenotypes in the embryo sac cells.

These analyses indicated that when there was LRE present in the synergid cytoplasm, it was associated with vacuoles. It was known that LRE can function as a chaperone for FER, therefore LRE may associate with the endomembrane system to transport FER to the plasma membrane. Confocal data suggests there was no co-localization with the endoplasmic reticulum, the Golgi apparatus, or peroxisomes (Liu et al. 2016). Therefore, LRE present in vacuoles was consistent with the confocal data findings and it would have made sense if LRE was acting as a chaperone for FER and transporting it through the endomembrane system.

## Genetic Variability and Morphology

Genetic mutations do not always lead to a phenotype in every individual. This was common knowledge in fields that worked with genetic diseases. There may have been a number of different reasons for this. In the real world there may have been additional genetic variation or environmental factors beyond that of the specific gene in question that could have explained the differences in penetrance of a disease (Burga et al., 2011). There could have been differences in the expression of a disease even if there were no detectable differences in the genome, epigenetics, or transcriptome as in the case of monozygotic twins where only one twin was affected with multiple sclerosis (Miller, 2010). These findings were also encountered in the lab with experimentation that controls for genetics and environment (Burga et al., 2011). It was known from genetic studies of diseases that simple Mendelian genetics were not enough to explain the patterns of genetic disease manifestation. Some diseases were monogenetic (controlled by one gene), oligogenic (controlled by several genes but still had a genetic basis), and polygenetic (which had a complex interaction with many genes and the environment) (Badano and Katsanis, 2002). If the LRE phenotype was simply monogenetic, then there should

have been a change in the means of the *lre-7/lre-7* measurements with regards to the WT measurement means, but this was not the case.

Even though there were not many differences in the sample means between the *lre-7* and the control group, the extreme difference in variation of the structures was well beyond what was encountered in wild types. Since fertility was necessary for the survival of the species, it stands to reason that a deletion in one gene alone would not have completely eliminated all fertility. It makes sense that *Arabidopsis* had evolved secondary and compensatory mechanisms that could have rescued seed viability if there were a small mutation in a protein that was important in fertility. Often gene networks were modular, so if one aspect was down regulated another signaling pathway would have been up regulated. Since such compensatory mechanisms would have been redundant and therefore not refined by natural selection the way the major pathways have been, it stands to reason redundant pathways would have rescued seed viability, but they would not have been as efficient or would completely complement the defects. In the case of LRE it was not surprising that *lre-7/lre-7* null mutants still have a small percentage of viable seeds, but that the total seed set was reduced.

It was also likely that functionally redundant pathways that existed would not have been under selection pressures, so they would have been free to accumulate mutations which could mean that such pathways may not be able to fully compensate for loss of the primary gene function (Nowak et al., 1997). This meant that genetic redundancy was a wide spread phenomenon in the genomes of higher organisms (Nowak et al., 1997). Freeing redundant pathways from major selection pressures could have also been a good thing since they would

have been free to evolve new functions, and thus it could have been an important mechanism for evolution.

## Evolutionary implications of structural variability

In evolutionary terms, the LORELEI/FERONIA pathway may have been co-opted from other sources such as the roots or leaves for use in reproduction. This means that it may have had similar functions to the FER pathway in other tissues such as the leaves and roots or it could have evolved new novel functions in fertility. Redundancy has been explored a little with regards to the *LRE* gene. It was known that the gene that was the closest relative of *LRE,* the LORELEI-like-GPI-anchored protein 1 (LLG1) which was also expressed in the ovule, had no fertility defects when knocked out and it would not have enhanced the fertility defects of *lre-5/lre-5* (Tsukamoto et al., 2010). This could have meant that if there was some redundancy that was contributing to the incomplete penetrance of the LRE phenotypes, it was not simply due to the LLG1 gene.

One of the patterns that emerges again and again in the structures that were measured was that there was increased variability in these structures as compared with the wild type. Note that the wild type data was obtained from two different wild type lines and pooled in order to maximize the within sample variation of the wild type lines. Since Colombia wild type was the background for the *lre* lines, there was more genetic variability between the pooled wild type lines than there should be between the Colombia wild type and *lre* lines. By pooling two genetically (Colombia WT and CW) different wild type accessions, the amount of structural variation encountered in a wild type accession would have been maximized. Since one of the tradeoffs of using electron microscopy was that it was a very resource intensive technique; it

was not possible to have a large sample size. Because data was pooled from two genetically different wild type lines, it would have maximized the structural variation encountered in wild type ovules, any between sample variation and extreme outliers in the *lre-7* data could have been attributed to knockout of the gene, instead of being an artifact of low sample size.

Increase in the variability of a phenotype has been noted in other studies. Depending on the function of the gene or protein in a pathway it was not uncommon to find an increase in structural variation of one or many characteristics, depending on where the gene or protein was in the pathway or what its function was. At the level of gene expression, Hasegawa et al. (2015) used variability in gene expression, rather than changes in the average gene expression, to detect patterns in gene expression in human embryos at different stages. Using single cell gene sequencing techniques, they found that even at the four-cell, eight-cell, morula and blastocyst stages, they were able to identify genes that had stable gene expression during all of these developmental stages. They found that stable gene expression was less likely to be associated with loss-of-function variant genes and recessive related diseases. They found a difference in the low variability gene expression at the earlier stages, which included DNA methylation, responses to hypoxia, and telomerase activity. At the blastula stage, the more stable genes were enriched for metabolic processes and telomerase signaling.

Genes with low-expression variance, or higher constraint, were significantly more connected to other networked members and tended to function as core members of a signal transduction pathway, whereas genes with higher gene expression variance had fewer network connections and also sit on the periphery of the cell (Mar et al., 2011). Variation in gene expression may have been important for the plasticity of neural development. Mar et al. (2011)

had found a reduction in variability of gene expression in neural stem cells from Schizophrenia patients in comparison to patients with Parkinson's disease and to a healthy control group.

This study suggested that, in addition to the cell-cell communication between the male and female gametophyte, LRE may have had additional roles earlier in morphological development of the cells of the embryo sac. These roles of LRE may have been similar to what has been observed in the vegetative tissue or it may have been interacting with other gene networks. In the future other potential roles for LRE, including its most likely indirect influence on the cell wall thickness, should be investigated further.

*TEM methods conclusions*

When optimizing the immunogold labeling protocol, it was found that the fast infiltration and thin embedment procedure was ideal for the ovules. Using it resulted in the production of many ovules that were correctly oriented for sectioning, as well as being well infiltrated and polymerized. Other embedding methods such as gelatin capsules, BEEM capsules, and microfuge tubes, and TAAB flat tubes resulted in ovules that were oriented randomly and often times they were not polymerized well at 50˚C. It was also found that a light coating of carbon evaporated onto sections following immunolabeling helped to stabilize the sections in the electron beam, and if there were holes in the sections resulting from suboptimal infiltration present, they did not expand when exposed to the electron beam.

# FUTURE DIRECTIONS

*Future FER pathway studies*

Although the ultrastructural evidence in this study was consistent with LRE acting in the FER pathway for ROS generation, future studies are needed to confirm this directly. Additional evidence that LRE acts in the FER pathway was that most of it was localized to the filiform apparatus, where it would have likely formed a co-receptor with FER. Even though the FER pathway to ROS generation explained the ultrastructural defects, it may not have been the only way LRE is influencing reproduction. There could have been many potential downstream effects for the FER pathway such as microtubule/actin rearrangement and hormone regulation. LRE functioning in the FER pathway also did not completely explain why LRE that lacked a transmembrane domain was able to compliment the fertility defects that were observed in *lre-7/lre-7* null mutants.

One way to confirm that LRE was acting in the FER pathway was to see if *fer* null mutants exhibited the same cell wall phenotypes that the LRE mutants expressed. Preliminary results from another ultrastructural project in the lab indicate that this was likely the case, however a larger sample size was needed to confirm this. If LRE had a novel function in embryo sac development that was independent of FER the same ultrastructural defects should not have been seen. Previous studies had also shown that LRE, FER, and NTA null mutant lines all had similar reproductive phenotypes and thus one would expect that they all function in the same pathway.

It would also be of interest to look for genes associated with ROS signaling such as *respiratory burst oxidase homologue* (*rboh)* genes which encoded the catalytic subunit of NADPH oxidase isoforms in plants. In the study by Andriunas et al. (2012), they measured several *rboh* genes and found that two of them were expressed when $H_2O_2$ was produced and that they were regulated by cross-talk with ethylene.

These results still did not answer the question as to why there was an increase in cell wall thickness in cells where extremely low levels of LRE were detected, such as the antipodal cells. Were these indirect large-scale effects that were due to communication between cells of the embryo sac? Were the phenotypes observed due to different functions temporally during development? It should also be determined if LRE was expressed earlier in the development of the ovule. Liu et al. (2016) showed that LRE was not expressed in the ovule at 11, 12a, and 12b floral stages, but it might be worth looking into earlier stages of floral development to see if lack of LRE might cause the cell wall defects. Can the cell wall defects happen in a rapid amount of time during the 12c floral stage, or do low levels of LRE signaling early in development help to generate proper cell wall thickness throughout the embryo sac during reproduction in general? It could have been that more nascent forms of LRE were acting as chaperones for FER and thus the cell wall defects were observed due to FER not localizing correctly during deposition of the cell wall. It was known that FER was expressed throughout the embryo sac. It was also known that LRE from other sources such as the cytoplasm and the induced expression of LRE in the pollen tube can complement the fertility defects. In other studies, on proteins with GPI anchors, both the native attached form and an introduced soluble form can still perform the correct function in the pathway (Worley et al., 2000). Perhaps the interaction with mobile

LRE and the FER pathway could be one possibility for why LRE could affect cell walls throughout the embryo (Figure 5.1).

Developmental differences in the synergid cells of some *lre-7/lre-7* ovules should be investigated in more detail. Although it was known that the aspect ratios of these cells differ from those in WT ovules. Though the synergid cells receive the pollen tube, it was unknown if there was a certain aspect ratio needed in order for the synergid cells to be 'mature' enough to receive the pollen tube. There may have been some optimal biomechanical advantage to having the cells be a certain size or it could just have been an artifact of growth over time. Even if the synergids would not have been able to reach a specific aspect ratio to mature, their large size may make them an easy metric to use as an indication of overall cell growth and the presence of cell wall defects. The aspect ratios of synergid cells should be investigated more in fertility mutants, particularly those in the FER pathway.

*Electron microscopy techniques:*

In the future ultrastructural studies should be done with the high pressure freezing and freeze substitution techniques to determine if there were any preservation artifacts in the chemically fixed samples. Preservation artifacts, especially of cell membranes, were possible with chemical fixation, but it should not detract from the validity of the present study since the same methods were used for preparation of both wild type and mutant tissue for comparison in this baseline study. A superior alternative fixation method, however, might reduce the background noise due to variability created by preservation artifacts and thus it may be possible to see more subtle ultrastructural defects that were not able to be measured in this study.

In the future three-dimensional reconstructions should be done to see the orientation of all of the cells that comprise the entire embryo sac using the technique of SEM array tomography. This could provide information about subtle changes in the size, shape and/or orientation of all of the cells that comprise the embryo sac that one would not be able to pick out easily with either light microscopy or TEM. For example, there may be cell growth defects that could only be determined by laborious serial section reconstruction with TEM the difficulty of which is compounded by the fact that TEM requires small sections that make it difficult to observe large multicellular structures such as an embryo sac. Although light microscopy of intact ovules would not require the sectioning process, it is difficult to measure the embryo sac enclosed within whole ovules due to the Rayleigh scattering of light, even if the ovules are cleared.

In conclusion, this study used high resolution TEM imaging that provided new insights into the role of LRE during sexual reproduction in plants that was previously unknown through light microscopy and molecular techniques alone. The data from this study should be used as a foundation for future studies on the role that LRE plays in the FER pathway and its relationship with cell wall development in the embryo sac.


Figure 5. 1 Electron micrograph of a *fer-4* egg cell showing cell wall thickenings near the nucleus of the egg cell, similar to what has been observed in some of the *lre-7/lre-7* mutants. LRE has been shown to form a co-receptor with FER, so it is not surprising that similar cell wall defects in the egg cell are also present in *fer-4* null mutants. The scale bar is 10 microns.

# REFERENCES


**Amien S, Kliwer I, Marton ML, Debener T, Geiger D, Becker D, Dresselhaus T** (2010) Defensin-like ZmES4 mediates pollen tube burst in maize via opening of the potassium channel KZM1. PLoS Biol **8:** e1000388

**Andriunas FA, Zhang HM, Xia X, Offler CE, McCurdy DW, Patrick JW** (2012) Reactive oxygen species form part of a regulatory pathway initiating trans-differentiation of epidermal transfer cells in Vicia faba cotyledons. J Exp Bot **63:** 3617-3629

**Badano JL, Katsanis N** (2002) Beyond Mendel: an evolving view of human genetic disease transmission. Nat Rev Genet **3:** 779-789

**Bleckmann A, Alter S, Dresselhaus T** (2014) The beginning of a seed: regulatory mechanisms of double fertilization. Front Plant Sci **5:** 452

**Boisson-Dernier A, Roy S, Kritsas K, Grobei MA, Jaciubek M, Schroeder JI, Grossniklaus U** (2009) Disruption of the pollen-expressed FERONIA homologs ANXUR1 and ANXUR2 triggers pollen tube discharge. Development **136:** 3279-3288

**Burga A, Casanueva MO, Lehner B** (2011) Predicting mutation outcome from early stochastic variation in genetic interaction partners. Nature **480:** 250-253

**Caron E** (2003) Rac signalling: a radical view. Nature Cell Biology **5:** 185

**Christensen CA, Gorsich SW, Brown RH, Jones LG, Brown J, Shaw JM, Drews GN** (2002) Mitochondrial GFA2 Is Required for Synergid Cell Death in Arabidopsis. The Plant Cell **14:** 2215-2232

**Dresselhaus T, Franklin-Tong N** (2013) Male–Female Crosstalk during Pollen Germination, Tube Growth and Guidance, and Double Fertilization. Molecular Plant (Oxford University Press / USA) **6:** 1018-1036

**Duan Q, Kita D, Johnson EA, Aggarwal M, Gates L, Wu HM, Cheung AY** (2014) Reactive oxygen species mediate pollen tube rupture to release sperm for fertilization in Arabidopsis. Nat Commun **5:** 3129

**Duan Q, Kita D, Li C, Cheung AY, Wu HM** (2010) FERONIA receptor-like kinase regulates RHO GTPase signaling of root hair development. Proc Natl Acad Sci U S A **107:** 17821-17826

**Ferluga C, Kosutic Z, Bacun-Kubovic M** (1971) [Clinical observations on epidemics of Q fever in northern Croatia]. G Mal Infett Parassit **23:** 962-963

**Gross-Hardt R, Kagi C, Baumann N, Moore JM, Baskar R, Gagliano WB, Jurgens G, Grossniklaus U** (2007) LACHESIS restricts gametic cell fate in the female gametophyte of Arabidopsis. PLoS Biol **5:** e47

**Hasegawa Y, Taylor D, Ovchinnikov DA, Wolvetang EJ, de Torrente L, Mar JC** (2015) Variability of Gene Expression Identifies Transcriptional Regulators of Early Human Embryonic Development. PLoS Genet **11:** e1005428

**Heydlauff J, Groß-Hardt R** (2014) Love is a battlefield: programmed cell death during fertilization. Journal of Experimental Botany **65:** 1323-1330

**Higashiyama T** (2002) The synergid cell: attractor and acceptor of the pollen tube for double fertilization. J Plant Res **115:** 149-160

**Holdorf MM, Owen HA, Lieber SR, Yuan L, Adams N, Dabney-Smith C, Makaroff CA** (2012) Arabidopsis ETHE1 encodes a sulfur dioxygenase that is essential for embryo and endosperm development. Plant Physiol **160:** 226-236

**Holloway SJ, Friedman WE** (2008) Embryological features of Tofieldia glutinosa and their bearing on the early diversification of monocotyledonous plants. Ann Bot **102:** 167-182

**Kagi C, Baumann N, Nielsen N, Stierhof YD, Gross-Hardt R** (2010) The gametic central cell of Arabidopsis determines the lifespan of adjacent accessory cells. Proc Natl Acad Sci U S A **107:** 22350-22355

**Kawashima T, Berger F** (2015) The central cell nuclear position at the micropylar end is maintained by the balance of F-actin dynamics, but dispensable for karyogamy in Arabidopsis. Plant Reprod **28:** 103-110

**Kessler SA, Grossniklaus U** (2011) She's the boss: signaling in pollen tube reception. Curr Opin Plant Biol **14:** 622-627

**Kessler SA, Shimosato-Asano H, Keinath NF, Wuest SE, Ingram G, Panstruga R, Grossniklaus U** (2010) Conserved molecular components for pollen tube reception and fungal invasion. Science **330:** 968-971

**Kumar P, Wagner CE** (2018) Temperature dependence of nonlinear susceptibilities in an infinite range interaction model. J Phys Condens Matter **30:** 345801

**Leshem Y, Johnson C, Sundaresan V** (2013) Pollen tube entry into the synergid cell of Arabidopsis is observed at a site distinct from the filiform apparatus. Plant Reprod **26:** 93-99

**Leydon AR, Tsukamoto T, Dunatunga D, Qin Y, Johnson MA, Palanivelu R** (2015) Pollen Tube Discharge Completes the Process of Synergid Degeneration That Is Initiated by Pollen Tube-Synergid Interaction in Arabidopsis. Plant Physiol **169:** 485-496

**Leydon AR, Tsukamoto T, Dunatunga D, Qin Y, Johnson MA, Palanivelu R** (2015) Pollen tube discharge completes the process of synergid degeneration that is initiated by pollen tube - synergid interaction in Arabidopsis. pp.00528.02015

**Li C, Wu HM, Cheung AY** (2016) FERONIA and Her Pals: Functions and Mechanisms. Plant Physiol **171:** 2379-2392

**Li C, Yeh FL, Cheung AY, Duan Q, Kita D, Liu MC, Maman J, Luu EJ, Wu BW, Gates L, Jalal M, Kwong A, Carpenter H, Wu HM** (2015) Glycosylphosphatidylinositol-anchored proteins as chaperones and co-receptors for FERONIA receptor kinase signaling in Arabidopsis. Elife **4**

**Lindner H, Kessler SA, Muller LM, Shimosato-Asano H, Boisson-Dernier A, Grossniklaus U** (2015) TURAN and EVAN mediate pollen tube reception in Arabidopsis Synergids through protein glycosylation. PLoS Biol **13:** e1002139

**Liu X, Castro C, Wang Y, Noble J, Ponvert N, Bundy M, Hoel C, Shpak E, Palanivelu R** (2016) The Role of LORELEI in Pollen Tube Reception at the Interface of the Synergid Cell and Pollen Tube Requires the Modified Eight-Cysteine Motif and the Receptor-Like Kinase FERONIA. Plant Cell **28:** 1035-1052

**Liu Y, Yan Z, Chen N, Di X, Huang J, Guo G** (2010) Development and function of central cell in angiosperm female gametophyte. Genesis **48:** 466-478

**Mansfield SG, Briarty LG, Erni S** (1991) Early embryogenesis in *Arabidopsis thaliana*. **I**. The mature embryo sac. . Canadian Journal of Botany **69:** 447-460

**Mar JC, Matigian NA, Mackay-Sim A, Mellick GD, Sue CM, Silburn PA, McGrath JJ, Quackenbush J, Wells CA** (2011) Variance of gene expression identifies altered network constraints in neurological disease. PLoS Genet **7:** e1002207

**McDonald KL** (2014) Rapid embedding methods into epoxy and LR White resins for morphological and immunological analysis of cryofixed biological specimens. Microsc Microanal **20:** 152-163

**Miller N** (2010) Genome, Epigenome and RNA sequences of Monozygotic Twins Discordant for Multiple Sclerosis. ; Lawrence Berkeley National Lab. (LBNL), Berkeley, CA (United States)

**Miyazaki S, Murata T, Sakurai-Ozato N, Kubo M, Demura T, Fukuda H, Hasebe M** (2009) ANXUR1 and 2, sister genes to FERONIA/SIRENE, are male factors for coordinated fertilization. Curr Biol **19:** 1327-1331

**Moll C, von Lyncker L, Zimmermann S, Kagi C, Baumann N, Twell D, Grossniklaus U, Gross-Hardt R** (2008) CLO/GFA1 and ATO are novel regulators of gametic cell fate in plants. Plant J **56:** 913-921

**Murgia M, Huang B, C. Tucker S, E. Musgrave M** (1993) Embryo Sac Lacking Antipodal Cells in Arabidopsis thaliana (Brassicaceae), Vol 80

**Ngo QA, Vogler H, Lituiev DS, Nestorova A, Grossniklaus U** (2014) A calcium dialog mediated by the FERONIA signal transduction pathway controls plant sperm delivery. Dev Cell **29:** 491-500

**Nowak MA, Boerlijst MC, Cooke J, Smith JM** (1997) Evolution of genetic redundancy. Nature **388:** 167-171

**Pagnussat GC, Alandete-Saez M, Bowman JL, Sundaresan V** (2009) Auxin-dependent patterning and gamete specification in the Arabidopsis female gametophyte. Science **324:** 1684-1689

**Palanivelu R, Brass L, Edlund AF, Preuss D** (2003) Pollen Tube Growth and Guidance Is Regulated by POP2, an Arabidopsis Gene that Controls GABA Levels. Cell **114:** 47-59

**Pereira AM, Masiero S, Nobre MS, Costa ML, Solis MT, Testillano PS, Sprunck S, Coimbra S** (2014) Differential expression patterns of arabinogalactan proteins in Arabidopsis thaliana reproductive tissues. J Exp Bot **65:** 5459-5471

**Pereira AM, Pereira LG, Coimbra S** (2015) Arabinogalactan proteins: rising attention from plant biologists. Plant Reprod **28:** 1-15

**Rotman N, Gourgues M, Guitton AE, Faure JE, Berger F** (2008) A dialogue between the SIRENE pathway in synergids and the fertilization independent seed pathway in the central cell controls male gamete release during double fertilization in Arabidopsis. Mol Plant **1:** 659-666

**Schiott M, Romanowsky SM, Baekgaard L, Jakobsen MK, Palmgren MG, Harper JF** (2004) A plant plasma membrane Ca2+ pump is required for normal pollen tube growth and fertilization. Proc Natl Acad Sci U S A **101:** 9502-9507

**Schultz C, Gilson P, Oxley D, Youl J, Bacic A** (1998) GPI-anchors on arabinogalactan-proteins: implications for signalling in plants. Trends in Plant Science **3:** 426-431

**Song X, Yuan L, Sundaresan V** (2014) Antipodal cells persist through fertilization in the female gametophyte of Arabidopsis. Plant Reprod **27:** 197-203

**Tsukamoto T, Qin Y, Huang Y, Dunatunga D, Palanivelu R** (2010) A role for LORELEI, a putative glycosylphosphatidylinositol-anchored protein, in Arabidopsis thaliana double fertilization and early seed development. Plant J **62:** 571-588

**Uhrig JF, Hülskamp M** (2001) Rop GTPases: Polarity and Cell Shape in Plants. *In* eLS. John Wiley & Sons, Ltd

**Volz R, Heydlauff J, Ripper D, von Lyncker L, Gross-Hardt R** (2013) Ethylene signaling is required for synergid degeneration and the establishment of a pollen tube block. Dev Cell **25:** 310-316

**Wodniok S, Brinkmann H, Glockner G, Heidel AJ, Philippe H, Melkonian M, Becker B** (2011) Origin of land plants: do conjugating green algae hold the key? BMC Evol Biol **11:** 104

**Worley DS, Pisano JM, Choi ED, Walus L, Hession CA, Cate RL, Sanicola M, Birren SJ** (2000) Developmental regulation of GDNF response and receptor expression in the enteric nervous system. Development **127:** 4383-4393

**Yu GH, Zou J, Feng J, Peng XB, Wu JY, Wu YL, Palanivelu R, Sun MX** (2014) Exogenous gamma-aminobutyric acid (GABA) affects pollen tube growth via modulating putative Ca2+-permeable membrane channels and is coupled to negative regulation on glutamate decarboxylase. J Exp Bot **65:** 3235-3248

CURRICULUM VITAE

# JULEEN DICKSON

**EDUCATION:**

***Doctor of Philosophy:*** Biological Sciences: Cell and Molecular Biology
University of Wisconsin-Milwaukee, Owen Laboratory
Dissertation: Ovule Ultrastructure and Immunogold Localization of LORELEI in *Arabidopsis*
Fall 2013-present

***Master of Science:*** Biology
California State University Fullerton, Dickson Laboratory.
Thesis: Development of the slow-twitch oxidative myotomal muscle in the yellowfin tuna (*Thunnus albacares*)
Feb. 2005-Aug. 2008

***Bachelor of Science***; Marine Science (Biology concentration)
Southampton College of Long Island University, Southampton, NY
Sept. 2000-Aug. 2004

**AWARDS/HONORS:**

**Peter J. Salamun Scholarship:** Spring 2018
**Midwest Plant Cell Dynamics Student Fellowship:** Summer 2017
**Graduate Student Pollen RCN internship:** Summer 2016
**Louise Neitge Mather Scholarship:** Spring 2016
**Plant Reproduction 2016 Registration Award:** Fall 2016
**Ruth Walker Grants-In-Aid of Research:** Spring 2015, 2017
**Ruth Walker Travel Grant:** Summer 2014, Summer 2017
**Advanced Opportunity Program Fellowship:** Fall 2013-present
**Grants-In-Aid of Research administered by Sigma Xi, the Scientific Research Society:** Spring 2012
**Charlotte Mangum Student Support Award:** Winter 2009, 2010, 2011, 2012

**RESEARCH EXPERIENCE:**

**University of Wisconsin-Milwaukee:** Dissertation Research, Owen laboratory, Fall 2015-present

- Developed skills for embedding, ultramicrotomy, and sample preparation for transmission electron microscopy (TEM).
- Developed Immunogold labeling protocol for GFP and cell wall components in plant ovule tissue.
- Experience with scanning electron microscopy (SEM) imaging of samples ranging from nanoparticles and mineral samples to plant and animal tissues.
- Worked with *Arabidopsis* lines including null mutants from T-DNA insertions and several transgenic lines with YFP and GFP reporters for various proteins involved in cell-to-cell signaling between pollen tubes and female gametophytes.
- Dark room experience, where I developed film for TEM negatives and enlargements on photographic paper.

- Used energy-dispersive X-ray spectroscopy (EDS) detectors for elemental detection and analyses on SEM.
- Assisted with high pressure freezing and freeze substitution protocols for plant tissues.
- Built macros in imageJ for immunogold labeling analyses.

**University of Wisconsin-Milwaukee:** Udvadia laboratory, Fall 2013-Spring 2015
- Experience with molecular techniques ranging from RNA extraction to qPCR.
- Primer design and optimization for qPCR.
- Utilized Fluorescence Activated Cell Sorting (FACS) to isolate neural crest cells from zebrafish embryos.
- Experience managing and screening 30 transgenic zebrafish lines including lines containing Cre recombinase and lines created with CRISPR technology.
- Conducted toxicological exposures of zebrafish embryos and larvae to varying concentrations of the environmental toxin Benzo(a)pyrene.
- Used Alcian Blue staining techniques to stain cartilage elements in craniofacial structures in fish larvae.
- Quantified morphological variation between exposure trials with geometric morphometric analyses to eliminate size and orientation bias among individuals within treatment groups.
- Collected Z-stacks and screened fish larvae on various fluorescent microscopes.

**University of Wisconsin-Milwaukee:** Oliver laboratory, Summer 2012-Summer 2013
- Synthesized gold and magnetite nanoparticles and conjugated them to various antibodies and proteins of interest for labeling purposes in electron microscopy.
- Performed phlebotomy, prepared human blood samples, and isolated platelets with sepharose column chromatography.
- Conducted experiments and SEM analyses on surface activated platelets labeled with nanoparticles using the transmission electron (TE) and backscattered electron (BSE) detectors.
- Tissue culture experience with model mammalian and insect cell lines, including CHO and HEK cell lines.
- Responsible for ordering lab supplies, record keeping, and coordinating with collaborators.

**University of Wisconsin-Milwaukee:** Janssen laboratory. Goby lateral line development. 2011-2012
- Used clearing and staining techniques to investigate bone ossification during larval fish development.
- Used immunofluorescent staining techniques to identify different lateral line sensory cells.
- Fixed, dehydrated, critical point dried, sputter coated, and imaged fish larvae with SEM.
- Conducted ANCOVA analyses in 'R' statistical software.

**University of Rhode Island:** Webb laboratory, Lateral line canal development in cichlids. 2008-2010
- Used standard histological methods to section, stain, and mount tissue for paraffin histology.
- Compared the pattern and timing of two different lateral line morphologies during development to test heterochrony hypotheses.
- Gained experience with cichlid husbandry including breeding, rearing larvae, and hatching live brine shrimp.

**California State University Fullerton:** Thesis: Slow-twitch oxidative muscle development in tunas
- Traveled to Achotines Laboratory in Panama where yellowfin tuna juveniles were raised and sampled.
- Specimens were cryofixed in liquid nitrogen, sectioned on a cryostat, and mounted on slides.
- Immunohistochemistry and enzyme histochemistry labeling techniques were used to identify slow-twitch oxidative muscle.
- Documented ontogenetic progression of medial slow-twitch oxidative muscle development in yellowfin tunas ranging from 40 to 188 mm fork length.
- Gained experience in writing grants, research proposals, scientific reports, and teaching biology laboratories.

**Friday Harbor Laboratories: Fish Swimming Course** San Juan Island, WA. Summer 2007
- In-depth study of fish kinematics and energetics using respirometry and flow tanks.
- In five weeks I designed, set-up, collected, and analyzed data for a publication-quality experiment.
- Conducted experiments on 'The effect of fatigue on schooling behavior' and 'Escape responses in Chimeras.'
- Participated in semi-weekly beach seines to collect fish for projects.

**Southampton College:** Marine Operations and Research, Southampton, NY. Spring 2004
- Conducted benthic sampling of Shinnecock, Moriches, and Quantuck Bay.
- Sediment sampling and grain size analysis at various geographic points.
- Benthic epifaunal and infaunal invertebrate identification.
- Calculated hard clam densities in different sediment types.
- Found correlations between sediment grain size and invertebrate community diversity.

**Southampton College:** Gobler laboratory, Southampton, NY, Sept 2003-Aug. 2004
- Brown tide (*Aureococcus sp.*) biological oceanography research.
- Growth rate experimentation with various *Aureococcus* strains infected with virus strains under different light levels.
- Maintained both phytoplankton and virus cultures in the lab.

**Scripps Institution of Oceanography:** Palenik laboratory, La Jolla, CA, Feb 2003- Aug 2003
- Used cloning techniques to generate both random and site-specific mutations in amino acid transporters in the cyanobacterium *Synechococcus.*
- Documented the effects of altering nitrogen levels and temperature on growth rates in coastal and oligotrophic strains of *Synechococcus sp*.
- Weekly field sampling to monitor phytoplankton populations.

**SEAmester West:** Baja California, Mexico, Spring 2002
- Lived and worked at sea for three months aboard the 19th century Sailing Vessel, *Californian.*
- Gained experience with sail handling, helm, and navigation while taking undergraduate courses.

**Great Lakes WATER Institute:** Milwaukee, Wisconsin, June 2001- Aug 2001
- Conducted larval yellow perch gut analysis to observe size related diet shifts.
- Experience with zooplankton identification in field samples from freshwater systems.
- Collected field samples on Lake Michigan using Tucker Trawl, Neuston Net, and various other field equipment.
- Daily husbandry for laboratory-reared larval perch and field-caught zooplankton maintained in laboratory.

**TEACHING EXPERIENCE:**

**University of Wisconsin-Milwaukee:** Bio 152L: Foundations in Biological Sciences II, Spring 2019
- Taught foundations of hypothesis writing, experimental design, and basic analyses with long term experiments.
- Introduced students to biological diversity in the five kingdoms, with emphasis on plants and animals.
- Introduced molecular cloning techniques with a bacterial transformation laboratory.
- Gave powerpoint lectures, designed, administered, and graded quizzes and various lab reports.

**University of Wisconsin-Milwaukee:** Bio 202L: Anatomy and Physiology I, Fall 2016-Fall 2018
- The first course in the Anatomy and Physiology for both biology and health science majors.
- Taught topics a wide range of topics including histology, bone, muscle, and neural anatomy.
- Had experimental laboratory on diffusion and osmosis.
- Created PowerPoint lectures and designed quizzes.

- Extensive experience with digital learning environments, including D2L, Blackboard, and Canvas platforms ranging from posting assignments, grading, and quizzing in a digital environment.
- Have experience with the external Anatomy web programs such as the Anatomy TV website, and also quizzing through the McGraw-Hill connect web site.

**University of Rhode Island, Kingston RI:** Bio 360L: Marine Biology, Spring 2009-Fall 2010

- Upper division class for marine biology majors.
- Taught topics ranging from phytoplankton diversity to marine ecology, including numerous dissections.
- Led numerous field trips including a trawl survey in the bay and intertidal field trips.
- Guest lectured for both the phytoplankton and ichthyology weeks in the lecture portion of the course.
- Designed an ichthyology laboratory which included interactive activities ranging from dissections to larval identification.

**University of Rhode Island, Kingston RI:** Bio 101L: Elements of Biology, Fall 2008

- Introductory biology laboratory for majors.
- Taught topics ranging from PCR to animal physiology.
- Assisted in lecture exam grading.

**Orange Coast College, Costa Mesa CA:** MS 100L: Oceanography laboratory, Spring 2008

- Introductory Oceanography laboratory offered through Marine Science Department for majors and non-majors.
- Activities that include navigation, bathymetry, wave predictions, water chemistry, and sediment analysis.
- Field activities include sediment sampling during an oceanographic cruise.
- Led nature walk through the Newport Back Bay estuary system and Long Beach Aquarium tour.

**California State University, Fullerton:** Biol 362L: Mammalian Physiology Laboratory. 2005-2008

- Upper division elective.
- Focused on understanding of physiological principles through laboratory experiments.
- Emphasized hypothesis testing, experimental design, data analysis, and interpretation with simple statistics.
- Graded weekly scientific reports, quizzes, and administered the final.
- Experiments included live frog models, computer models, or monitoring basic vital signs among peers.

**California State University, Fullerton:** Biol 171L: Evolution and Biodiversity Laboratory, Spring 2005-Spring 08

- First core course for biology majors that met twice a week.
- Experience giving short lectures, supervising lab work, and field trips.
- Field trips: Mojave Desert, Intertidal, Chaparral.
- Emphasized experimental design, and diversity of the five kingdoms.
- Graded student assignments and designed quizzes.

**California State University, Fullerton:** Biol 101L: General Biology Laboratory, Spring 2005

- Biology for non-majors.
- Topics included respiration, photosynthesis, reproduction, development, evolution, energy transport.
- Organized field trips to tide pools, grunion run, Cabrillo Marine Aquarium.
- Designed weekly quizzes and graded post-lab assignments.
- For final class period students gave poster presentation on biology topic of their choosing that was relevant to society, such as stem cell research, genetically modified organisms, endangered species and had to discuss the pros and cons of the topic.

**REFERENCES:**

**Heather Owen (PhD Advisor/Director of Electron Microscopy Facility).** Phone: (414) 229-6816 E-mail: owenha@uwm.edu
Address: University of Wisconsin-Milwaukee, Department of Biological Sciences, 3209 N. Maryland Ave, Milwaukee, WI, 53211, USA

**Julie Oliver (Committee member/ PI for SEM platelet project).** Phone: (414) 229-4317 E-mail: joliver@uwm.edu
Address: University of Wisconsin-Milwaukee, Department of Biological Sciences, 3209 N. Maryland Ave, Milwaukee, WI, 53211, USA

**Doug Steeber (Committee member).** Phone: (414) 229-4371 E-mail: steeber@uwm.edu
Address: University of Wisconsin-Milwaukee, Department of Biological Sciences, 3209 N. Maryland Ave, Milwaukee, WI, 53211, USA

**Kathryn Dickson (Master's advisor).** Phone: (657) 278-3614 E-mail: kdickson@fullerton.edu
Address: California State University, Fullerton, Department of Biological Sciences, Fullerton, CA 92834, USA

**PUBLICATIONS:**

**Dickson, J., Dickson, K. A.** (*in review*) Ontogenetic Change in the Amount and Position of Slow-Oxidative Myotomal Muscle in Relationship to Regional Endothermy in Juvenile Yellowfin Tuna *Thunnus albacares.* Journal of Fish Biology.

**Dickson, J., Janssen, J. A.** (2018) Proliferation of Superficial Neuromasts During Lateral Line Development in the Round Goby, *Neogobius melanostomus.* (*preprint*). https://doi.org/10.1101/386169

**Dickson, J.M.**, **Maia, A., and Domenici, P.** (*in prep*). Three-Dimensional Escape Response of White Spotted Ratfish, *Hydrolagus colliei*.

**Webb, J.F., Bird, N.C., Carter, L., Dickson, J.** (2014) Comparative development and evolution of two lateral line phenotypes in lake Malawi cichlids. Journal of Morphology. 275:678-692.

**Dickson, J.** (2008). Development of the slow-twitch oxidative myotomal muscle in the yellowfin tuna (*Thunnus albacares*). M.S. thesis, California State University, Fullerton, CA. pp. 1-57.

**RESEARCH PRESENTATIONS:**

**Dickson, J.M.,** Palanivelu, R., and Owen, H.A. (2017) Ultrastructural analysis of *Arabidopsis thaliana* ovule maturation. Midwest Plant Cell Dynamics. (Paper and poster presentation)

**Dickson, J.M.,** Palanivelu, R., and Owen, H.A. (2017) Immunogold localization of cell wall components and ovule ultrastructure in Arabidopsis. UWM Biological Sciences Symposium.

**Dickson, J.M.,** Palanivelu, R., and Owen, H.A. (2016) Ovule Ultrastructure and Localization of LORELEI, A GPI Anchor Protein Involved in Pollen Tube Reception. UWM Biological Sciences Symposium.

**Dickson, J.M,** Cheung, A., Palanivelu, R., and Owen, H.A. (2016) Ultrastructural Analysis of *Arabidopsis thaliana* ovules. 24th International Congress on Sexual Plant Reproduction.

**Dickson, J.M.**, O'Connor, B.D., and Udvadia, A.J. (2015) Craniofacial Malformation Resulting from Exposure to Benzo(a)pyrene at Different Time Points During Development. Midwest Zebrafish Conference.

**Dickson, J.M.**, O'Connor, B.D., and Udvadia, A.J. (2015) Craniofacial Malformation Resulting from Exposure to Benzo(a)pyrene at different time points during development. UWM Biological Sciences Symposium.

O'Connor, B.D., **Dickson, J.M.**, and Udvadia, A.J. (2015) Effect of Benzo(a)pyrene on the Craniofacial Development of Zebrafish. National Council on Undergraduate Research Meeting.

**Dickson, J.M.,** Hammond-Weinberger, D.R., and Udvadia, A.J. (2014) Exploring Mechanisms Underlying Craniofacial Malformations Resulting from Developmental Exposure to Benzo(a)pyrene. 11th International Conference on Zebrafish Development and Genetics.

**Dickson, J.M.** and Udvadia, A.J. (2014) Craniofacial Malformation Resulting from Developmental Exposure to an Environmental Toxin, benzo(a)pyrene. UWM BioScience Symposium.

**Dickson, J.M.** and Udvadia, A.J. (2014) Impacts of Benzo(a)pyrene on Cranial Neural Crest Cell Development. UWM Neuroscience Symposium.

**Dickson, J.M.**, Udvadia, A.J., and Janssen, J.A. (2012). Reduced Lateral Line Canal Development in the Round Goby, *Neogobius melanostomus*. Society of Integrative and Comparative Biology.

**Dickson, J.M.**, Udvadia, A.J., and Janssen, J.A. (2012). Reduced Lateral Line Canal Development in the Round Goby, *Neogobius melanostomus*. Science Education Partnership Award Conference.

**Dickson, J.M.** and Webb, J.F. (2011). Comparative Post-Embryonic Development of the Cranial Lateral Line Canal System in Cichlid Fishes: Temporal and Spatial Patterns. Society of Integrative and Comparative Biology.

**Dickson, J.M.** and Webb, J.F. (2010). Comparative Development of Lateral Line Canals in Three Lake Malawi Cichlids: Insights into the Evolution of Widened Canals. Society of Ichthyologists and Herpetologists.

**Dickson, J.M.** and Webb, J.F. (2010). The Development of Widened Lateral Line Canals in a Lake Malawi cichlid: Insights into Lateral Line Evolution. Society of Integrative and Comparative Biology.

**Dickson, J.M.**, Maia, A., and Domenici, P. (2010). Three-Dimensional Escape Response of White Spotted Ratfish, *Hydrolagus colliei*. Society of Experimental Biology.

**Dickson, J.M.**, Maia, A., and Domenici, P. (2009). Three-Dimensional Escape Response of White Spotted Ratfish, *Hydrolagus colliei*. Society of Integrative and Comparative Biology.

**Dickson, J.M.**, Maia, A., and Domenici, P. (2009). Three-Dimensional Escape Response of White Spotted Ratfish, *Hydrolagus colliei*. Bodies in Motion- URI graduate student conference.

**Dickson, J.M.**, Maia, A., and Domenici, P. (2008). Three-Dimensional Escape Response of White Spotted Ratfish, *Hydrolagus colliei*. The American Elasmobranch Society.

Bohaboy, E., Cleary, A., **Dickson, J.M.**, Longval, B., and Szczepanski, J. (2009). Functional Diversity in Temperate Coastal Fish Communities. Society of Integrative and Comparative Biology. American Society of Ichthyologists and Herpetologists.

**Dickson, J.M.** and Dickson, K.A. (2008). Development of the Slow-Twitch Oxidative Myotomal Muscle in the Yellowfin tuna (*Thunnus albacares*). American Society of Ichthyologists and Herpetologists.

**Dickson, J.M.** and Dickson, K.A. (2008). Slow-Twitch Oxidative Muscle Development in Yellowfin Tuna, *Thunnus albacares*. Society of Integrative and Comparative Biology.

**Dickson, J.M.** and Dickson, K.A. (2007). Red Muscle Development in the Yellowfin Tuna (*Thunnus albacares*). Graduate Women in Science.

**Dickson, J.M.** and Dickson, K.A. (2007). Medial Red Muscle Development in the Yellowfin Tuna (*Thunnus albacares*). Southern California Academy of Science.

**Dickson, J.M.** and Dickson, K.A. (2007). Medial Red Muscle Development in Tunas (Family Scombridae). Tuna Conference.

**RELAVENT COURSE WORK:**

Quantitative Fluorescence Microscopy
Principles of Fluorescence Techniques
Transmission Electron Microscopy
Scanning Electron Microscopy
Genetics
Eukaryotic Gene Regulation
Molecular Biology
Advanced Cell Biology
Neuroscience Seminar
Cell and Molecular Bio Seminar
Microbiology
Experimental Design
Statistics and R for the Life Sciences
Introduction to Linear Algebra and Matrix Algebra
Statistical Inference and Modeling for High throughput Experiments
Experimental Animal Learning
Marine Operations and Research
Developmental Biology
Fish Development
Developmental Neurobiology
Development, Ecology, and Evolution Marine Ecology
Field Work in Coastal Ecology
Human Impacts on Coastal Environments
Marine Phylogeography
Chemical Oceanography
Physical Oceanography
Biological Oceanography
Making Sense of Climate Denial
Marine Bioacoustics
Navigation and Seamanship
Biology of Plankton
Phycology
Vertebrate Zoology
Invertebrate Zoology
Tropical Marine Biology
Evolution
Diversity of Fishes
Ichthyology (west coast)
Ichthyology (east coast)
Fish Swimming: Kinematics, Ecomorphology, Behavior and Environmental Physiology

**PROFESSIONAL SOCIETY MEMBERSHIP:**

Midwest Microscopy and Microanalysis Society
International Conference on Arabidopsis Research

Midwest Plant Cell Dynamics
American Association for the Advancement of Science
International Association of Sexual Plant Reproduction Research
Sigma Xi
Genetics Society of America
Society of Integrative and Comparative Biology
Society of Experimental Biology
Southern California Academy of Science
American Society of Ichthyologists and Herpetologists
American Elasmobranch Society
American Association of University Professors
Western Society of Naturalists
National Center for Science Education